1985

The description of chemical reactions by the method of the Full Optimized Reaction Space. The ring-opening of unsubstituted and substituted cyclopropylidene to allene

Petros Valtazanos
Iowa State University

Valtazanos, Petros

THE DESCRIPTION OF CHEMICAL REACTIONS BY THE METHOD OF THE FULL OPTIMIZED REACTION SPACE. THE RING-OPENING OF UNSUBSTITUTED AND SUBSTITUTED CYCLOPROPYLIDENE TO ALLENE

Iowa State University PH.D. 1985

The description of chemical reactions by the method of the Full Optimized Reaction Space. The ring-opening of unsubstituted and substituted cyclopropylidene to allene

by

Petros Valtazanos

A Dissertation Submitted to the
Graduate Faculty in Partial Fulfillment of the
Requirements for the Degree of
DOCTOR OF PHILOSOPHY
Department: Chemistry
Major: Physical Chemistry

Approved:

Signature was redacted for privacy.

In Charge of Major Work

Signature was redacted for privacy.

For the Major Department

Signature was redacted for privacy.

For the Graduate College

Iowa State University
Ames, Iowa

1985

TABLE OF CONTENTS

I. INTRODUCTION

Surely, theoretical science has existed for as long as experimental science. From the first discernment of a pattern, when observing natural phenomena, the scientifically minded must have had an urge to develop a theory to fit the facts and, if possible, to predict what would happen under somewhat different circumstances. For a long time, however, theory and experiment tended mostly to be coupled in the sense that the same persons would develop theories and perform experiments. Only in relatively recent times, with the coming of increased specialization in all forms of human endeavor, have pure theorists emerged as a separate species and claimed their place among the various branches of science.

Theoretical chemistry in its modern sense was made possible by the development of quantum mechanics in the 1920s which led to the formulation of chemical problems in terms of a mathematical formalism which would, in principle, describe all physical properties of molecules and their reactions. However, even though the equations now exist, their solution is far from trivial. In fact, the only quantum chemical problem which can be solved exactly is that of the hydrogen atom. No other molecule can be solved analytically, and theoreticians have therefore concentrated

their efforts on obtaining approximate solutions of sufficiently high accuracy to the exactly formulated problems.

Such approximate solutions can vary widely in the level of the approximations employed. Since even the simplest of them require large amounts of numerical computations, in the old days (and still today in certain areas) most chemical problems were attacked via empirical or semi-empirical methods. These approaches are based on the expedient of substituting, for the most difficult and time-consuming quantities in the quantum mechanical equations, numerical parameters whose values are determined by fitting the results of the calculation to existing experimental or, in some cases, well-established theoretical data. This method is extremely economical in comparison to nonempirical methods, and it has had impressive successes for certain limited classes of molecules. Nonetheless it is fraught with problems. Foremost among these is the assumption that identical empirical parameters can be used when a compound or reaction is expected to have characteristics or behavior similar to another compound or reaction. This procedure is inherently dangerous even when based on a well-developed chemical intuition. Especially when phenomena are investigated about which there exists little evidence or where the evidence is conflicting, can a priori assumptions

about similarities with other cases lead to results that are wrong or at least suspect.

The alternative to the semi-empirical methods is the ab-initio approach, a term which, roughly translated, means "from scratch". It should be appreciated that ab-initio calculations do contain a certain amount of empirical information, such as basis sets and the scaling of primitive exponents. The difference betwen them and semi-empirical methods is that this "empirical" information does not change arbitrarily with the system under investigation but has been established by two decades of numerical experimentation in finding reliable quantitative approximations to the exact solutions of the Schrodinger equation by rigorous mathematical procedures such as the variation principle. It is for this reason that ab-initio methods lend themselves well to the study of those chemical problems for which little experimental information is available, provided that their use is economically feasible.

One of the main theoretical strengths as well as economical difficulties of ab-initio calculations is the rigorous evaluation of all energy integrals, in particular two-electron repulsion integrals which are the most expensive to evaluate. The other feature of ab-initio calculations which makes them more accurate and more difficult is the ability to account for electron correlation. Because of

these technical problems, ab-initio calculations involving relatively large systems were extremely rare before the early seventies. With the advances in modern high speed electronic computing, however, theoreticians have become able to perform non-empirical calculations of ever increasing accuracy for real chemical problems of ever increasing complexity. Apart from the fact that it has improved the quality of the calculations, the inclusion of electron correlation has made possible the correct study of reactions, rearrangements, dissociations, and other chemically interesting processes where changes in electronic configuration during the process makes the use of single-determinant SCF calculations questionable.

* * * * *

The organic compounds known as carbenes are among the more interesting and less understood chemical species. The fact that they are frequently thought to be intermediates in important synthetic reactions, provides chemical justification for a desire to understand their properties. At the same time, their low-lying singlet and triplet excited states make them challenging as well as difficult objects of study, both theoretically and experimentally.

Another interesting and challenging category of organic compounds, is that containing strained-ring species.

Strained-ring molecules tend to break the ring to relieve the strain, thus providing many noteworthy reactions, intermediates and products.

Cyclopropylidene is the smallest carbene undergoing bond-fission due to ring-strain. Left alone, it will open up to give allene, a compound of great and varied synthetic usefulness (for a review of the synthetic value of allene see Brady (1980)):

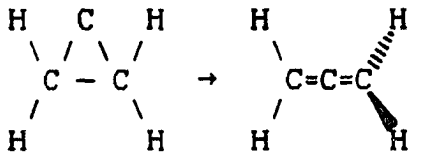

Cyclopropylidene Allene

Thus this reaction, contains all the ingredients mentioned above to make it especially challenging, and it has therefore long been of interest to chemists, both experimental and theoretical. Theoretical attempts have been made in the past to attack the problem, but the complexity of the project and the oversimplified approximations used has largely defeated these efforts.

In the present investigation, the problem is approached in a more accurate and complete fashion. In Chapter II, an account of past work is given. In Chapter III arguments are presented to justify the method to be used and the results of

a complete energy surface study of the reaction of the unsubstituted compound are also presented in that Chapter.

In Chapter IV, some theoretical implications of certain features of the surface calculated in Chapter III, are dicussed, analyzed and generalized.

In Chapter V, the geometries obtained during the calculations of Chapter III are used in conjunction with a greatly improved basis set to improve the quantitative accuracy of the work done in that Chapter.

Finally, in Chapter VI, an attempt is made to study the influence of substituents on the ring-opening of cyclopropylidene, and hence to explain some of the less well-understood experimental evidence about this reaction.

The resulting energy surface probably represents the most complete study ever done on any one reaction. The conclusions are instructive and, in some cases, unexpected. They explain in a satisfactory manner the observations which have been made by experimentalists. It is hoped that the approach taken here can be of use in future studies of other systems of chemical interest.

II. PREVIOUS WORK

A. Experimental Results

Allene is a well-known and stable compound, whose geometry, energy and other important data are well-documented. Lord and Venkatesvarlu (1952), Almenningen et al. (1959), Maki and Toth (1965) and Hegelund et al. (1977) all have reported experimental results for allene and a thorough review of these and other experimental and theoretical results is given by Runge (1980).

Cyclopropylidene, on the other hand, is a transient metastable species, which has never been isolated experimentally, at least in its unsubstituted form. What little experimental evidence exists on the stereospecificity of the reaction, seems to suggest that it can indeed be documented that the reaction is at least partially stereospecific. Thus Jones et al. (1963), Jones and Wilson (1965), Walbrick et al. (1968), and Jones and Walbrick (1969), all report obtaining more or less optically active allene when starting with optically active cyclopropylidene. It must be noted, however, that all their experiments are performed using heavily substituted species rather than the unsubstituted parent compound, and they do point out that, in all likelihood, the observed partial stereospecificity is due

to the bulk of the substituents rather than to any inherent electronic reasons. An exception to this is a more recent communication by Jones and Krause (1971), wherein certain experimental results are interpreted as providing evidence for electronic effects playing a role in the formation of one or the other of the possible stereoisomers. Specifically they point out that if cis-2-phenyl-3-p-methylphenylcyclopropylidene gives an allene which is partially optically active, then cis-2-p-bromophenyl-3-p-methylphenylcyclopropylidene should give a product which has either lower optical purity or a reversed configuration, due to the fact that bromine is larger that hydrogen. In actual fact however, an allene of higher optical activity and the same relative configuration is obtained, and this result is taken as an indication that effects other than those deriving from steric hindrance, i.e. electronic effects, contribute in determining the product. It should be pointed out, in passing, that part of these authors' arguments were based on a reaction mechanism which, even in the absence of the present work, is not today thought to be correct.

There is no experimental evidence whatsoever on the nature of the transition state. As to the activation energy barrier itself, Chapman (1974) points out that at temperatures as low as 77 K cyclopropylidene gives allene spontaneously, which would tend to indicate a quite low

barrier. Even though the experiment in question is inconclusive and there seems to be some doubt as to whether the true ground state of cyclopropylidene was indeed involved, the fact remains that the reaction always proceeds with ease and consequently the barrier cannot be high.

B. Theoretical Calculations

In view of the slim experimental evidence, there have been a number of attempts to explain theoretically what happens in the course of this reaction. Borden (1967) suggested that, for orbital symmetry reasons, the reaction should proceed via a monorotatory path, which means that only one CH_2 group rotates as the C-C-C angle opens. Bodor, Dewar and Maksic (1973), using the MINDO/2 semi-empirical model, concluded that the ring opens in a nonrotatory fashion (i.e. without rotation of the CH_2 groups) to yield planar D_{2h} allene, which then undergoes internal rotation to give the final D_{2d} product. They calculated the barrier height to be 13.7 kcal/mole and determined that the reaction is exothermic by less than 40 kcal/mole. The transition state (which would have C_{2v} symmetry like cyclopropylidene) was placed at a C-C-C opening angle of approximately 85^{o}. Dillon and Underwood (1977), in a Simplex-INDO semi-empirical calculation, found that the reaction starts out as disrotatory, reverses its

motion to give a nonrotated transition state, and thereafter continues to its conclusion via a conrotatory path. They placed the transition state at a C-C-C opening angle of 96°, estimated the barrier to be 72 kcal/mole and the overall exothermicity of the reaction about 25 kcal/mole. It should be noted, however, that their surface had no minimum corresponding to the cyclopropylidene geometry! Pasto, Haley and Chipman (1978), using ab-initio methods for the first time, concluded that the conversion involves three distinct processes: (a) initial disrotatory opening proceeding almost to the transition state; (b) a rapid transformation from the disrotatory structure to distorted monorotatory at an opening angle of between 90 and 100°; and (c) nonrotatory conversion of the 100° structure to allene. The transition state was estimated to lie between 90 and 94.5°, the activation energy was calculated to be about 18 kcal/mole, and the overall reaction exothermicity about 74 kcal/mole. Finally, Honjou, Pacansky and Yoshimine (1984), using very sophisticated calculation methods, arrived at a barrier of 10.2 kcal/mole and an overall reaction exothermicity 62.6 kcal/mole. However, they did not attempt to elucidate the reaction pathway nor did they identify the transition state.

III. THE UNSUBSTITUTED REACTION

A. Method of Calculation

1. The FORS model

Since semi-empirical methods depend heavily on parametrizations based on related experimental or reliable theoretical information, it would be more than risky to try to extract meaningful conclusions from anything but an unbiased ab-initio calculation for a reaction about which so little is known. Until the early seventies, ab-initio calculations were almost exclusively based on the Hartree-Fock SCF approximation. This single-determinant approximation has by now become standardized (see for example Roothaan (1951), Pople and Nesbet (1954), Schaefer (1977) and Carsky and Urban (1980) and references therein). Its main drawback is its failure to take electron correlation into account. Nonetheless it is still very useful for the calculation of molecular geometries that can be described in terms of a single electronic configuration (single determinant) wavefunction.

In view of the substantial computational savings, its use in the present problem could be justified if it could be shown that the reaction is dominated by a single configuration throughout. In fact such is not the case

however and, therefore, a wavefunction with the capacity to adapt to the changing dominant configurations is called for. There exist various types of such correlated wavefunctions, and among them perhaps one the most elegantly simple and easily interpretable is the FORS model.

The model of the Full Optimized Reaction Space (FORS) was first introduced by Ruedenberg and Sundberg (1976) and Cheung, Sundberg and Ruedenberg (1979), and further developed by Ruedenberg, Schmidt, Gilbert and Elbert (1982). It has been applied to a number of reactions by Dombek (1977), Feller (1979), Johnson and Schmidt (1981), Feller, Schmidt and Ruedenberg (1982), Schmidt (1982), Lam and Johnson (1983), Lam (1984), and Valtazanos and Ruedenberg (1985). The FORS model is unique in its attempt to combine consistently the concept of a full valence space with the principle of orbital optimization and to explore systematically the implication of such a framework. The concept has been generalized by Siegbahn et al. (1980), Roos et al. (1980), Roos (1980) and Siegbahn et al. (1981) to the "Complete Active Space Self-Consistent Field (CASSCF)" procedure, which has also proven to be very successful.

The FORS model describes the electronic structure of a molecule in terms of the best wavefunction that can be obtained by a superposition of <u>all</u> configurations that are generated by <u>all possible occupancies and couplings</u> from a

"formal minimal basis" of those valence orbitals on the constituent atoms which are actively involved in the reaction. These configurations span the "Full Reaction Space", and MCSCF optimization (see for example Ruedenberg, Cheung and Elbert (1979) or Yaffe and Goddard (1976)) of the orbitals in terms of an extended set of quantitative basis orbitals determines the "Full Optimized Reaction Space".

For the system at hand, Figure 3.1 represents a schematic picture of the orbitals of the reactant and the product. There are nine core orbitals, which we will label $|c_1\rangle \ldots |c_9\rangle$, namely three carbon 1s inner shells (not shown), two carbon-carbon sigma bond orbitals and four carbon-hydrogen bond orbitals, both of which are indicated by bond-lines. These core orbitals can be safely assumed to remain doubly occupied throughout the reaction. Then there are four reaction orbitals labeled $|1\rangle, |1'\rangle, |2\rangle$ and $|3\rangle$ and they are explicitly shown on Figure 3.1. They clearly change both in character and occupation as the reaction progresses from the reactant to the products. Thus for orbital $|1\rangle$ one has a change from σ^2 to π_x^1; for orbital $|1'\rangle$, from π^0 to π_y^1; for orbital $|2\rangle$, from σ^1 to π_x^1; and for orbital $|3\rangle$, from σ^1 to π_y^1, where the superscripts denote occupations. Since the whole reaction surface is to be studied, a single configuration Hartree-Fock SCF wavefunction would clearly be inappropriate in this case. The FORS wavefunction with 18

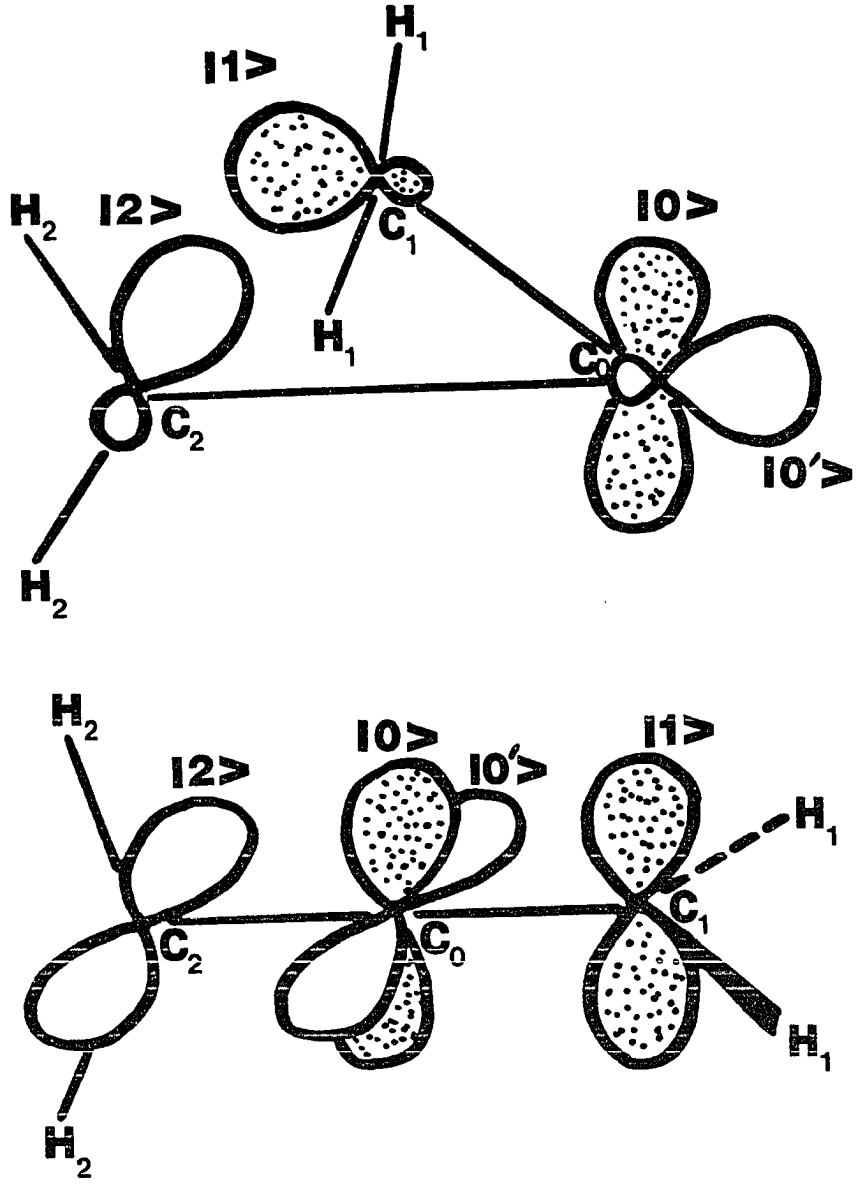

Figure 3.1. Reaction orbitals (denoted by $|0\rangle, |0'\rangle, |1\rangle$ and $|2\rangle$) of cyclopropylidene (top) and allene (bottom)

core electrons in the 9 core orbitals and 4 reactive electrons in the 4 reaction orbitals embodies all possible rearrangements among the four reactive orbitals and is therefore sufficiently flexible to account for the configuration changes that can be expected during the progress of the reaction. At the same time, it involves only 20 configurations and is sufficiently compact to permit the extensive calculations which are needed.

The molecular FORS wavefunction is thus a superposition of 20 configurations

$$\Psi^{SM} = \Sigma_{Kt} C_{Kt} \Phi^{SM}_{Kt}$$

where each configuration Φ^{SM}_{Kt} is a normalized spin-adapted antisymmetrized product (SAAP) of CGOs (configuration generating orbitals, i.e. all MOs which are occupied in any of the configurations of the wavefunction). A SAAP is an N electron wavefunction of the form

$$\Phi^{SM}_{Kt}(\text{space},\text{spin}) = N_K A\{U_K(\text{space})\theta^{SM}_t(\text{spin})\}$$

where θ^{SM}_t is a spin eigenfunction, S and M being the eigenvalues of S^2 and S_z; U_K is a product of CGOs; $A = (N!)^{-1/2}\Sigma_p(-1)^p P$ is the conventional antisymmetrizer, and $N_K = 2^{-\pi(K)/2}$ with $\pi(K)$ being the number of doubly occupied

CGOs in U_K. Properties of SAAPs are described by Ruedenberg (1971), Salmon, Cheung and Ruedenberg (1972), and Ruedenberg and Poshusta (1972).

The ground states of both cyclopropylidene and allene are singlets. There was some controversy on this point as regards cyclopropylidene. While Dillon and Underwood (1977) found singlet cyclopropylidene to be lower than the triplet, Pasto et al. (1978) claimed that the triplet is the true ground state. More recent calculations by Stierman and Johnson (1985), Honjou, Pacansky and Yoshimine (1985) plus minimal and extended basis set geometry optimizations performed in the present work, have however confirmed beyond any reasonable doubt that the singlet is indeed considerably lower in energy. Assuming only C_1 symmetry throughout, the full singlet configuration space generated by the four reaction orbitals is spanned by the 20 SAAPs which can be characterized as follows:

$$|i^2j^2\rangle = 2^{-1}A\{Core|i\rangle^2|j\rangle^2\theta_0\} \quad : \quad 6 \text{ SAAPs}$$

$$|i^2jk\rangle = 2^{-1/2}A\{Core|i\rangle^2|j\rangle|k\rangle\theta_0\} \quad : \quad 12 \text{ SAAPs}$$

$$|11'23S\rangle = A\{Core|1\rangle|1'\rangle|2\rangle|3\rangle\theta_0\} \quad : \quad 1 \text{ SAAP}$$

$$|11'23T\rangle = A\{Core|1\rangle|1'\rangle|2\rangle|3\rangle\theta_1\} \quad : \quad 1 \text{ SAAP}$$

where:

A = antisymmetrizer

i,j,k = all possible choices of 1,1',2,3

$\theta_0 = (\alpha\beta-\beta\alpha)(\alpha\beta-\beta\alpha)/2$, singlet coupling

$\theta_1 = \{\alpha\alpha\beta\beta+\beta\beta\alpha\alpha-(\alpha\beta+\beta\alpha)(\alpha\beta+\beta\alpha)/2\}/\sqrt{3}$, triplet coupling

Core = $c_1^2c_2^2\ldots c_9^2(\alpha\beta-\beta\alpha)^9/2^{9/2}$

2. Atomic orbital basis sets

There remains the question of the basis set to be used for this study. In this context it must be born in mind that the surface to be determined requires tens of thousands energy calculations, all of the multi-configuration FORS-MCSCF type. Questions of feasibility cannot, therefore, be taken lightly. It was therefore decided at first to get good geometries and on this basis, later to improve the energetics of the reaction. The STO-3G minimal basis set developed by Hehre, Stewart and Pople (1968, 1969), Hehre, Ditchfield, Stewart and Pople (1970) and Stewart (1970) is an obviously useful choice for the first step since it is very economical and, at the same time, has been proven to give reliable geometries, especially for hydrocarbons (see for example Carsky and Urban (1980) and Dykstra and Schaefer (1980)). The shortcomings of this basis set in terms of reliable energies will subsequently be remedied through use of the extended basis set described in Chapter VI.

3. Reduction of internal coordinates

Since C_3H_4 has 7 atoms, its geometry is fully characterized by 21 Cartesian coordinates. They can be reduced to 15 internal coordinates, by taking out the 6 coordinates corresponding to translation and free rotation of the molecule. This means that the full reaction surface must be imagined as a 15 dimensional surface in a 16 dimensional space, namely the energy as a function of 15 independent variables. This poses certain problems, both because of the staggering magnitude of the task of calculating properly a surface in a 15 dimensional parameter space, and because of the difficulty of interpreting such a surface, assuming one could calculate it. It is therefore imperative to reduce the dimensions of the surface in such a manner that (i) the calculation becomes feasible, (ii) it can be meaningfully interpreted, (iii) it includes all meaningful features of the reaction and gives an accurate description of what is happening.

Figure 3.2 shows the 15 internal coordinates that we chose to describe the geometry of the molecule. They are: 6 bond lengths (2 C-C bond lengths and 4 C-H bond lengths), 5 valence angle bends (the 4 C-C-H angles and the C-C-C ring-opening angle Φ), 2 out-of-plane bends (the angle between each C-C bond and the corresponding CH_2 plane), and 2 dihedral angles (the angles between the C-C-C plane and each

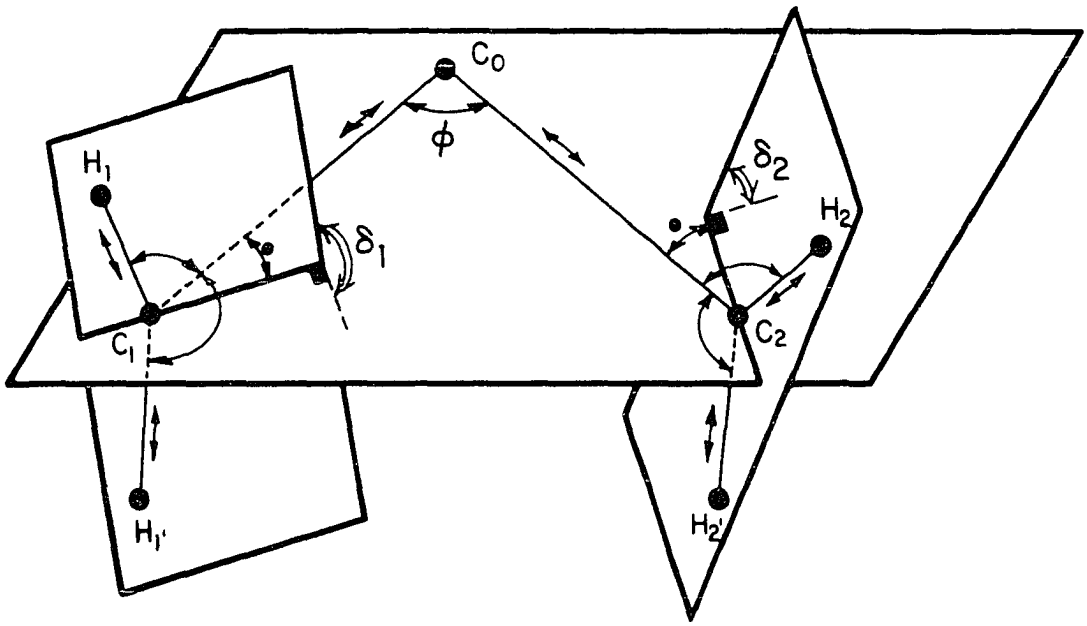

Figure 3.2. Internal coordinates of C_3H_4. Φ, δ_1 and δ_2 are chosen as reaction coordinates

of the two CH_2 planes) which we shall call δ_1 and δ_2. Of these 15 coordinates, the angles Φ, δ_1 and δ_2 are the most interesting ones for the reaction, because Φ shows the extent of the ring-opening whereas δ_1 and δ_2 describe the rotations of the hydrogens during this ring-opening. We would expect the other twelve internal coordinates to change much less during the course of the reaction. We therefore choose (Φ,δ_1,δ_2) as "reaction coordinates", i.e. we will follow the reaction explicitly in terms of these three variables. The other twelve coordinates will not be ignored, however. For each (Φ,δ_1,δ_2) triple, the geometry will be completely optimized with respect to the remaining twelve variables.

Probably the most efficient means of optimizing geometries is the gradient method developed by McIver and Komornicki (1971) and implemented as a computer algorithm by Dupuis and King (1978). It uses the energy gradient with respect to the geometric coordinates as a guide to the steepest descent path towards the energy minimum (optimum geometry). Dupuis, Spangler and Wendoloski (1980) incorporated this method into the GAMESS (General Atomic and Molecular Electronic Structure System) MCSCF computer program. This program was heavily modified by M. W. Schmidt of North Dakota State University and S. T. Elbert of the Ames Laboratory, USDOE, Iowa State University. It incorporates for example Schlegel's (1982) geometry optimization and

saddle point location algorithm. Furthermore, the formalism of a new internal coordinate, namely the dihedral angle between two planes having only one point in common, was developed by K. Ruedenberg in analogy to the standard internal coordinates (such as given for example by Wilson, Decius and Cross (1955)), and implemented by S. T. Elbert.

The geometry optimization with respect to twelve internal coordinates means that for every set of values for the opening angle Φ and the hydrogen plane twisting dihedral angles δ_1 and δ_2, the molecular energy is minimized with regard to all other nuclear parameters. Thereby these 12 internal coordinates become functions of Φ, δ_1, δ_2 and thus the energy surface itself becomes a function of these three internal reaction coordinates. Its form can be visualized in terms of contour surfaces $E(\Phi,\delta_1,\delta_2)$=constant which are two-dimensional surfaces in the three-dimensional parameter space spanned by Φ, δ_1, δ_2. For a graphical representation, it is expedient to display the intersections of these surfaces E=constant with various planes Φ=constant. The resulting contour lines $E(\delta_1,\delta_2,\Phi_0)$=constant, for a fixed value $\Phi=\Phi_0$=constant, exhibit the dependence of the energy upon the dihedral rotation angles δ_1, δ_2 for a given value of the CCC opening angle Φ. The entire energy surface is thus covered by a sequence of such panels corresponding to various values of Φ. The nature of the reaction surface turns out to be

such that an adequate description of its pertinent features is obtained by examining about 20 panels corresponding to the following values of the ring opening angle:

$$\Phi=50(10)70(5)80(2)82(1)88(2)90(5)100(20)180$$

where the numbers in parentheses indicate step sizes (e.g. 90(5)100 means: 90,95,100).

Since δ_1 and δ_2 both can vary from -180° to 180°, it still seems at first sight as if an enormous number of (δ_1,δ_2) points are needed for each panel. However, since the energy is optimized with respect to the remaining 12 coordinates, it is readily seen that, for a given value of Φ, the energy is unchanged

(i) when the CH_2 planes are rotated by 180°,

(ii) when the molecule is reflected by the CCC plane,

(iii) when the left and right parts of the molecule are interchanged.

This means that the contours in a plane Φ=constant are invariant under the following operations:

(i) translation by 180° in the δ_1 direction

(ii) translation by 180° in the δ_2 direction

(iii) inversion, i.e. replacing (δ_1,δ_2) by $(-\delta_1,-\delta_2)$

(iv) exchanging the values of δ_1 and δ_2, i.e. reflection by the line $\delta_1=\delta_2$.

It follows that the energy has the same value for all points indicated by cross marks on the sample panel displayed

in Figure 3.3 which implies that the contour map of each panel Φ=constant possesses the two-dimensional lattice symmetry illustrated in the same figure. Consequently, it is only necessary to calculate energies for points in a region equivalent to the shaded area in the figure, which is 1/16 of the entire panel.

It turns out that around fifty points are required in this primitive area in order to obtain good isoenergetic curves. They were taken to be the points given by the values

$$\delta_1 = 20n_1 + 10n_2 \ , \ \delta_2 = 10n_2$$

with

$$n_1 = 0,1,2...(9-n_2) \ , \ n_2 = 0,1,2...9$$

From these 55 energy values, those for the 880 equivalent points on the panel shown in Figure 3.3 were generated and these were used to draw energy contours by using an interpolation procedure.

As mentioned before, each of the 55 points involves a minimization with respect to the other 12 internal coordinates. This gradient procedure requires on the average about a dozen evaluations of the molecular energy for a given set of the 15 internal coordinates. The determination of the

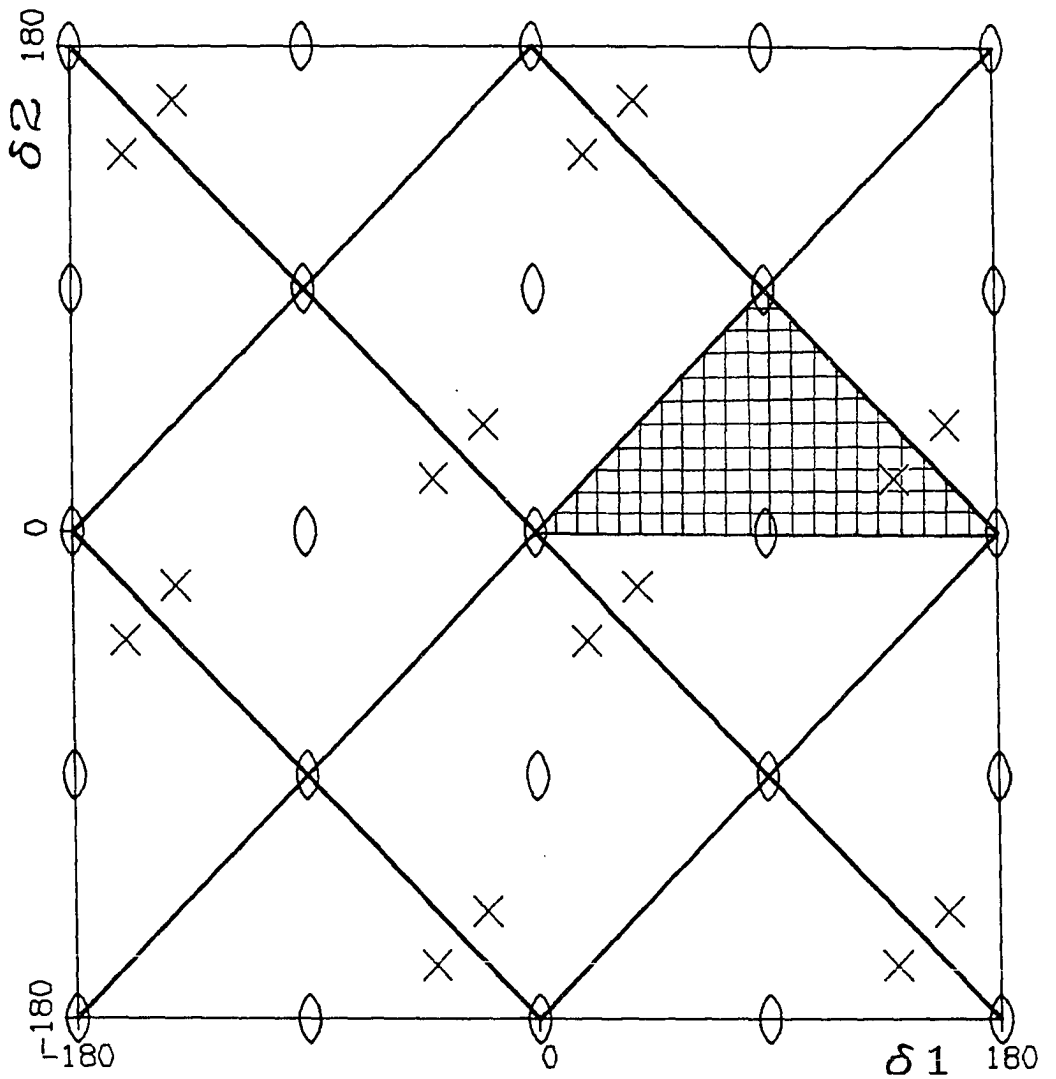

Figure 3.3. Lattice symmetry of energy surface for a panel Φ=constant. Crosses indicate equivalent points. Heavy diagonal lines indicate reflection planes. Oval symbols denote digonal axes. Shaded area shows a primitive region

entire energy surface therefore involved approximately

19(panels) x 55(points/panel) x 12(energies/point) = 12500

evaluations of the molecular energy. Every such energy evaluation is a multiconfiguration-self-consistent-field calculation involving 20 configurations based on 9 inactive and 4 active molecular orbitals.

B. Reaction Surface Obtained from the STO-3G Basis

1. Variation of the energy along the "Reaction Path"

For the reaction at hand, it appears natural to consider the opening angle Φ as the "reaction coordinate". While it is not the "intrinsic" reaction coordinate, we shall verify later on that it is not an unreasonable approximation to it. The calculation outlined in the preceding section therefore yields a series of contour panels depicting the energy as a function of δ_1 and δ_2 for various values of this reaction coordinate. Choosing the minimum energy on each of these panels we then obtain the plot of the optimal energy as a function of the reaction coordinate Φ.

This plot is exhibited in Figure 3.4. It begins with $\Phi=50^{\circ}$ in order to show that cyclopropylidene, corresponding to $\Phi=59.5^{\circ}$, is indeed a (meta)stable species. The plot

Figure 3.4. Reaction energy as a function of the ring-opening angle Φ. Notice the minima for cyclopropylidene and allene. The shadings shown here provide a key for those used in all subsequent panels for Φ=constant. Areas with higher energy than those shown here will be left unshaded

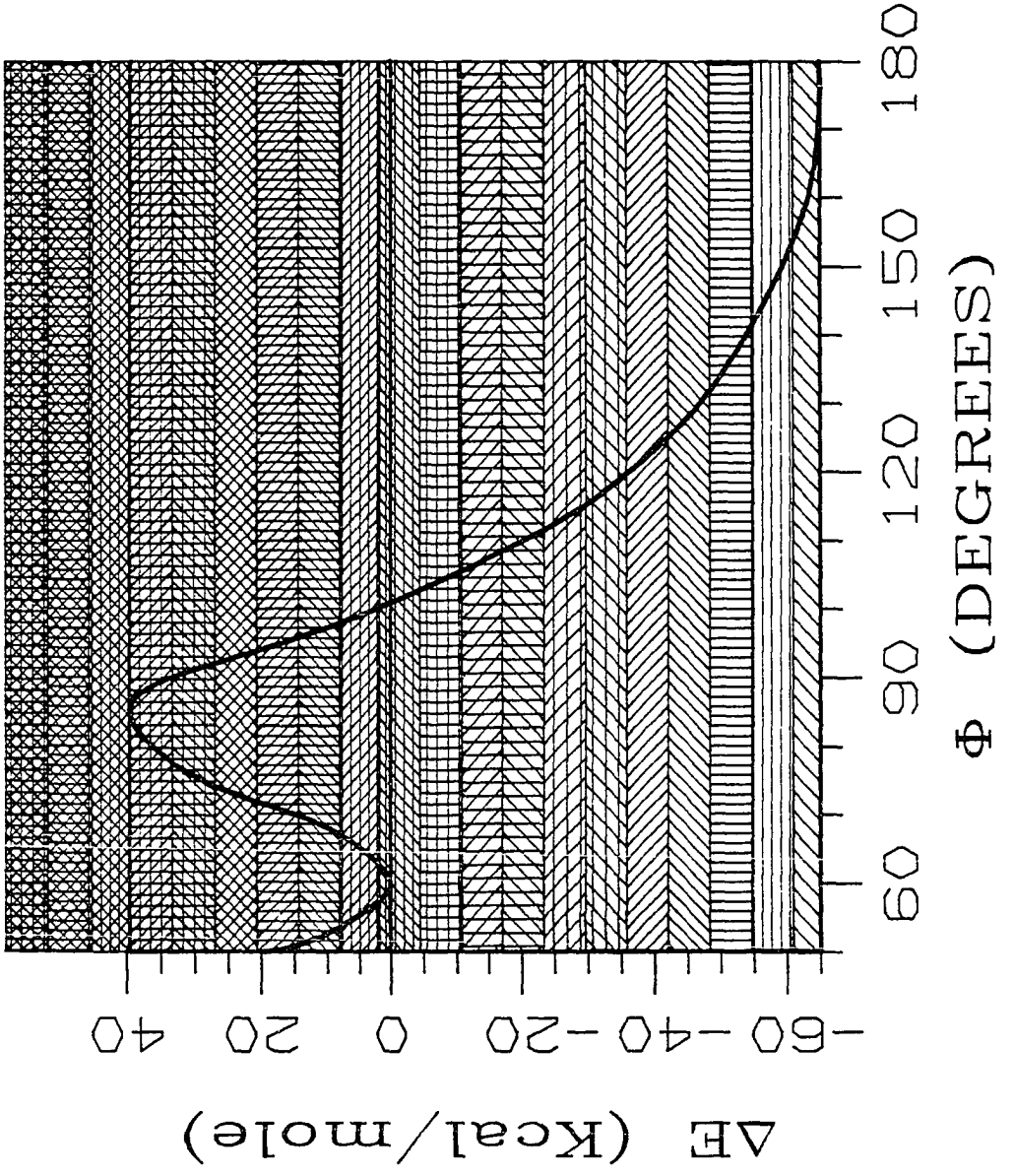
ΔE (Kcal/mole)
-60 -40 -20 0 20 40
60 90 120 150 180
Φ (DEGREES)

furthermore shows that the transition state occurs for $\Phi=84.2^{o}$ with an activation energy of 40 kcal/mole for the STO-3G basis. Deployment of the extended basis further on will yield a considerably lower barrier.

Figure 3.4 also illustrates a shading scheme which identifies the various energy ranges. The shading changes every 10 millihartree (~6 kcal/mole). This shading scheme will be adhered to throughout the rest of this presentation. On all subsequent contour maps contours will be drawn at 10 millihartree increments, corresponding to the horizontal lines on Figure 3.4, and the areas between the contours will be filled by the same shadings as those in Figure 3.4. In this manner it will be straightforward to compare energies on different contour maps. Figure 3.4 therefore provides the key for identifying the energies on all those maps. In some of these there occur areas with energies higher than any of those occurring in Figure 3.4. Such areas will be left blank between contours.

2. Reaction energy as a function of (δ_1,δ_2) for various values of Φ

The energy contours $E(\delta_1,\delta_2)$=constant for the various values of the reaction coordinate Φ are displayed in Figures 3.5.1 to 3.5.19. A sequential examination of these maps will disclose a number of interesting aspects of the reaction.

a. Cyclopropylidene (Fig. 3.5.1) The starting compound was found to have a Φ angle of 59.5^{o} by means of a geometry optimization involving all 15 internal coordinates. It exhibits very pronounced minima (m) for the four equivalent positions $(\delta_1=90^{o},\delta_2=90^{o})$, $(\delta_1=90^{o},\delta_2=-90^{o})$, $(\delta_1=-90^{o},\delta_2=-90^{o})$, $(\delta_1=-90^{o},\delta_2=90^{o})$. Since for the unsubstituted compound there is no difference between the four we shall, for reasons of simplicity, follow only the reaction of the species which is situated at $(\delta_1=90^{o},\delta_2=90^{o})$. This (like the other three) clearly corresponds to the two CH_2 planes being exactly perpendicular to the C-C-C plane, as one might expect. As one would also expect, the maximum (M) on this panel occurs for $(\delta_1=0^{o},\delta_2=0^{o})$, corresponding to the two CH_2 planes lying flat in the C-C-C plane, causing maximal steric hindrance of the hydrogens.

b. $\Phi=50^{o}$ (Fig. 3.5.2) This panel was calculated purely as an aid to interpolation beyond the cyclopropylidene minimum. It is highly unlikely that the molecule would ever find itself there. Its basic characteristics are the same as for the Cyclopropylidene panel, except that all energies are considerably higher. The minimum is about 30 millihartree higher.

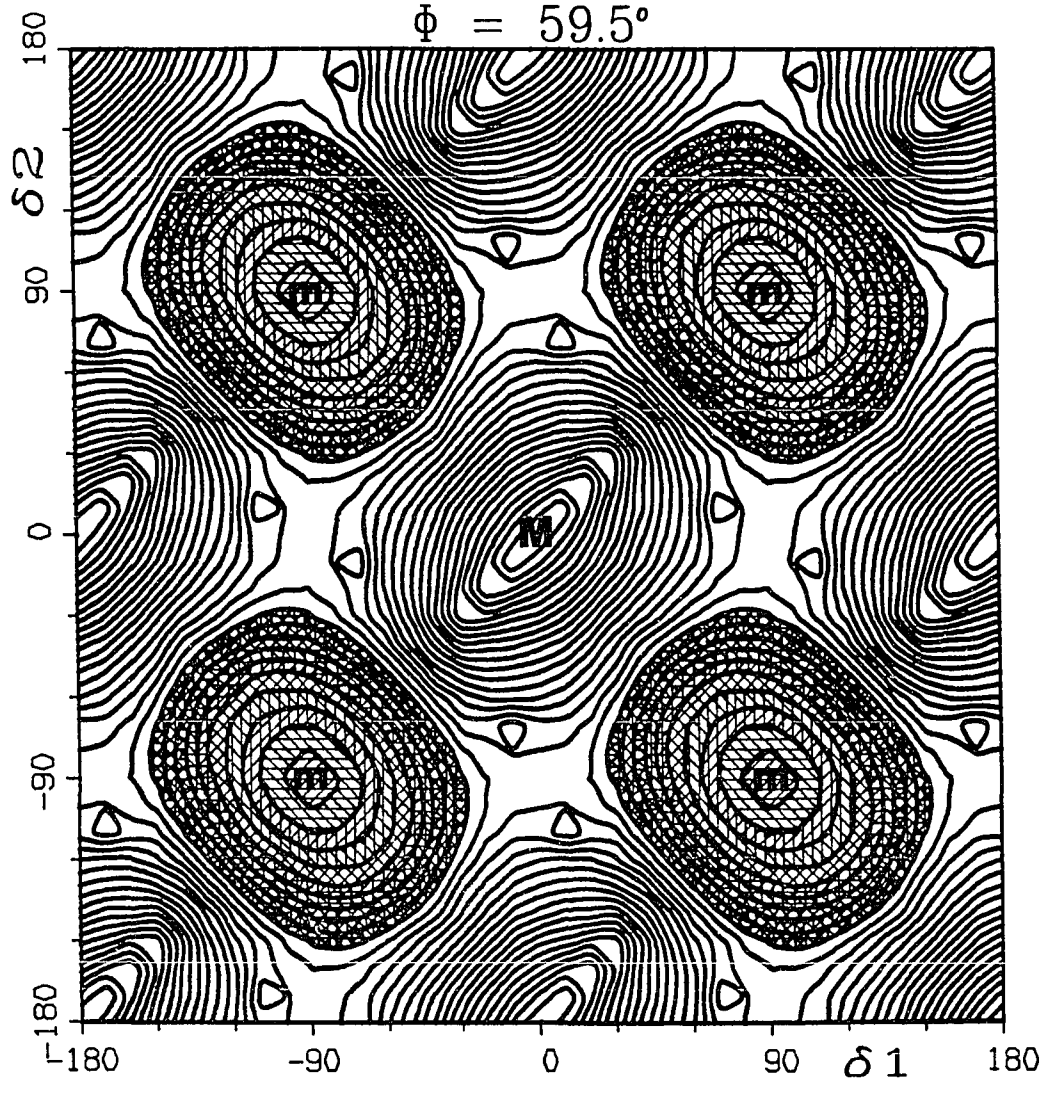

Figure 3.5.1. Energy surface over dihedral angle (δ_1 and δ_2) plane for Φ=59.5^{o} (cyclopropylidene). Note the four minima (m) and the maximum (M). Only the minimum situated at (δ_1=90^{o},δ_2=90^{o}) will be followed in the sequel, for reasons of simplicity

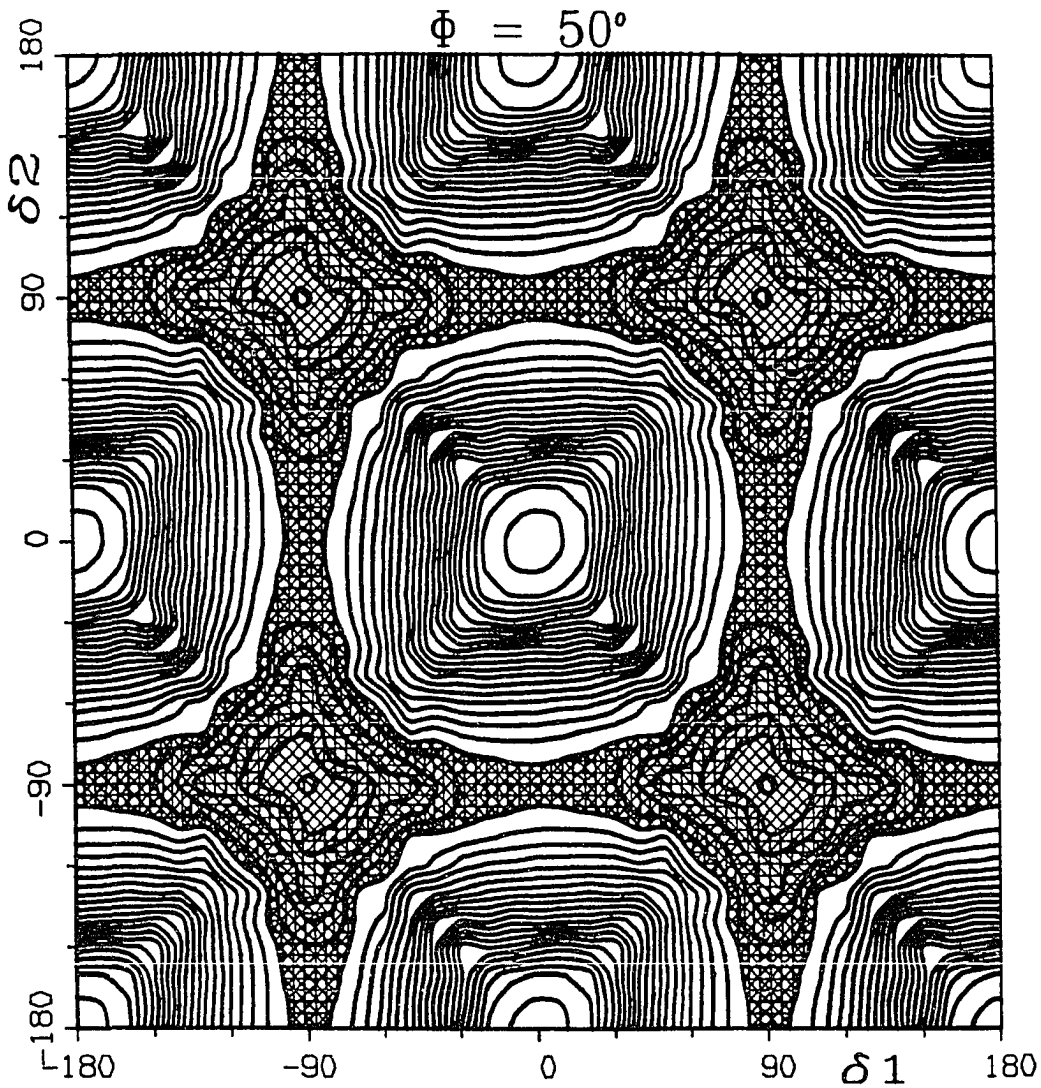

Figure 3.5.2. Energy surface over dihedral angle plane for $\Phi=50^{\circ}$. This panel has the same characteristics as cyclopropylidene, except that all energies are higher

c. $\Phi=70^{o}$ (Fig. 3.5.3) The minimum (m) is still located at ($\delta_1=90^{o},\delta_2=90^{o}$). Its energy has now increased, however, by about 20-30 millihartree. Moreover the area around the minimum is elongated, giving the CH_2 planes a greater ease for rotational motion. It should be noted here that the direction of the elongation of the minimum valley along the line $\delta_1+\delta_2=180^{o}$ is the disrotatory direction (see Figure 3.3), with the direction perpendicular to it, i.e $\delta_1-\delta_2$=constant, being the conrotatory one. Finally, it can be observed that the maximum is no longer at ($\delta_1=0^{o},\delta_2=0^{o}$). In fact, the maximum has now separated in two (M_1 and M_3) along the conrotatory path and a saddle point has developed at ($\delta_1=0^{o},\delta_2=0^{o}$).

d. $\Phi=75^{o}$ (Fig. 3.5.4) There is little qualitative difference between this panel and 70^{o}. One should note however the flattening out of the surface as a whole, i.e. there is now much less variation in energy between the various parts over the entire panel. Related to this is the increased elongation of the minimum area (m). In addition, the two maxima (M_1 and M_3) have moved farther apart (in fact the minimum valley is now sandwiched between two maxima (M_1 and M_2)). The saddle point at the origin has split into two and a new maximum is rising up at ($\delta_1=0^{o},\delta_2=0^{o}$).

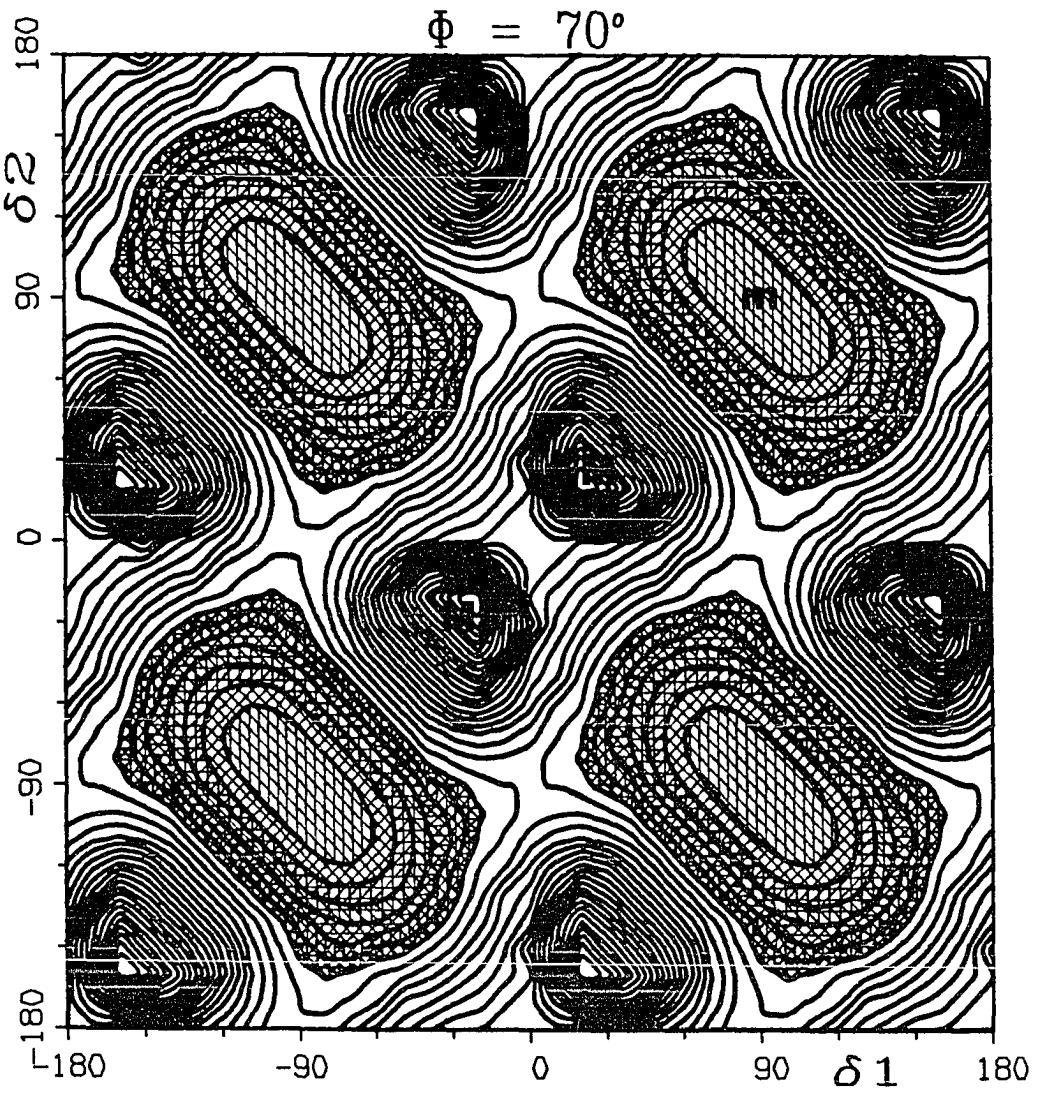

Figure 3.5.3. Energy surface over dihedral angle plane for $\Phi=70^{O}$. The minimum (m) is still at ($\delta_1=90^{O}$,$\delta_2=90^{O}$), but the area around it has elongated in the disrotatory direction. The maximum has separated in two (M_1 and M_2) along the conrotatory direction

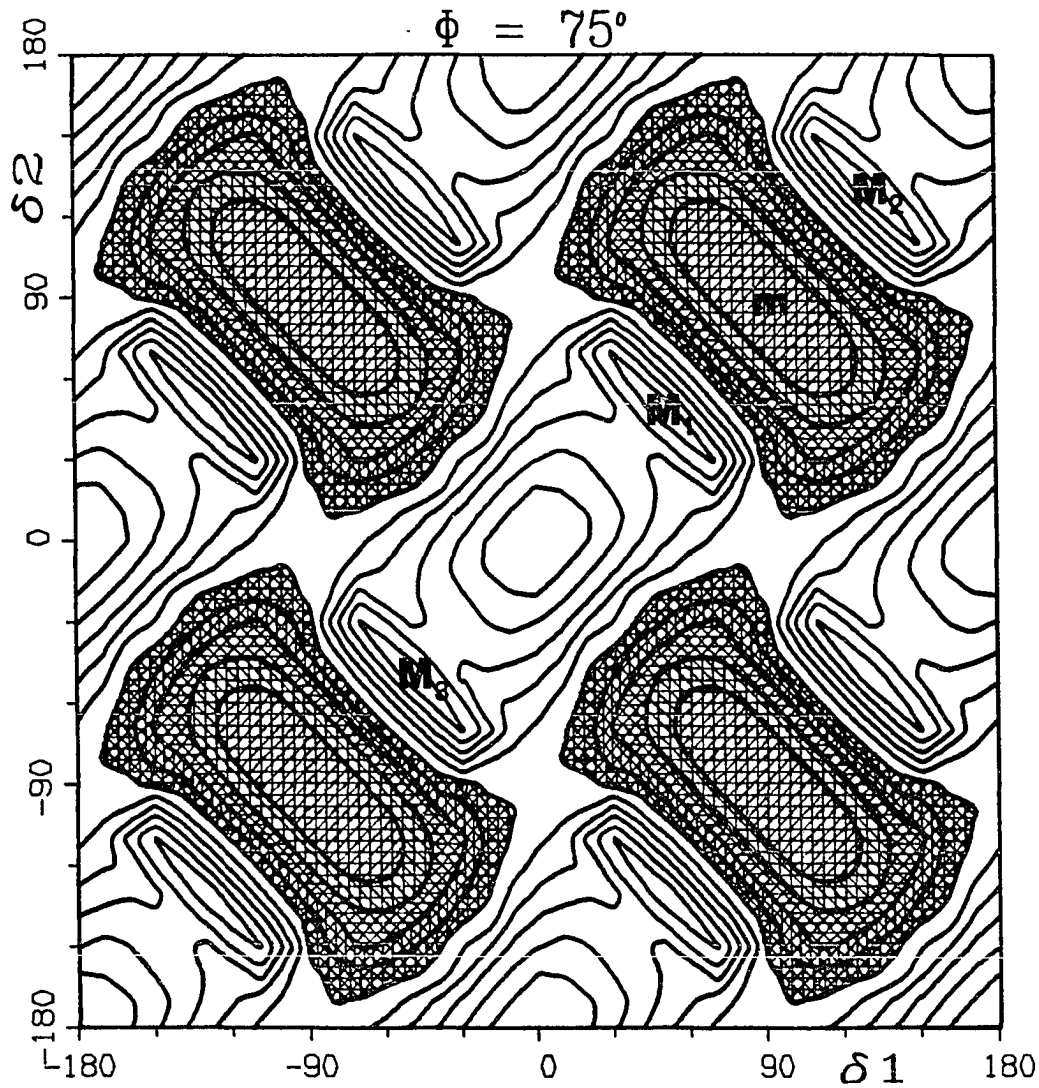

Figure 3.5.4 Energy surface over dihedral angle plane for $\Phi=75^{o}$. There is increased elongation around the minimum (m) and the surface has flattened out overall. The two maxima (M_1 and M_3) have moved farther apart, and the minimum valley is sandwiched between two maxima (M_1 and M_2). Note the reappearance of the maximum (M) at ($\delta_1=0^{o}, \delta_2=0^{o}$)

e. $\Phi=80^{o}$ (Fig. 3.5.5) The essential difference from the previous panels is that the minimum has now separated in two (m_1 and m_2), almost as if the two maxima (M_1 and M_2) had squeezed the minimum valley on either side, breaking it up. This split in two minima implies a disrotatory motion of the CH_2 planes as the Φ angle opens and the molecule moves up towards the transition state. We are, in effect, seeing the first bifurcation in the reaction path, corresponding to two equivalent motions: Either the top two hydrogens come closer together and the two bottom ones move farther apart or vice versa. Again for reasons of simplicity, we shall limit our discussion to only one of the two cases, namely the path moving to the right (m_1). Once more it should be noted that the absolute value of the minimum has gone up.

f. $\Phi=82^{o}$ (Fig. 3.5.6) This panel is a clear evolution from the previous one. The barrier between the minima on the same disrotatory $\delta_1+\delta_2$=constant (m_1 and m_2) has increased, while the barrier between minima on the conrotatory line $\delta_1+\delta_2$=constant (m_1 and m_3) has decreased. The maxima (M_1 and M_2) converging on the ($\delta_1=90^{o},\delta_2=90^{o}$) point along the conrotatory line are getting closer together (and farther from the ($\delta_1=0^{o},\delta_2=0^{o}$) point (M) from which they originally sprang).

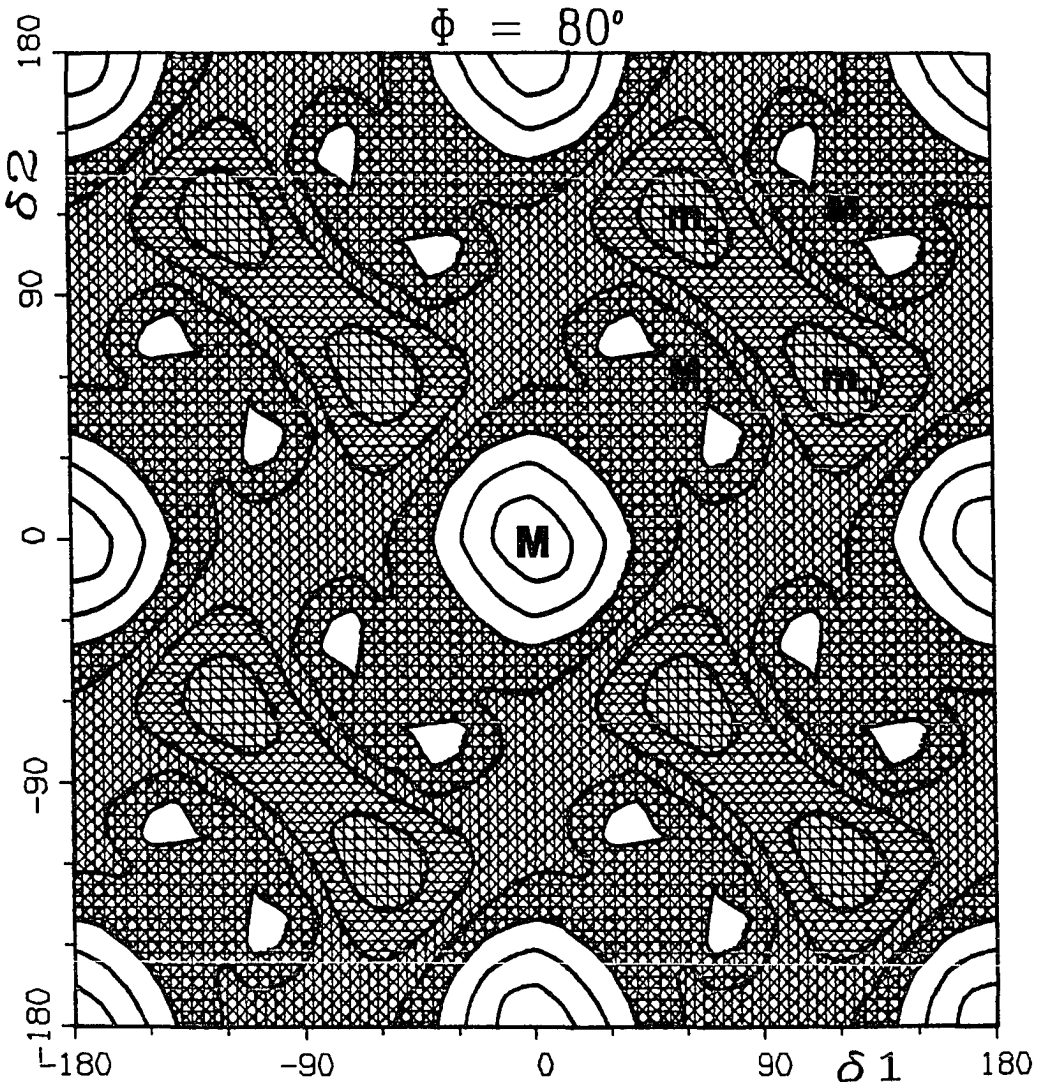

Figure 3.5.5. Energy surface over dihedral angle plane for $\Phi=80^{o}$. Note the separation of the minimum into two (m_1 and m_2) along the disrotatory path. For simplicity we will, henceforth, follow only the minimum (m_1)

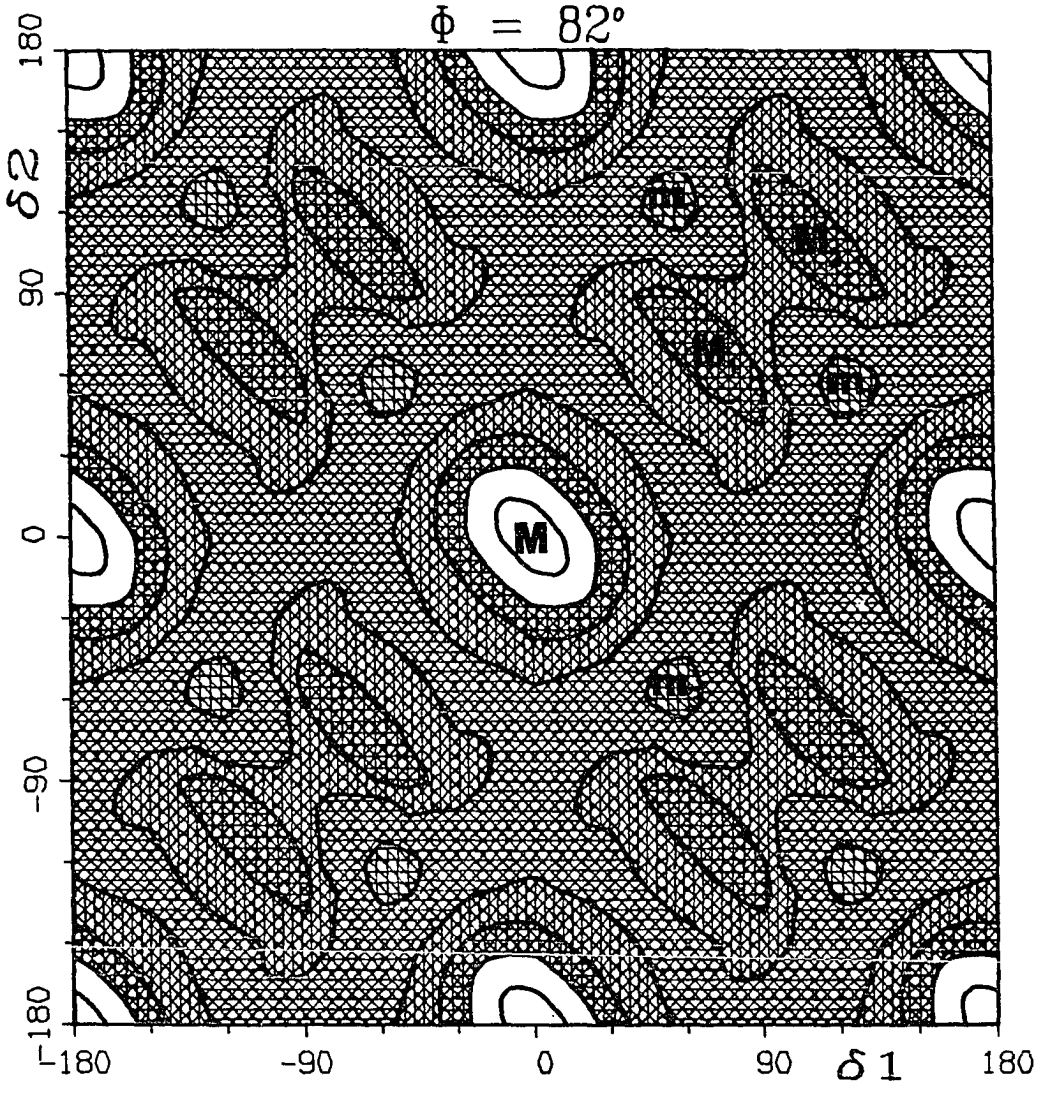

Figure 3.5.6. Energy surface over dihedral angle plane for $\Phi=82^{o}$. The two minima (m_1 and m_2) have moved farther apart on the disrotatory path

g. $\Phi=83^{o}$ (Fig. 3.5.7) Except for the fact that the minimum (m_1) has moved further along the disrotatory motion path, the important feature to notice is the appearance of a new minimum (m) at around ($\delta_1=90^{o},\delta_2=0^{o}$). A little reflection will show that this second minimum is the one corresponding to the relative positions which the two CH_2 planes have in Allene. An energy barrier, denoted as the saddle point S, separates the two minima (m_1 and m_2). The new minimum is slightly higher in energy. This is not easily apparent on the figure, but the calculation shows an energy difference of about 6 kcal/mole between the m_1 and m_2. The minimum energy position (m_1) where the molecule is situated has again gone up in energy.

h. $\Phi=84^{o}$ (Fig. 3.5.8) This panel is similar to the one for $\Phi=83^{o}$, except that the new minimum (m) at ($\delta_1=90^{o},\delta_2=0^{o}$) is now lower in energy than the original one (m_1) on the line $\delta_1+\delta_2=180^{o}$. There still exists a saddle point (S) between the two minima however. In the quasistatic reaction path picture of the reaction, the system would therefore continue to reside at the original minimum m_1.

Of particular interest is the fact that the new minimum (m) is extremely shallow in the disrotatory direction. It is really a low-lying valley along the line $\delta_1+\delta_2=90^{o}$. A motion along this line corresponds to the following disrotatory

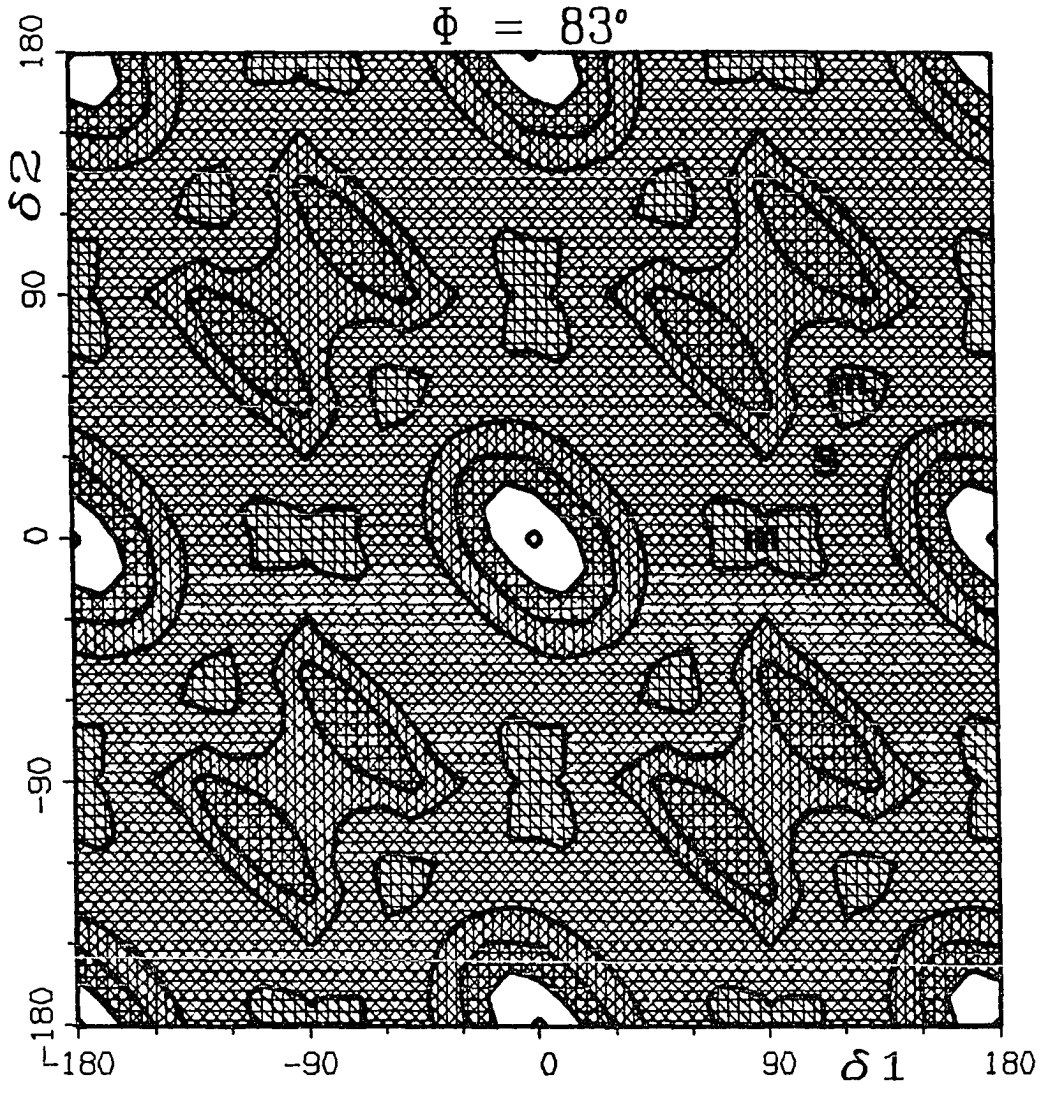

Figure 3.5.7. Energy surface over dihedral angle plane for $\Phi=83^{o}$. Notice the appearance of a second minimum (m) at ($\delta_1=90^{o},\delta_2=0^{o}$). The original minimum (m_1) is lower in energy

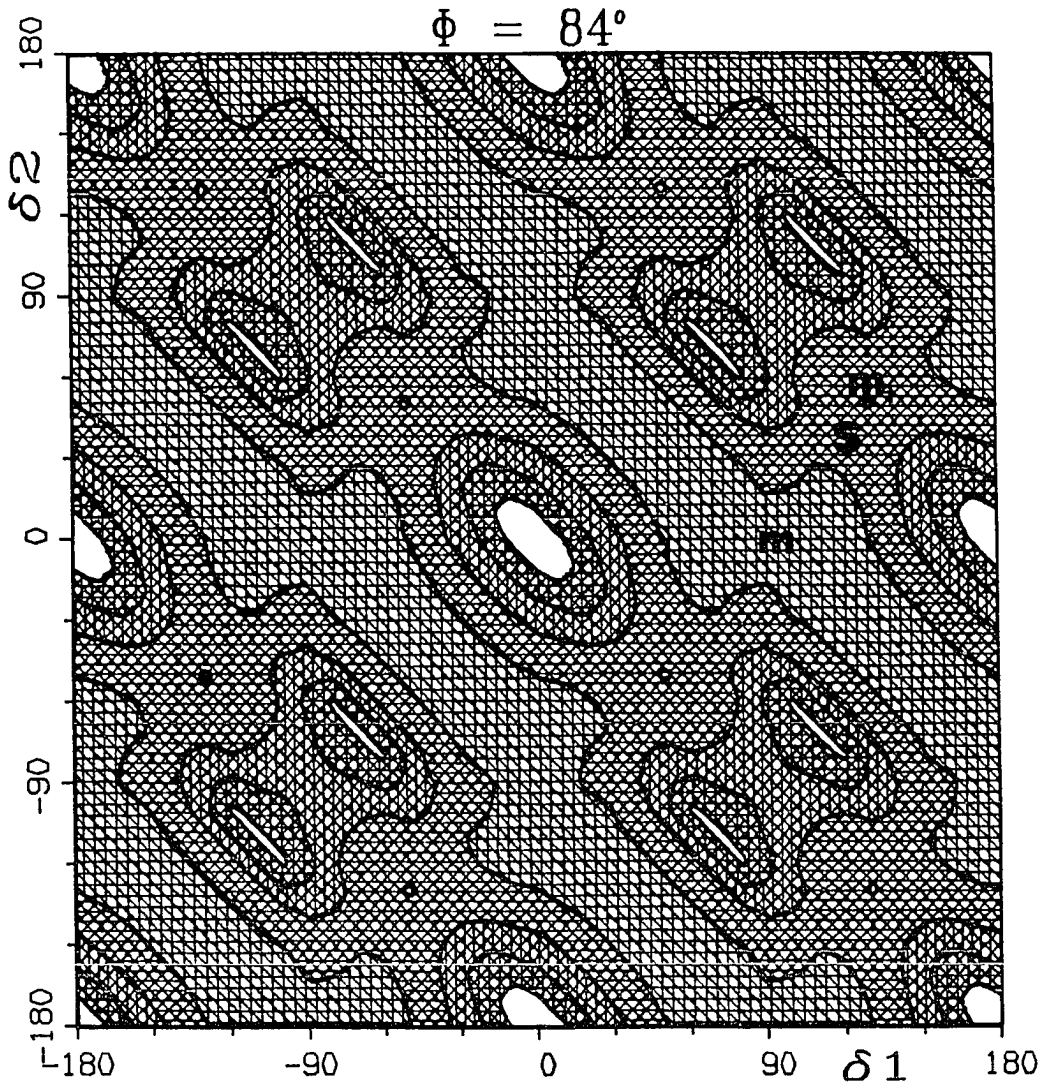

Figure 3.5.8. Energy surface over dihedral angle plane for $\Phi=84^{\circ}$. The new minimum (m) has turned into a valley which is lower in energy than the original minimum (m_1). It is still separated by a saddle point (S) from the original minimum (m_1)

synchronized rotation of the two CH_2 planes:

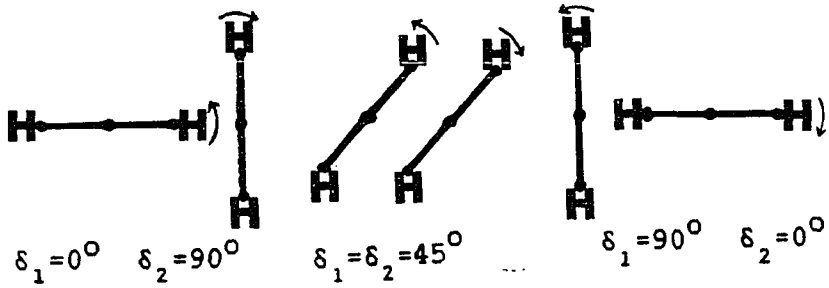

For $\Phi=84^{\circ}$ there clearly exists very little resistance against such a cogwheel-like, chirality preserving rotation.

i. $\Phi=85^{\circ}$ (Fig. 3.5.9) There is no longer a minimum on the line $\delta_1+\delta_2=180^{\circ}$. Instead the minimum m_1 of the preceding panel has now turned into a saddle point (S). In fact, this saddle point has come about through the merging of the saddle points which, in the preceding panel, were located on either side of what used to be the minimum m_1. The molecule is now free to slide down to the new minimum.

At this stage it must be noted that there are in fact two valleys on Figure 3.5.9, one on each side of the saddle S. They are labeled m_1 and m_2 respectively and correspond to two sets of geometries which are each others' stereoisomeric chiral images. It is evident that the system can descend from the saddle point (S) in either direction and we therefore have a second bifurcation on the reaction path. It is furthermore apparent that this bifurcation as well as the

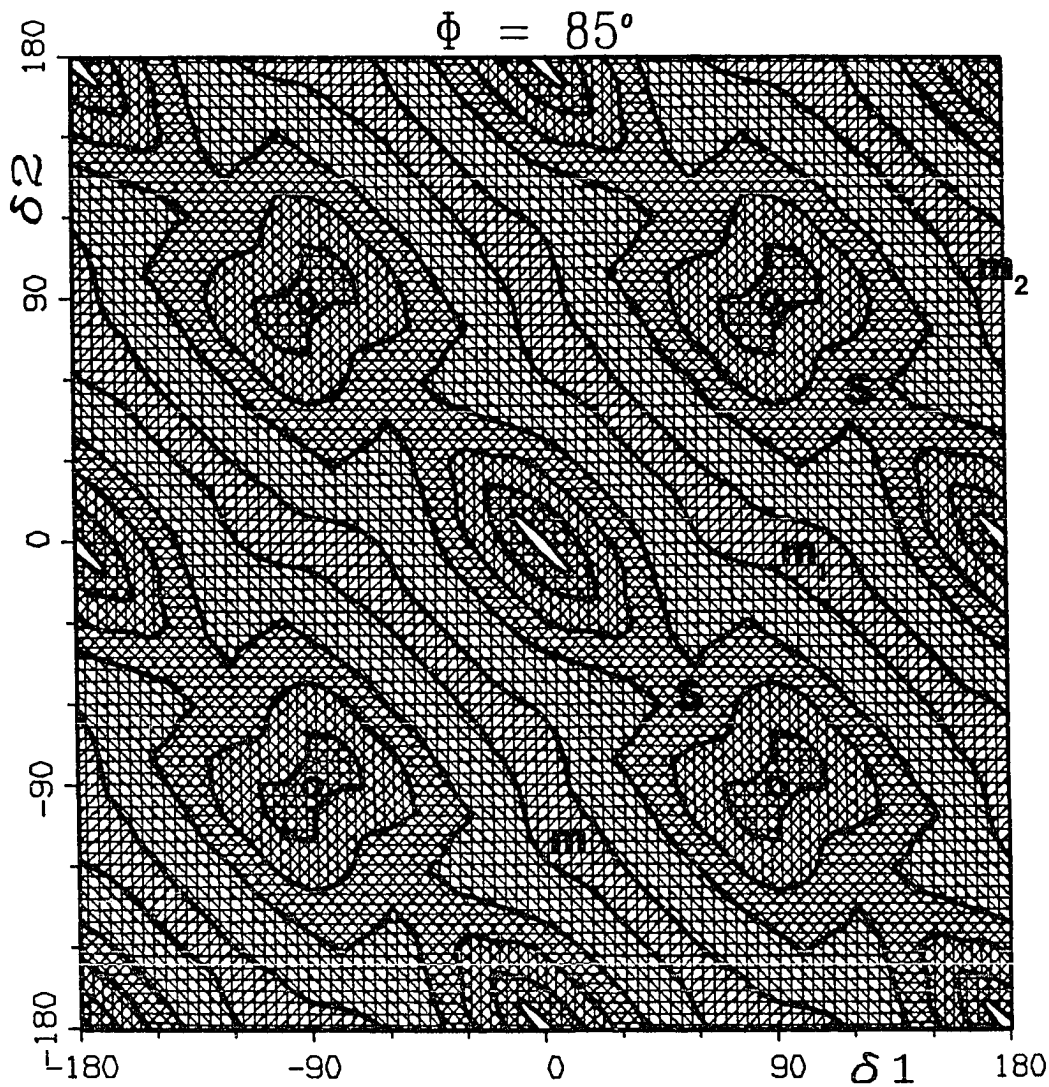

Figure 3.5.9. Energy surface over dihedral angle plane for $\Phi=85^{o}$. The original minimum is now a saddle point (S), and the molecule is free to move down to either of two valleys (m_1 or m_2), which stereoisomeric. This panel is just past the bifurcating transition region. Note that the two maxima (M_1 and M_2) have almost merged into one

highest point on the reaction path, i.e. the transition state, both occur between $\Phi=84^{o}$ and 85^{o}.

Because of the symmetry of the reaction surface there clearly exists no preference for the valley m_1 or the valley m_2, when the system descends from the transition state. Both stereoisomeric products will therefore occur with equal probability, i.e. the reaction would not be stereospecific if one could distinguish the four hydrogens. From this we infer that the ring-opening of the appropriately deuterium-substituted cyclopropylidene would presumably not be stereospecific (aside from a possible small dynamic stereospecificity due to the different masses of H and D in the kinetic energy tensor). We infer furthermore that in other substituted cyclopropylidenes, where stereospecificity has been observed experimentally, it is presumably not caused by covalent electronic interactions, but by steric or long-range electrostatic effects between the substituents. We shall return to this question later.

Finally, it may be noted in Figure 3.5.9 that the maxima (M_1 and M_2), converging on the ($\delta_1=90^{o},\delta_2=90^{o}$) point, have now almost merged into one.

j. $\Phi=86^{o}$ to 95^{o} (Figs. 3.5.10 - 3.5.14) The only feature which is really different from the $\Phi=85^{o}$ panel is that the entire surface is getting progressively lower in

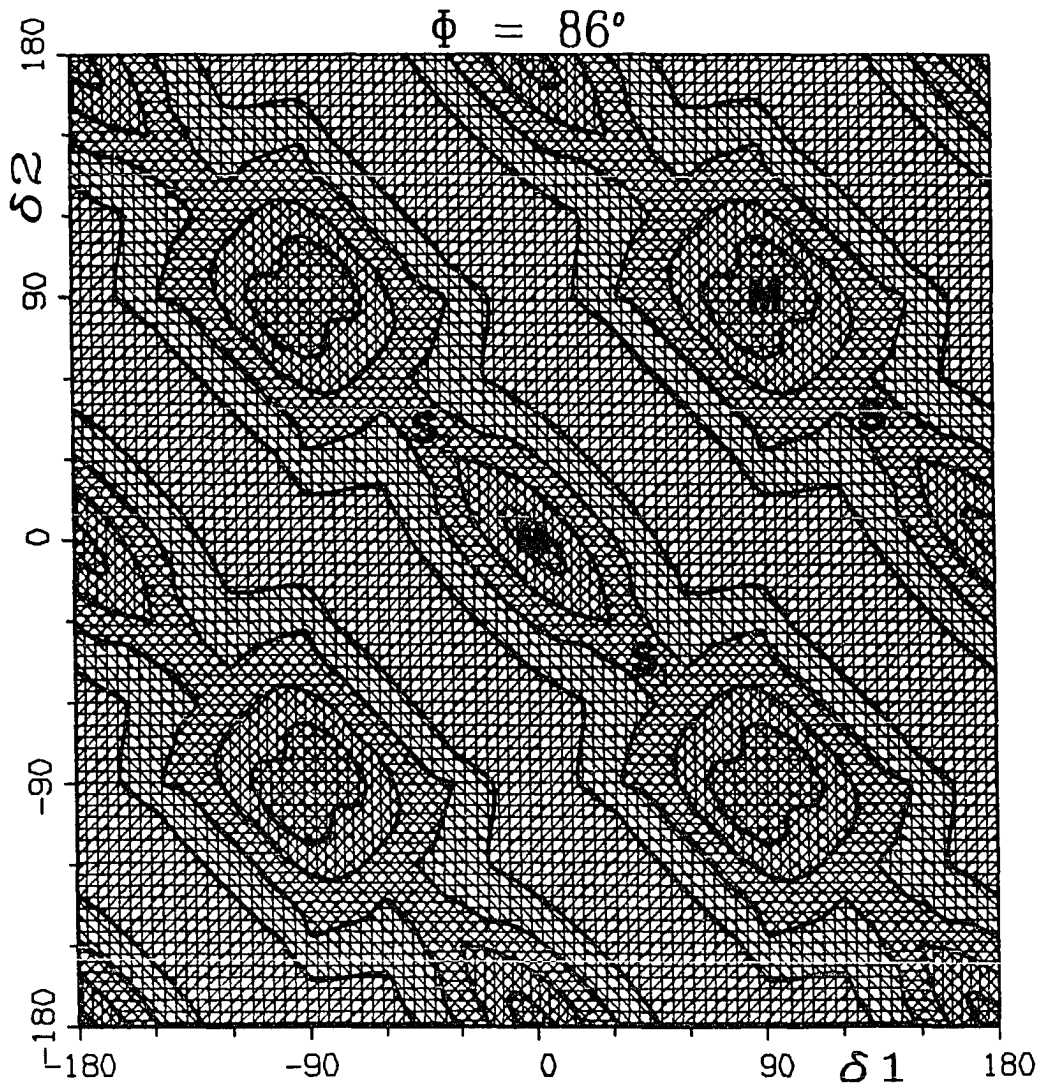

Figure 3.5.10. Energy surface over dihedral angle plane for $\Phi=86^{o}$. Overall pattern similar to that for 85^{o}. There is now a maximum (M) at $(\delta_1=90^{o},\delta_2=90^{o})$

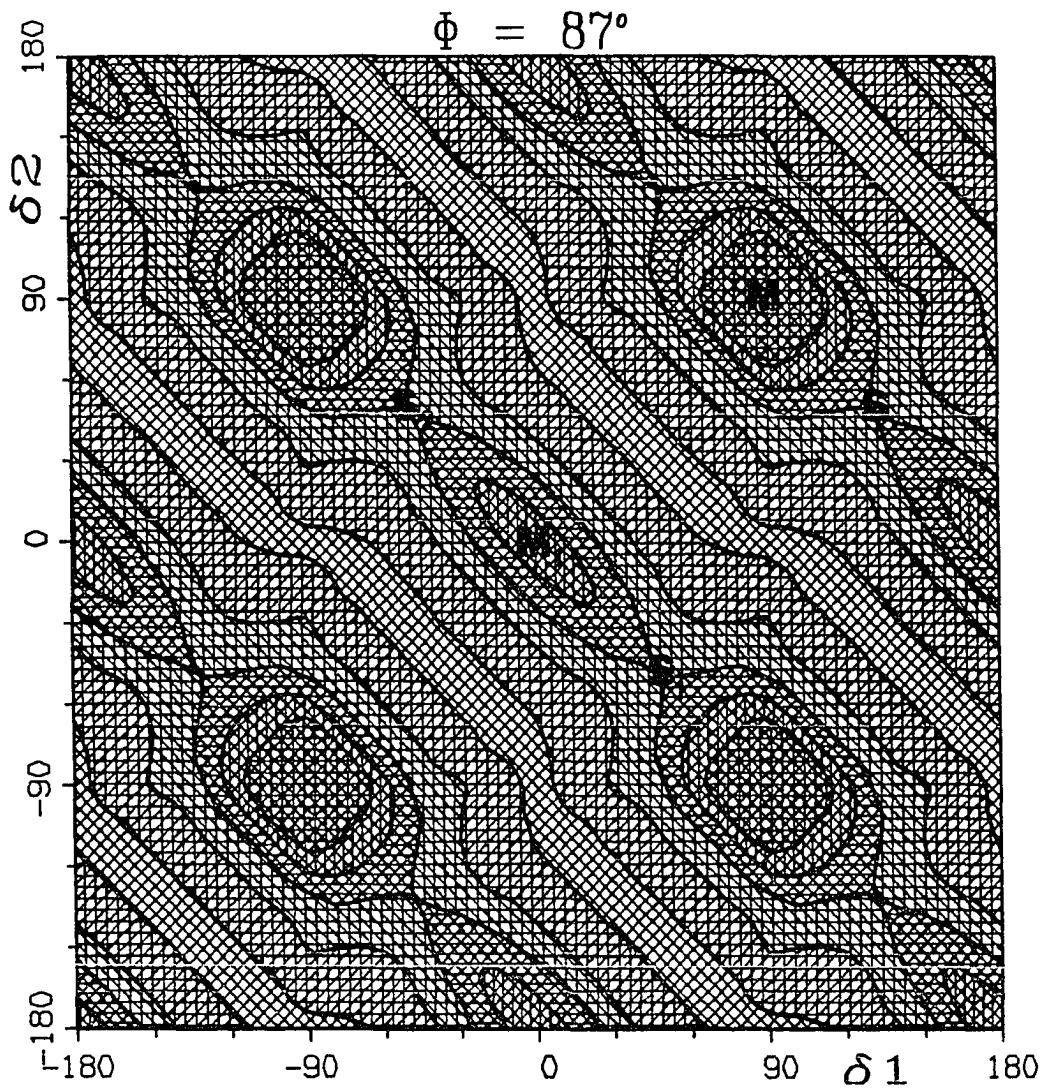

Figure 3.5.11. Energy surface over dihedral angle plane for $\Phi=87^{\circ}$. Very similar to the panel for 86°. Note that the entire surface is becoming lower in energy

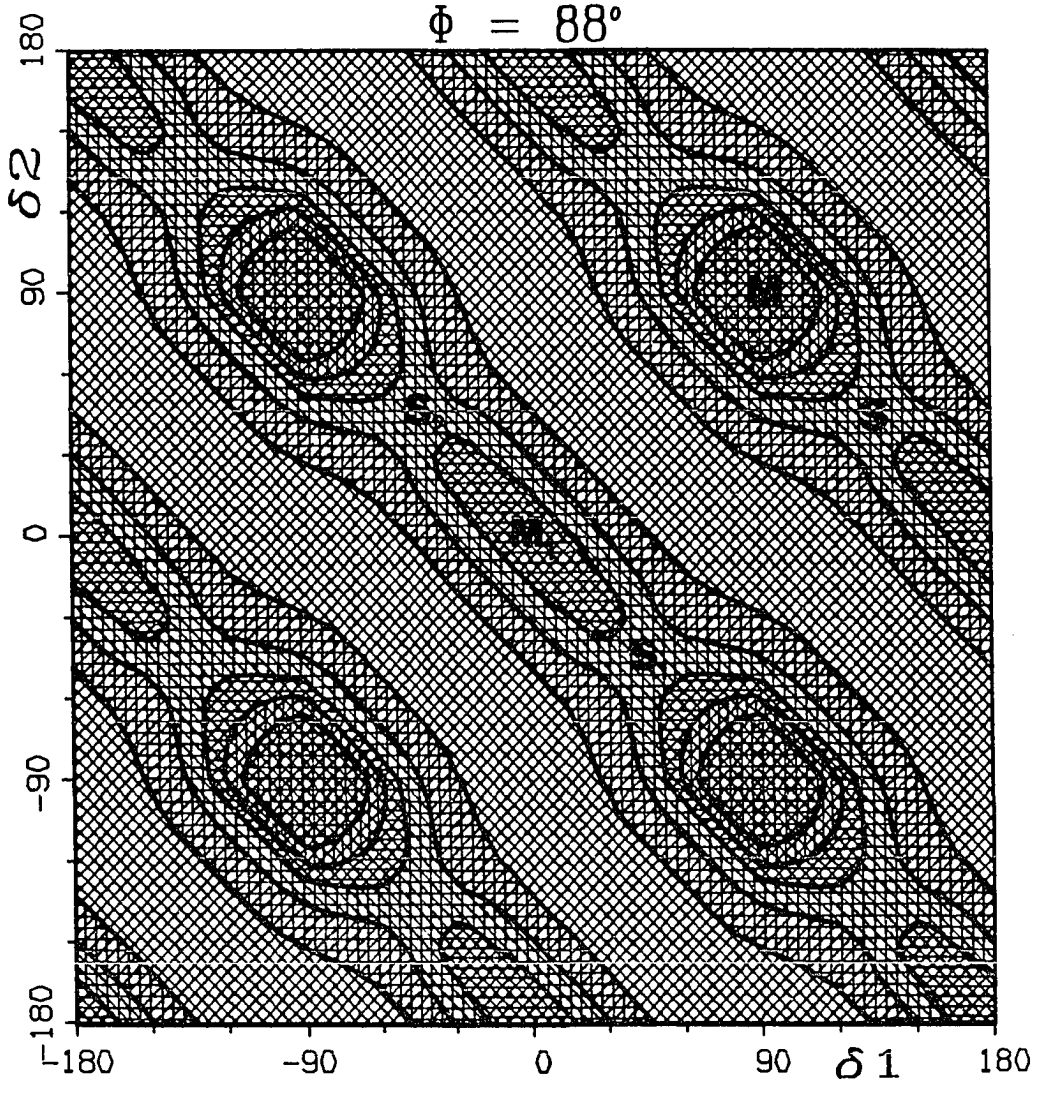

Figure 3.5.12. Energy surface over dihedral angle plane for $\Phi=88^{o}$. Again very little different from previous panels except for the overall energy lowering

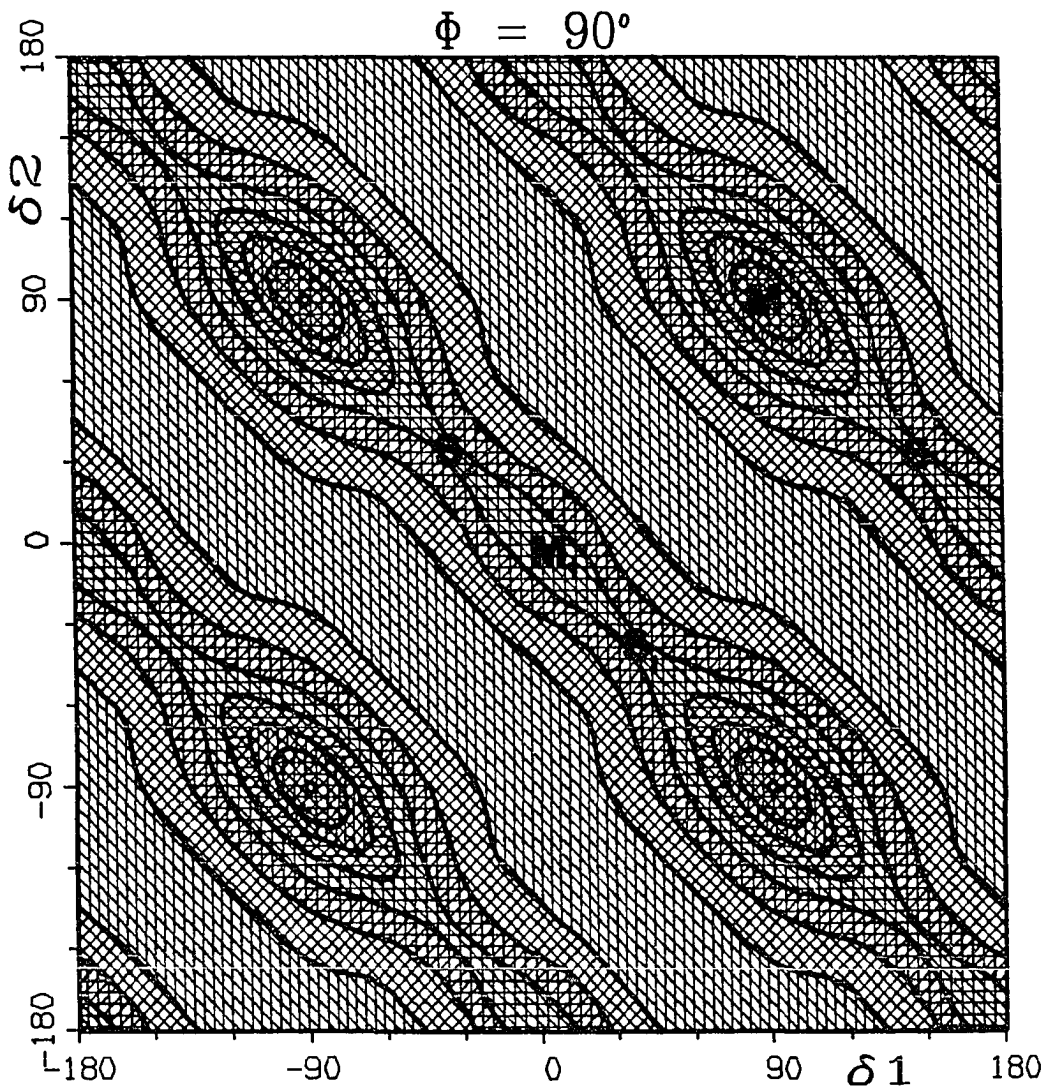

Figure 3.5.13. Energy surface over dihedral angle plane for $\Phi=90^{o}$. Overall pattern similar to previous panels. The maximum (M_1) at ($\delta_1=0^{o},\delta_2=0^{o}$) is slowly being sandwiched between two saddle points (S_1 and S_2)

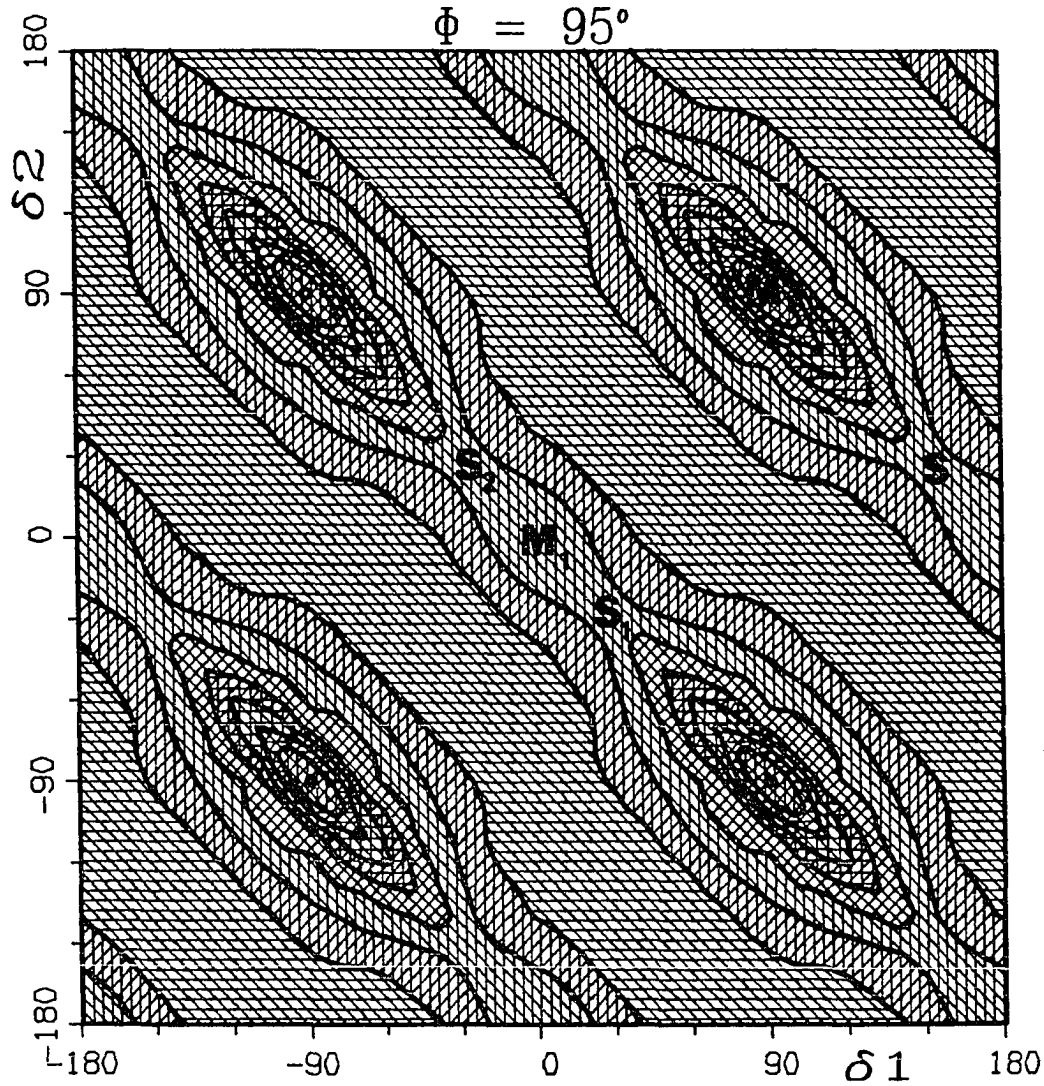

Figure 3.5.14. Energy surface over dihedral angle plane for Φ=95^{o}. Similar to Φ=90^{o}, except for overall energy lowering

energy as Φ opens from 85^{o} to 95^{o}. The reaction path is presumably well on its way downhill to the valley on its move down the energy curve towards the product. We have now one maximum (M) at ($\delta_1=90^{o},\delta_2=90^{o}$) and another ($M_1$) at ($\delta_1=0^{o},\delta_2=0^{o}$). The saddle points ($S_1$ and S_2) correspond to the old minima on the lines $\delta_1+\delta_2=180^{o}$ or equivalent lines. It is seen that the saddles (S_1 and S_2) approach the maximum (M) from both sides as Φ inreases.

k. $\Phi=100^{o}$ to 160^{o} (Figs. 3.5.15 - 3.5.18) The molecule is now moving rapidly on the downhill side of the energy curve. There are two notable features compared to previous panels. First the two saddle points (S_1 and S_2) from panel 3.5.14 have come together and coalesced at the point where the maximum M_1 was on Figure 3.5.14. We now have a saddle point (S), not a maximum at ($\delta_1=0^{o},,\delta_2=0^{o}$). Secondly, the low-lying valleys become straighter and straighter.

l. $\Phi=179^{o}$ (Allene, Fig. 3.5.19) The calculations were performed for $\Phi=179^{o}$ instead of 180^{o} so that the same computer program could be used, which was contingent upon being able to define the C-C-C plane. The contours seem to represent a series of perfectly straight valleys and ridges implying completely uninhibited motions along lines $\delta_1+\delta_2$=constant. The valleys (V) correspond to the staggered

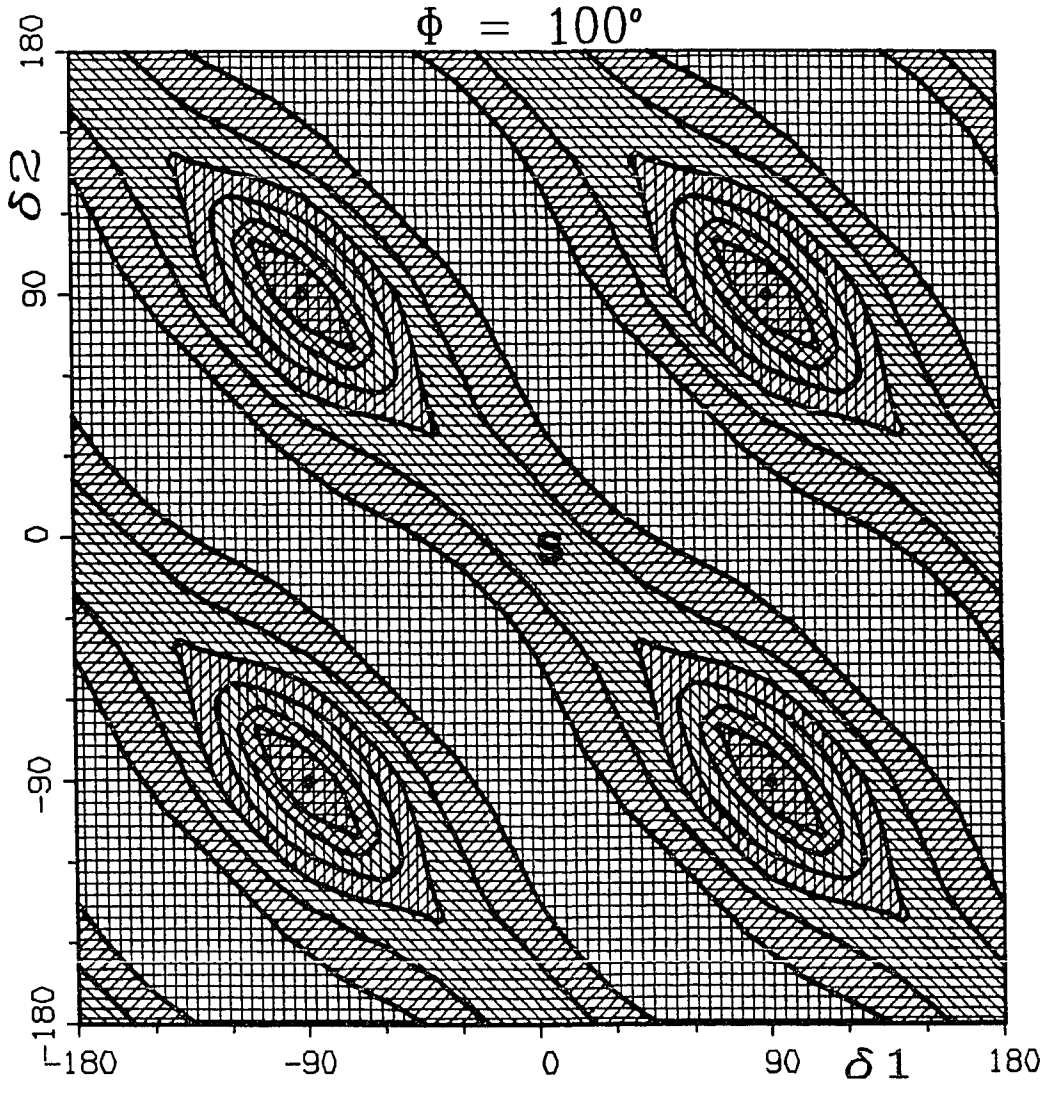

Figure 3.5.15. Energy surface over dihedral angle plane for $\Phi=100^{\circ}$. The maximum at ($\delta_1=0^{\circ}$,$\delta_2=0^{\circ}$) has turned into a saddle point (S). Notice that the minimum valleys are becoming straighter

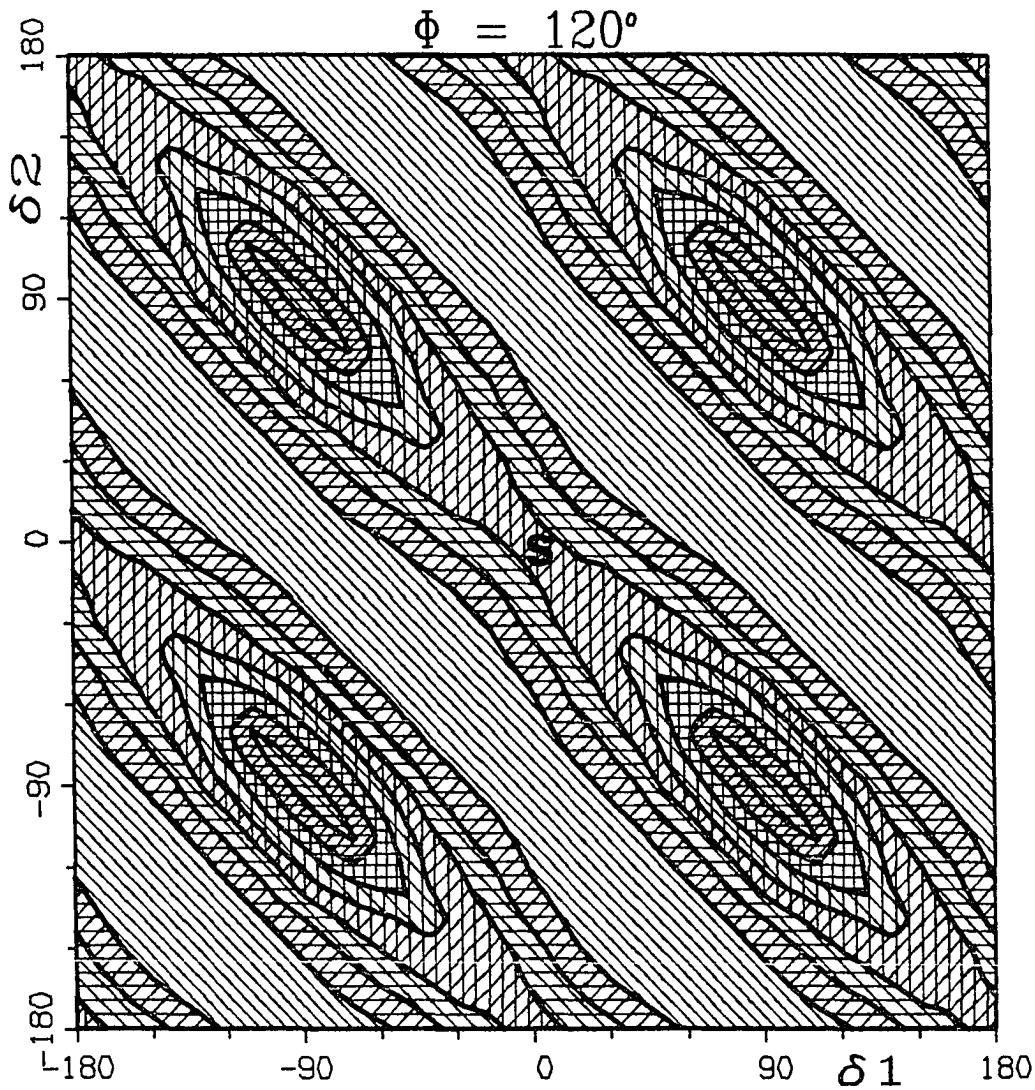

Figure 3.5.16. Energy surface over dihedral angle plane for Φ=120°. Very similar to the surface for 100°, except that the overall energy is lower and the minimum valleys are even straighter

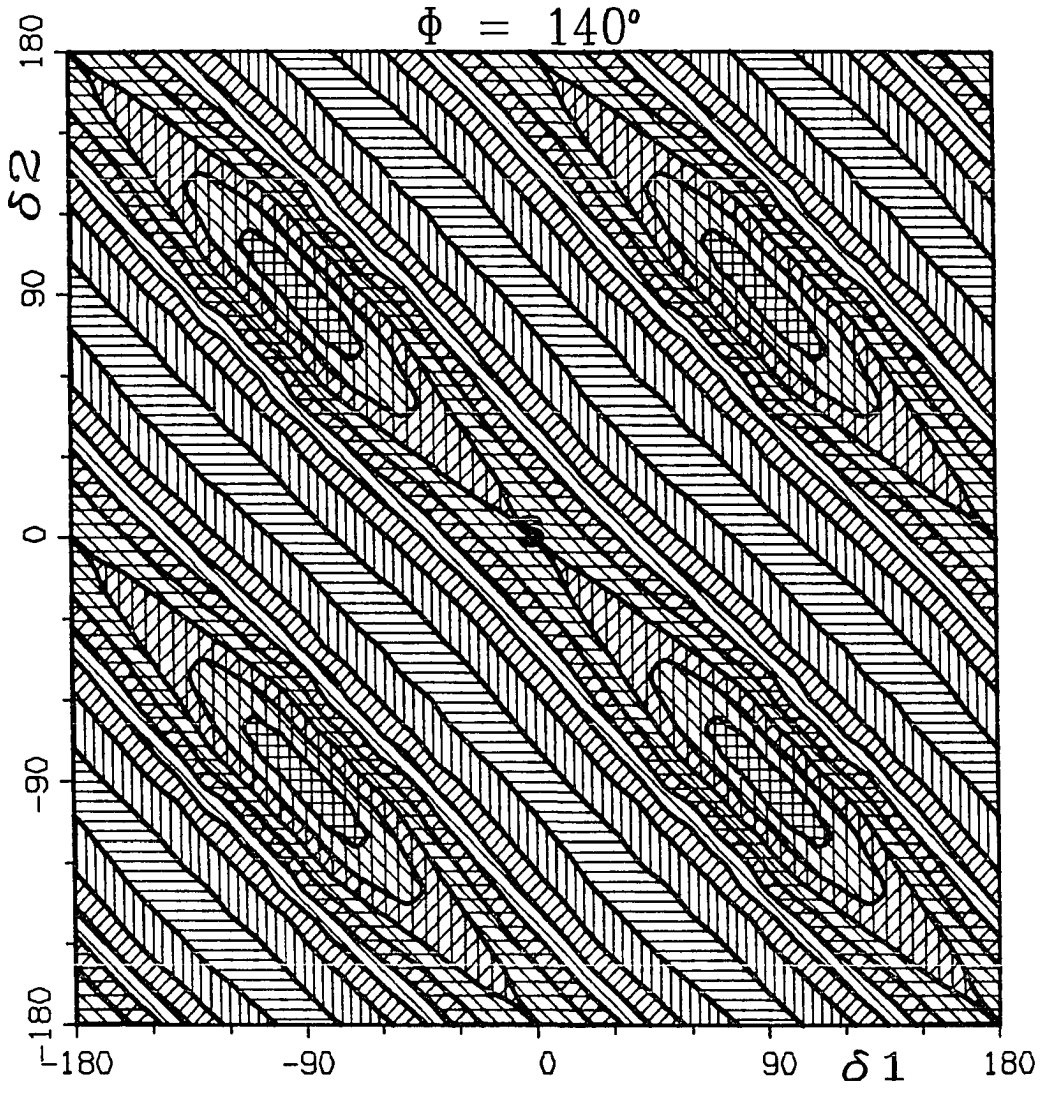

Figure 3.5.17. Energy surface over dihedral angle plane for $\Phi=140^{\circ}$. The minimum valleys are still straighter

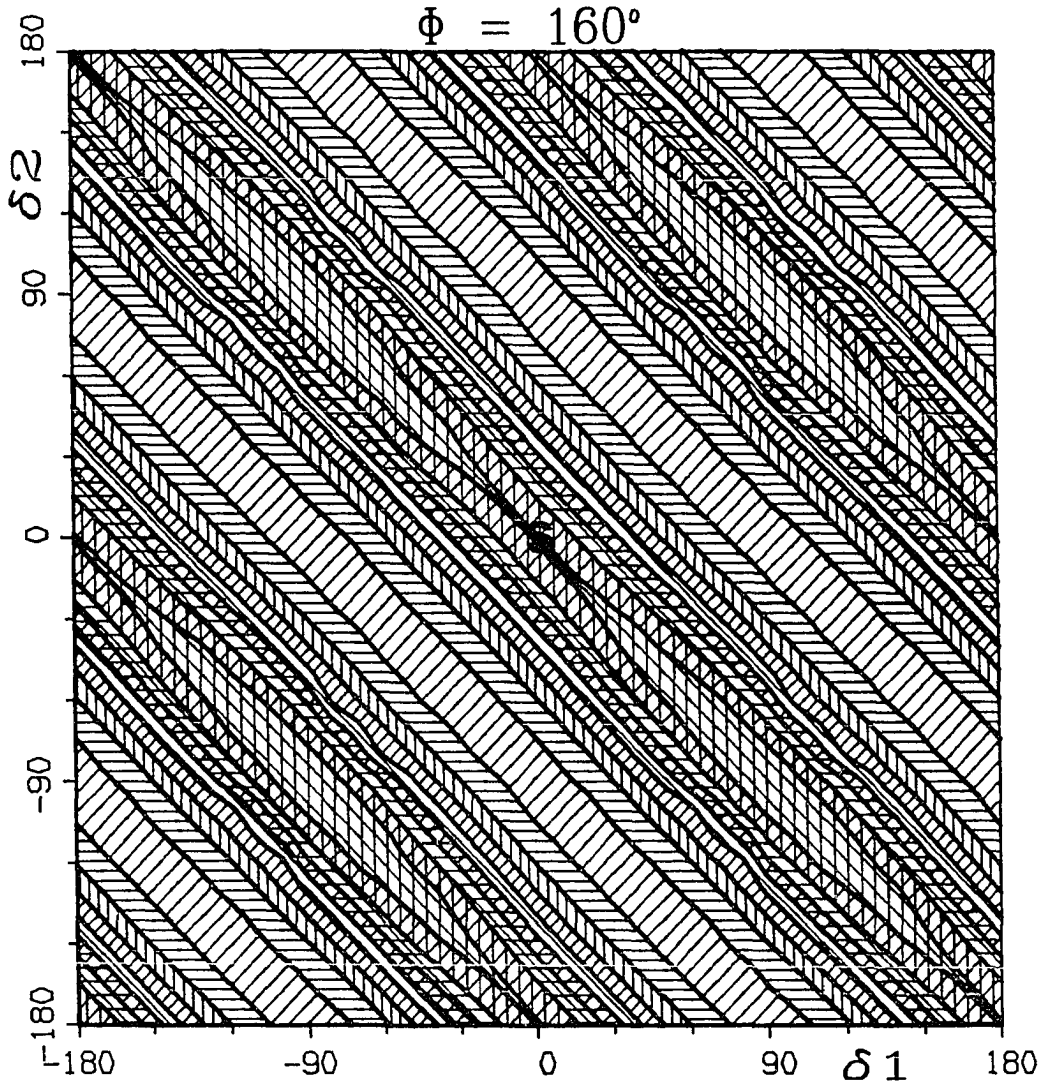

Figure 3.5.18. Energy surface over dihedral angle plane for $\Phi=160^{\circ}$. Basically the same as on previous panels, except that the minimum valleys are now almost completely straight. The saddle point at ($\delta_1=0^{\circ}$,$\delta_2=0^{\circ}$), however, still exists

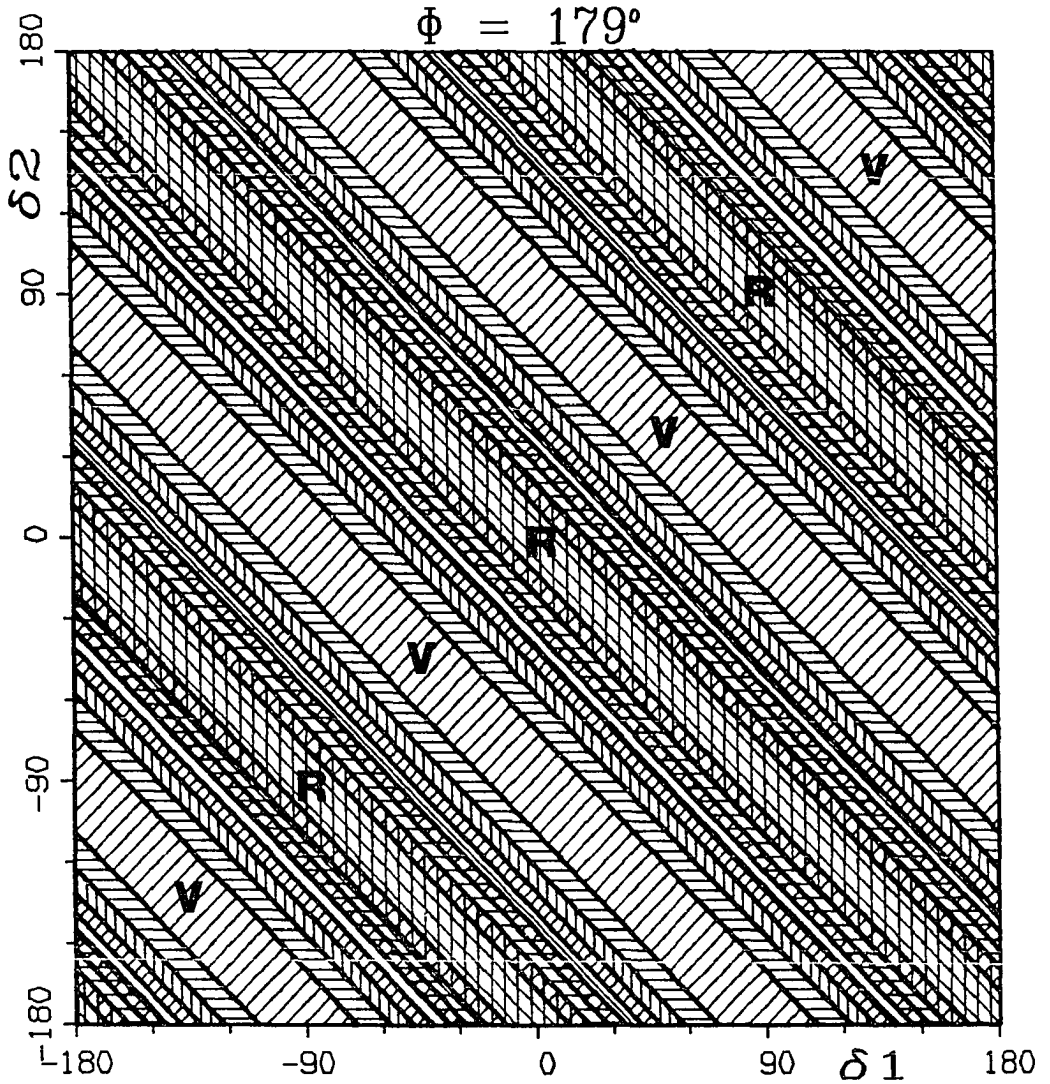

Figure 3.5.19. Energy surface over dihedral angle plane for $\Phi=179^{o}$ (allene). Note the perfectly straight valleys and ridges, corresponding to free rotations about the C-C-C axis. The valleys (V) correspond to the staggered (D_{2d}) configuration of allene, while the ridges (R) correspond to the eclipsed or planar (D_{2h}) configuration

(D_{2d}) configuration of Allene and the ridges (R) to the eclipsed (D_{2h}) configuration. This result is easy to understand, because motions along the valleys and ridges correspond to rigid rotations of the molecule about the linear C-C-C axis. This means that for $\Phi=180^{o}$, the average $(\delta_1+\delta_2)/2$ ceases to be an internal coordinate, so that motion in this direction is indeed free.

It stands to reason that for values of Φ which are not much smaller than 180^{o}, a similar behavior exists, i.e. motions along lines $\delta_1+\delta_2$=constant represent approximately rigid rotations around an axis which goes approximately through the three carbon atoms and hence are approximately free. Such an interpretation must clearly break down however when Φ becomes sufficiently small. Thus, for $\Phi=140^{o}$ (Figure 3.5.17) it is seen that a free motion exists only along the valleys $\delta_1+\delta_2\approx 90^{o}$, but not anymore along the ridges $\delta_1+\delta_2\approx 0^{o}$. This free motion along the valleys persists for Φ values all the way back to the transition state (see Figures 3.5.8 to 3.5.19). As was explained in the discussion of the panel for $\Phi=84^{o}$ (Figure 3.5.8), these motions along the valleys correspond to cogwheel-like synchronized rotations of the two hydrogen pairs. This is a result which could not have been foreseen without an explicit ab-initio calculation. How can it be explained? From Figure 3.5.20 it can be seen that for $\delta_1=0^{o}$ and $\delta_2=90^{o}$, there will exist:

(i) a strong bond between the π orbital on the central carbon and that p-orbital on C_1 which is perpendicular to the CCC plane,

(ii) a weaker bond between the σ orbital on the central carbon and the p orbital on C_2 which lies in the CCC plane.

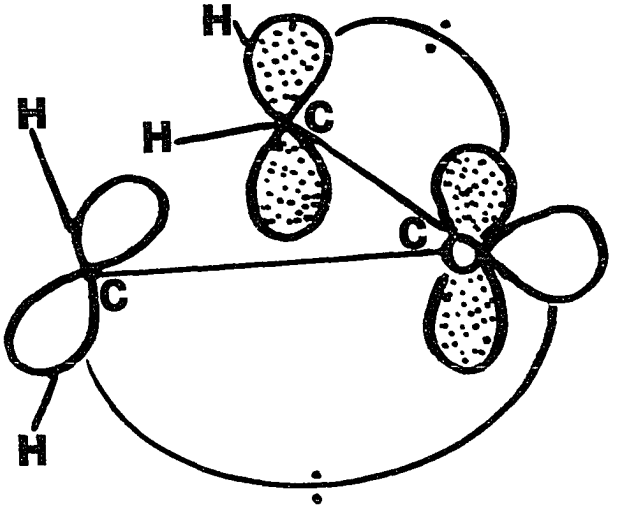

Figure 3.5.20. Formation of C-C π-like bonds

The situation is reversed if $\delta_1=90^{\circ}$ and $\delta_2=0^{\circ}$. It has to be inferred that the energy lost in breaking these bonds on one carbon is just about gained by reforming the same bond on the other carbon when the two hydrogen planes turn in a cogwheel-like fashion.

m. Isomerization of allene From an examination of the various contour panels, the following observation can be made with respect to the isomerization of allene. From Figure 3.5.19, the height of the barrier between the two valleys $\delta_1+\delta_2=90^o$ and $\delta_1+\delta_2=-90^o$, which correspond to the two different stereoisomers, is seen to be approximately 90 millihartrees (55kcal/mole). If one looks however at Figure 3.5.17, which corresponds to $\Phi=140^o$, one sees that the lowest part of the isomerization barrier, i.e. the point S, is considerably lower in absolute energy than 90 millihartree. It is therefore energetically advantageous for allene to bend by almost 40^o before rotating the two CH_2 planes with respect to each other. A saddle point optimization was carried out according to the method originally developed by McIver and Komornicki (1972), implemented in the GAMESS computer program by Dupuis, Spangler and Wendoloski (1980), and recently improved upon by Schlegel (1982). The results show a barrier of around 42 kcal/mole and a bending angle $\Phi=133.3^o$. These results can be compared to the values 46.3 kcal/mole and 134.29^o by Angus, Schmidt and Johnson (1985), 50.1 kcal/mole and 135.4^o by Seeger et al. (1977), 49 kcal/mole (with linear geometry) by Dykstra (1977), 52 kcal/mole (with linear geometry) by Staemmler (1977) and 53 kcal/mole and 137.4^o by Krogh-Jespersen (1982), as well as to an estimated experimental barrier of about 50 kcal/mole (this estimate is

based on an extrapolation from the measured barrier of the dimethylated compound by Roth, Ruf and Ford (1974)). We shall comment on these values above when reporting the results of our calculations with a better basis set, and we have ascertained the influence of substituents on this barrier (see Chapter V).

3. Reaction energy as function of Φ and $\delta=(\delta_1+\delta_2)/2$

Whereas the plot given in Figure 3.4 shows the variation of the energy with the "primary" reaction coordinate Φ, the plots in Figures 3.5.1-19 exhibit the variation of the molecular energy with all three reaction coordinates Φ, δ_1, δ_2. While the latter representation is necessary to obtain information about the rotations of the hydrogens, it makes it more difficult to visualize the reaction path in its entirety. It is therefore useful also to consider an intermediate representation, namely to examine the energy as a function of Φ and the "average conrotatory rotation angle" $\delta=(\delta_1+\delta_2)/2$. These energy values are obtained by finding, for each panel Φ=constant and on each line $\delta_1+\delta_2$=constant, the energy minimum with respect to the "disrotatory" variable $\delta_-=(\delta_1-\delta_2)/2$. The new independent variable δ shows how far off the C_s symmetry line ($\delta=90^o$) the molecule is. It might be mentioned that, although there are now 13 optimized internal coordinates and only two independently varying ones,

the new surface could hardly have been generated without first generating the lerger surface of the preceding section because the appropriate choice of coordinates becomes obvious only after studying the previous results.

Contours of this intermediate reaction surface are displayed in Figure 3.6. The contouring increments and the shading scheme are the same as before. The average conrotatory dihedral angle δ is the x-axis and the ring-opening angle Φ is the y-axis. The reactant, denoted by C, is at the clearly defined minimum for ($\delta=90^{o}$,$\Phi=59.5^{o}$), representing cyclopropylidene. As the reaction proceeds, the molecule moves upwards in the increasing Φ direction. It should be noted that the $\delta=90^{o}$ line represents either nonrotatory or disrotatory behavior of the CH_2 planes in such a way that the molecule retains C_s symmetry. Deviation from this line means breaking of the C_s symmetry, and can represent any mixture of conrotatory, monorotatory or asymmetric disrotatory motion of the CH_2 planes.

The floor of the valley in which the molecule is moving keeps rising, and we can distinguish a clear maximum on the $\delta=90^{o}$ line at a Φ angle of about 84.5^{o}. There are two things which are very interesting about this maximum region. First, it is apparent that, instead of going over the maximum, it would be energetically advantageous for the molecule to go around it and over one of two saddle points situated on

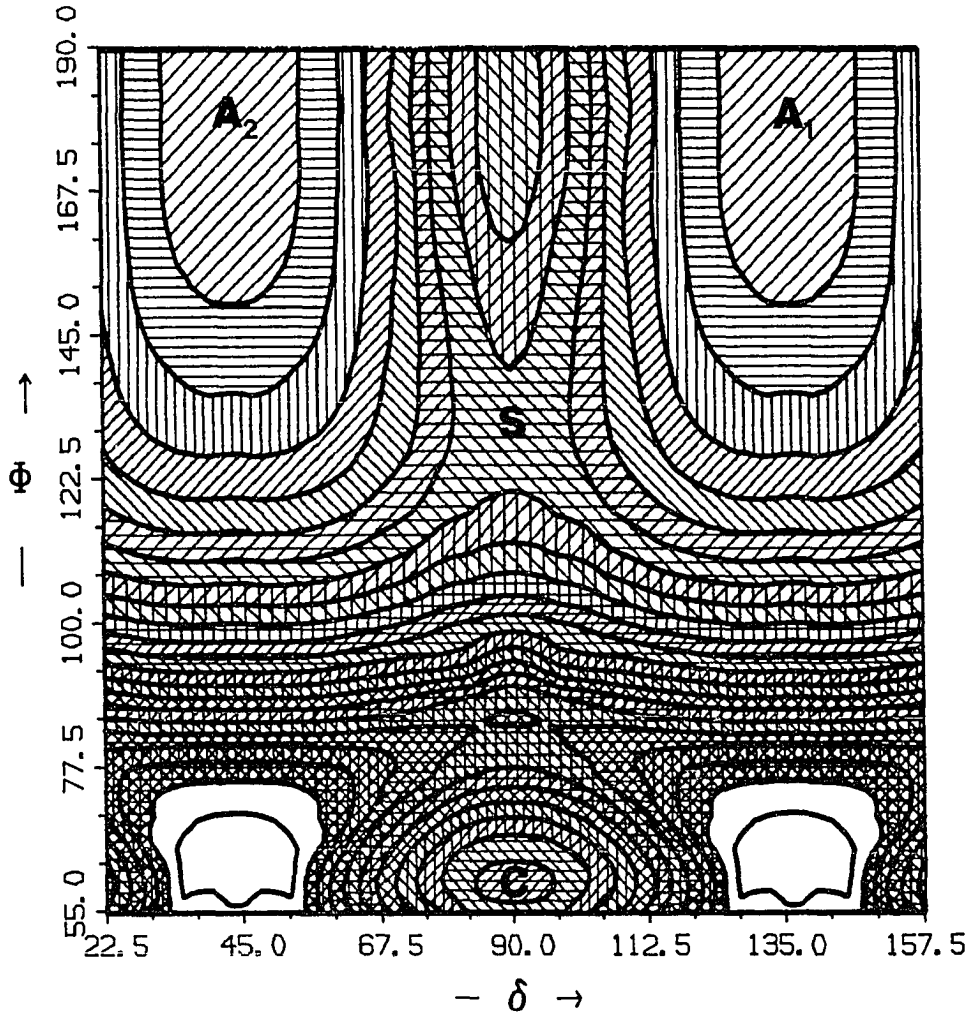

Figure 3.6. Contour plot of the energy as a function of Φ and δ. The shading scheme is the same as that used in the Φ=constant panels. Note the minima for cyclopropylidene (C) and the two allene stereoisomers (A_1 and A_2), the allene stereoisomerization saddle point (S), and the bifurcating transition region. The energy difference between the two saddle points and the maximum is ~2 kcal/mole

either side. Second, after the maximum the $\delta=90^{o}$ line is no longer a valley but a ridge. The presence of this potential ridge will cause the molecule to fall away from the C_s symmetry line and move towards one or the other of the two product minima A_1 and A_2. There is, of course, no reason why the molecule would move in one direction rather than in the other, i.e. towards one allene stereoisomer rather than to the other. In other words, we have typical conditions for a bifurcation. Thus the reaction path could follow the line $\delta=90^{o}$ from cyclopropylidene to close before the maximum for $\phi=84.5^{o}$. It would then bifurcate over the two saddles and follow the steepest descent lines to A_1 and A_2. It should be noted that <u>this bifurcation is in close vicinity of the transition region</u> and that the energy difference between the two saddles and the maximum is only a couple kcal/mole. We shall elaborate on this point in a later section.

The contour plot of Figure 3.6 also clearly exhibits for the first time the saddle point (S) which is the transition state for the internal rotation of allene. It is apparent from this surface that this molecule will bend to facilitate the hydrogen rotation and that this motion of twisting and bending is a concerted one.

4. Variation of the twelve remaining internal coordinates with (Φ,δ_1,δ_2)

As was mentioned earlier, the geometry optimizations for each (Φ,δ_1,δ_2) triple yields the other twelve internal coordinates as functions of Φ, δ_1, δ_2. An examination of those functional dependences is of interest for several reasons. First, it reveals more about the geometry changes of the molecule during the reaction and thereby yields a better understanding of the reaction mechanism. Secondly, the continuity or possible discontinuity of the functions in the neighborhood of the reaction path reveals whether the choice of Φ, δ_1, δ_2 as reaction coordinates is in fact a good one.

Accordingly, a series of additional energy calculations were performed for several panels Φ=constant, in the neighborhood of that point (δ_1^o,δ_2^o) at which the reaction path intersects those panels. Eight additional points were chosen as defined by the relations

$$\{(\delta_1+\delta_2)/2 - (\delta_1^o+\delta_2^o)/2\} = 0^o,+5^o,-5^o$$
$$\{(\delta_1-\delta_2)/2 - (\delta_1^o+\delta_2^o)/2\} = 0^o,+5^o,-5^o$$

effectively surrounding the intersection point. The complete results of these special calculations are shown in the tables of the Appendix, but some partial results are depicted graphically in this section in order to illustrate a few points.

a. The four C-H bond distances Their values remain at 1.089 ± 0.011 A throughout all of these calculations. Moreover, they change even less within each Φ panel. Thus the issue of discontinuity does not arise at all.

b. C-C bond lengths We are interested in the bonds C_0-C_1 and C_0-C_2. Figure 3.7 displays a plot of the values of these two nonbreaking C-C bond lengths at the points of intersection of the reaction path with the Φ panels, as functions of Φ. The "error bars" show the fluctuation of these values within each Φ panel, and it is apparent that they do not change enough for any question of discontinuity to arise. The equality of the two C-C bond lengths up to the bifurcation point is of course a consequence of the C_s symmetry. For very large Φ values, it is a consequence of the similarity to allene.

c. The four C-C-H bond angles Figure 3.8 displays a plot of the values at the intersection. The two bond angles above the CCC plane (C_0-C_1-H_1 and C_0-C_2-H_2) are drawn in bold lines, while the two angles below the CCC plane (C_0-C_1-H_1, and C_0-C_2-H_2,) are drawn in thin lines. It is apparent that all deviations from smoothness occur near the transition region, and it should be noted that in this region each "bottom" angle behaves more or less in the opposite fashion from that of the "top" angle at the same carbon. No error bars are drawn here, because the fluctuations of the

values within a particular Φ panel are, in some cases, greater than the entire range shown in Figure 3.8. These fluctuations can be seen from Figure 3.9, which shows contours of the four bond angles as function of $\delta=(\delta_1+\delta_2)/2$ and $\delta_-=(\delta_1-\delta_2)/2$ for $\Phi=60^o$. This value of Φ=constant was chosen, because the fluctuations are by far the largest for this panel. It is apparent that there exist no discontinuities, the relatively large changes notwithstanding. It is also interesting to note the perfect symmetry of the changes, since the panels for the "top" bends are related to each other by a diagonal rotation around the $\delta_-=0$ axis, while they are each related to the corresponding "bottom" bend by a rotation around the $\delta+\delta_-=0$ axis.

d. The two C-C-H-H out-of-plane bends (angles between each C-C bond and the corresponding CH_2 plane) Figure 3.10 depicts the changes in the values at the reaction path intersection points, as functions of Φ. In accordance with the C_s symmetry, the angles are seen to start out at exactly opposite values, and then change by equal and opposite amounts during the disrotatory C_s preserving phase of the reaction until they both become equal to 0^o near the transition region. From then on, they change in the same direction, although not always by the same amount. After the molecule has reached the slopes of the free synchronized CH_2 plane rotation valleys, the two bends become again

Figure 3.7. Change of C-C bond distances as a function of Φ. Note that C_0-C_1 and C_0-C_2 are essentially equal, except around the transition region and during the descent from the transition state to the valleys of synchronized rotation of the hydrogen planes, where the two C-C lengths change effectively in opposite ways. Error bars indicate fluctuations within a particular Φ=constant panel

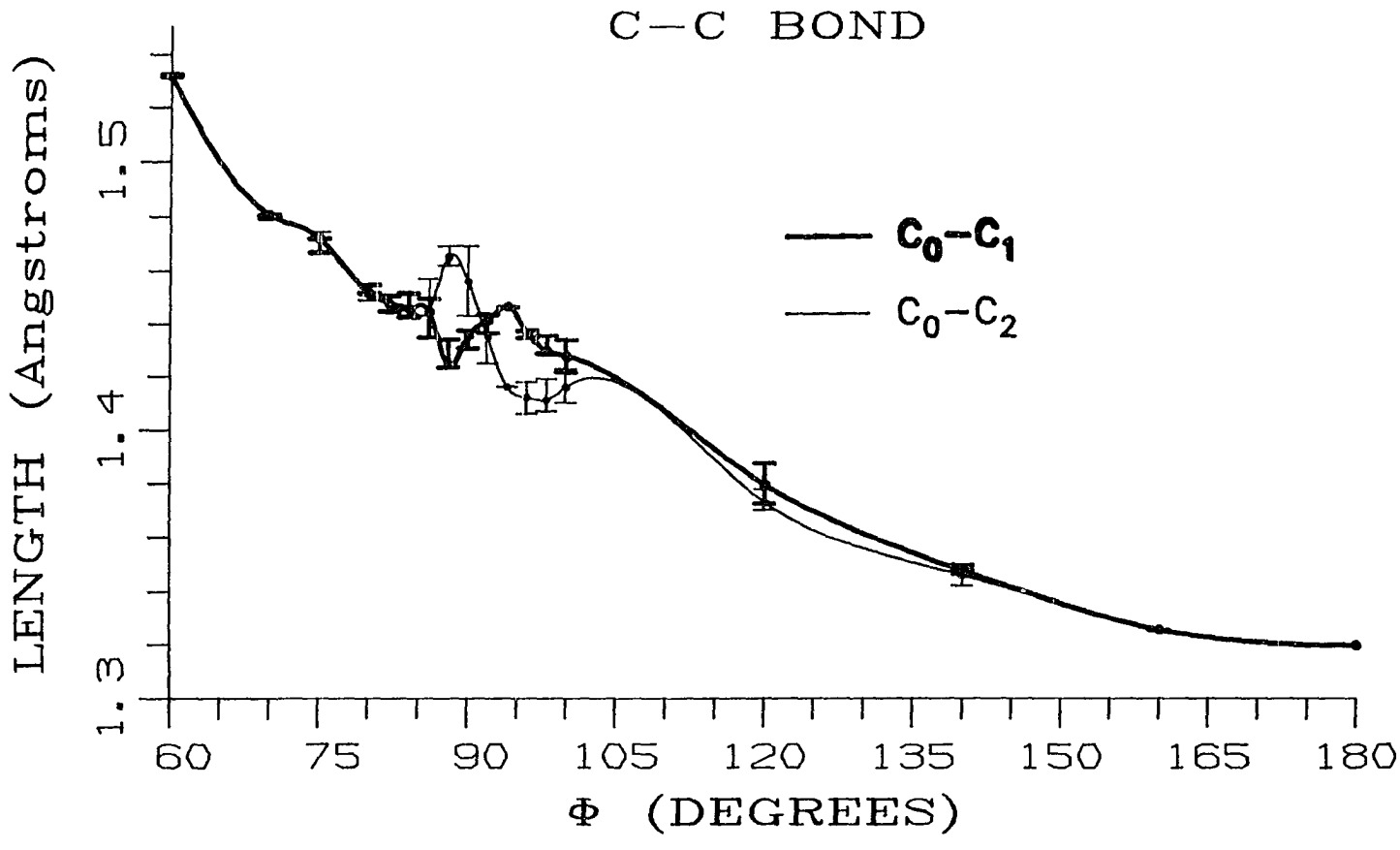
C—C BOND
LENGTH (Angstroms)
1.3
1.4
1.5
60
75
90
105
120
135
150
165
180
Φ (DEGREES)
C_0–C_1
C_0–C_2

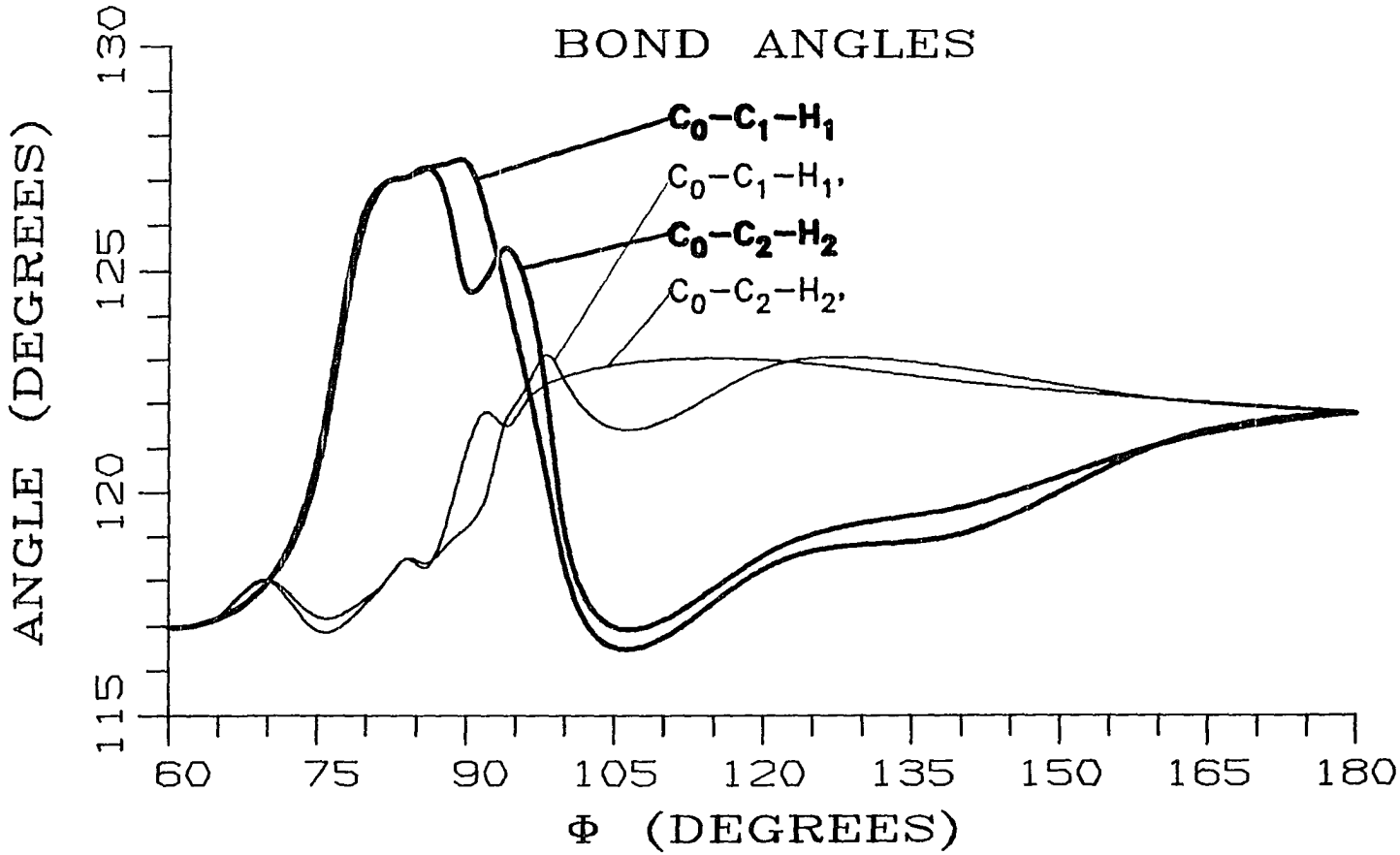

Figure 3.8. C-C-H bond angles as a function of Φ. "Top" and "bottom" angles change more or less in opposite ways

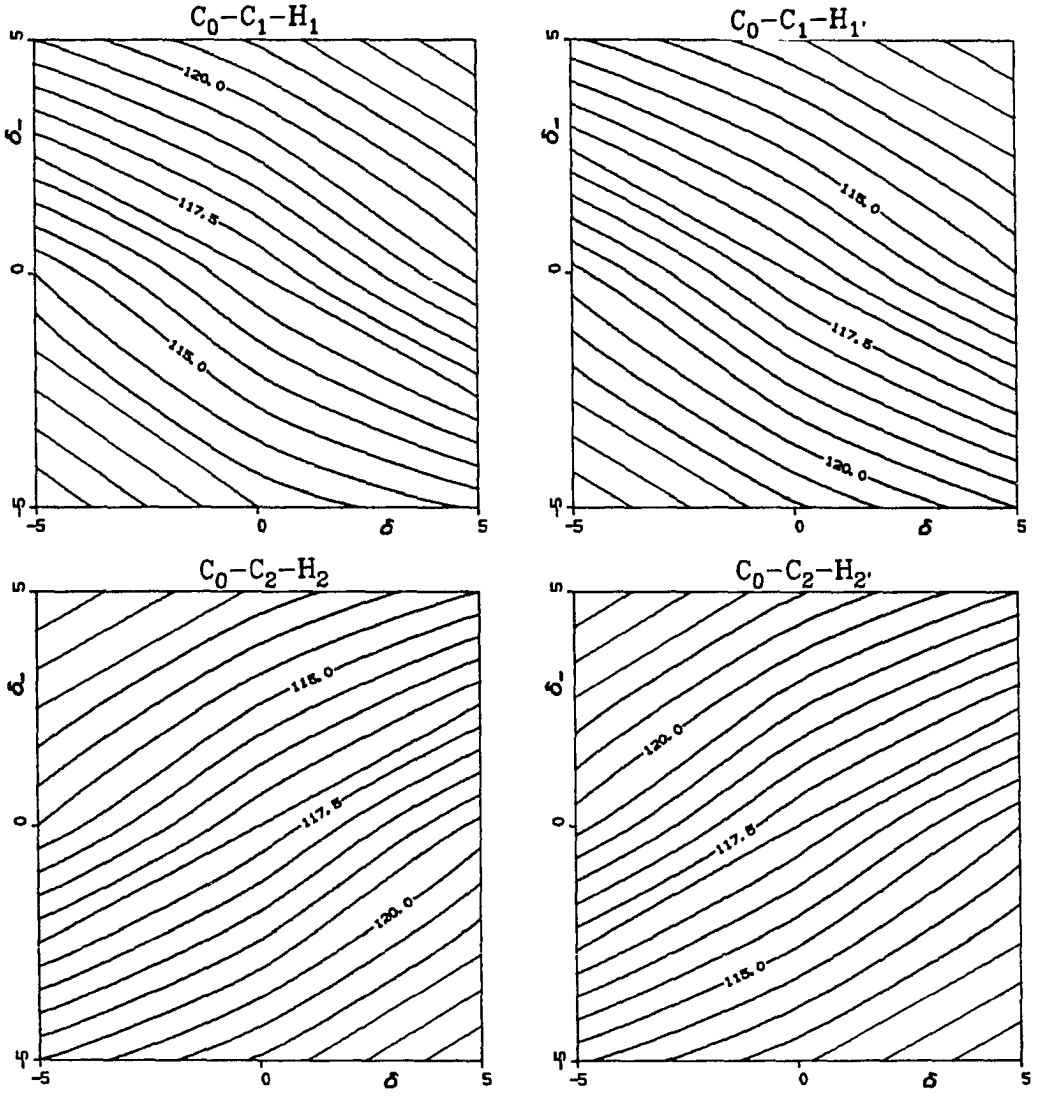

Figure 3.9. Fluctuation of the C_7C-H bond angles as a function of δ and δ_-, for $\Phi=60^{o}$. Contours are at 0.5 degree intervals. Note the absence of any discontinuities

approximately equal and remain so until the end of the reaction. The error bars indicate the fluctuations of the angle values within each Φ panel. Some of these are quite large. To make sure that no discontinuities exist, we again plot the values of the bends as functions of δ and δ_-. Contour plots for some Φ panels are shown in Figure 3.11. They are selected from those showing the largest change. Once more it is apparent that no discontinuities are present.

C. Conclusions

The preceding results may represent one of the most complete energy surfaces calculated for a reaction. What conclusions can be drawn from this work, and what are its implications?

The successive reduction of the dimensionality of the problem from 16 dimensions down to 4 to begin with and finally to just 3, clearly allows the mapping out of the reaction path and this is shown in Figure 3.12, where perspective drawings of the appropriate geometries of the molecule at various points along the energy curve are shown. The explicit geometries of four important species along the reaction path, viz. cyclopropylidene, allene, the ring-opening transition state and the allene isomerization saddle point, are shown on Table 3.1. Also, the energies and nature

Figure 3.10. C-C-H-H out-of-plane bends as function of Φ. Error bars show the fluctuations within each Φ=constant panel. Note that the bends change in opposing fashion while the reaction path is disrotatory and change essentially together when the path becomes more or less conrotatory

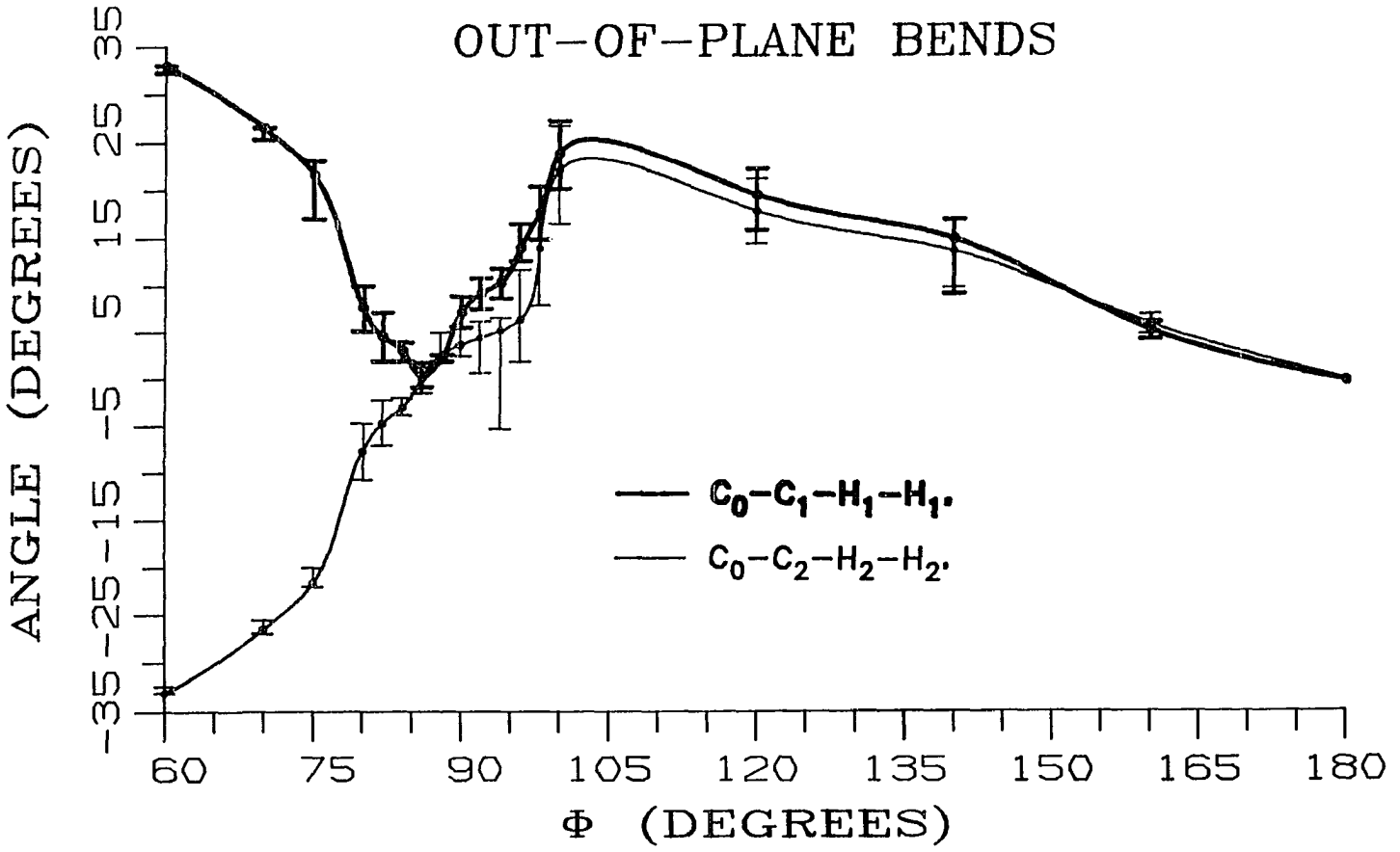
OUT–OF–PLANE BENDS
ANGLE (DEGREES)
35
25
15
5
-5
-15
-25
-35
60
75
90
105
120
135
150
165
180
Φ (DEGREES)
C0–C1–H1–H1'
C0–C2–H2–H2'

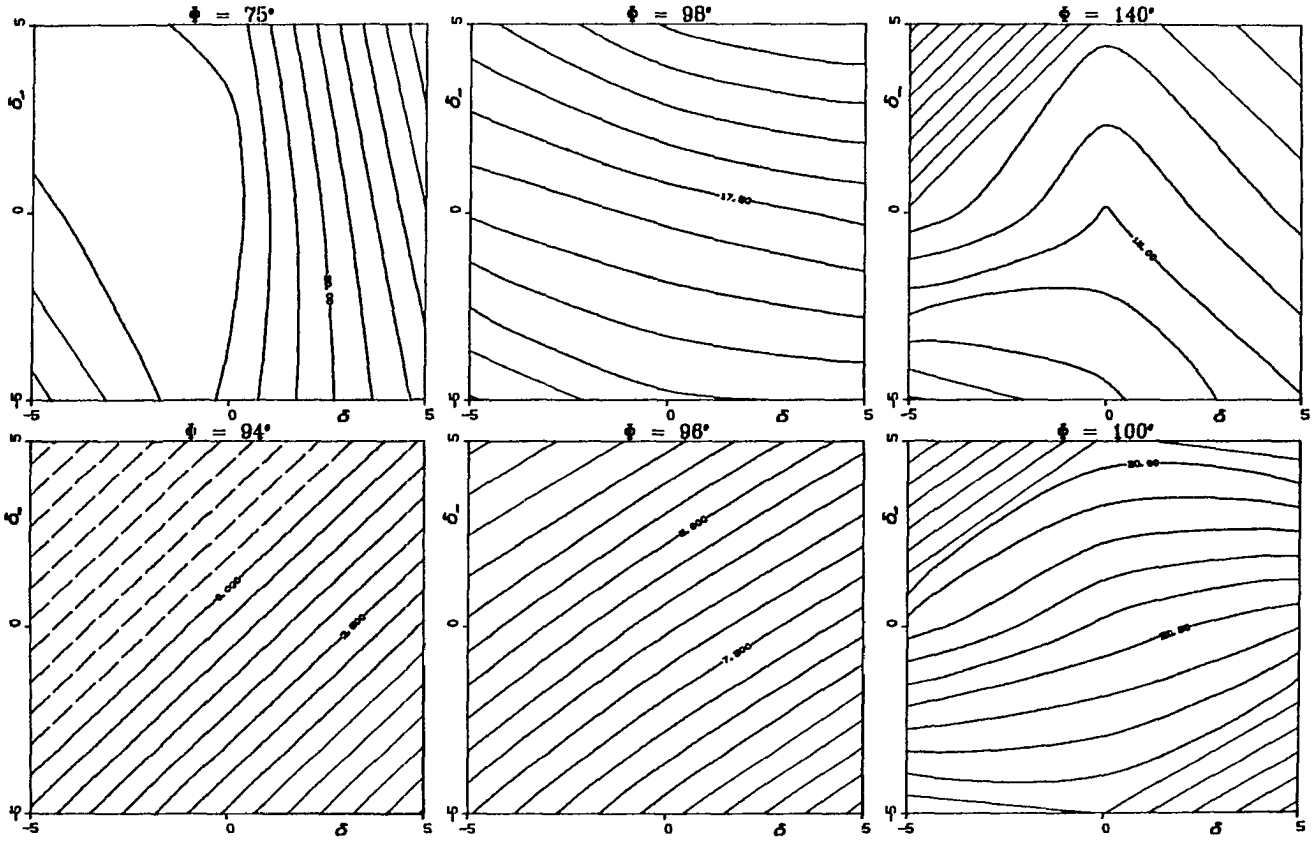

Figure 3.11. Fluctuation of the C-C-H-H out-of-plane bends as functions of δ and δ_ for some values of Φ. Contours are at 0.5 degree intervals

Figure 3.12. Geometry changes along the reaction path as a function of Φ. Each molecule is situated at the point where it cuts the energy curve, except where indicated by lines joining the molecule to the reaction curve

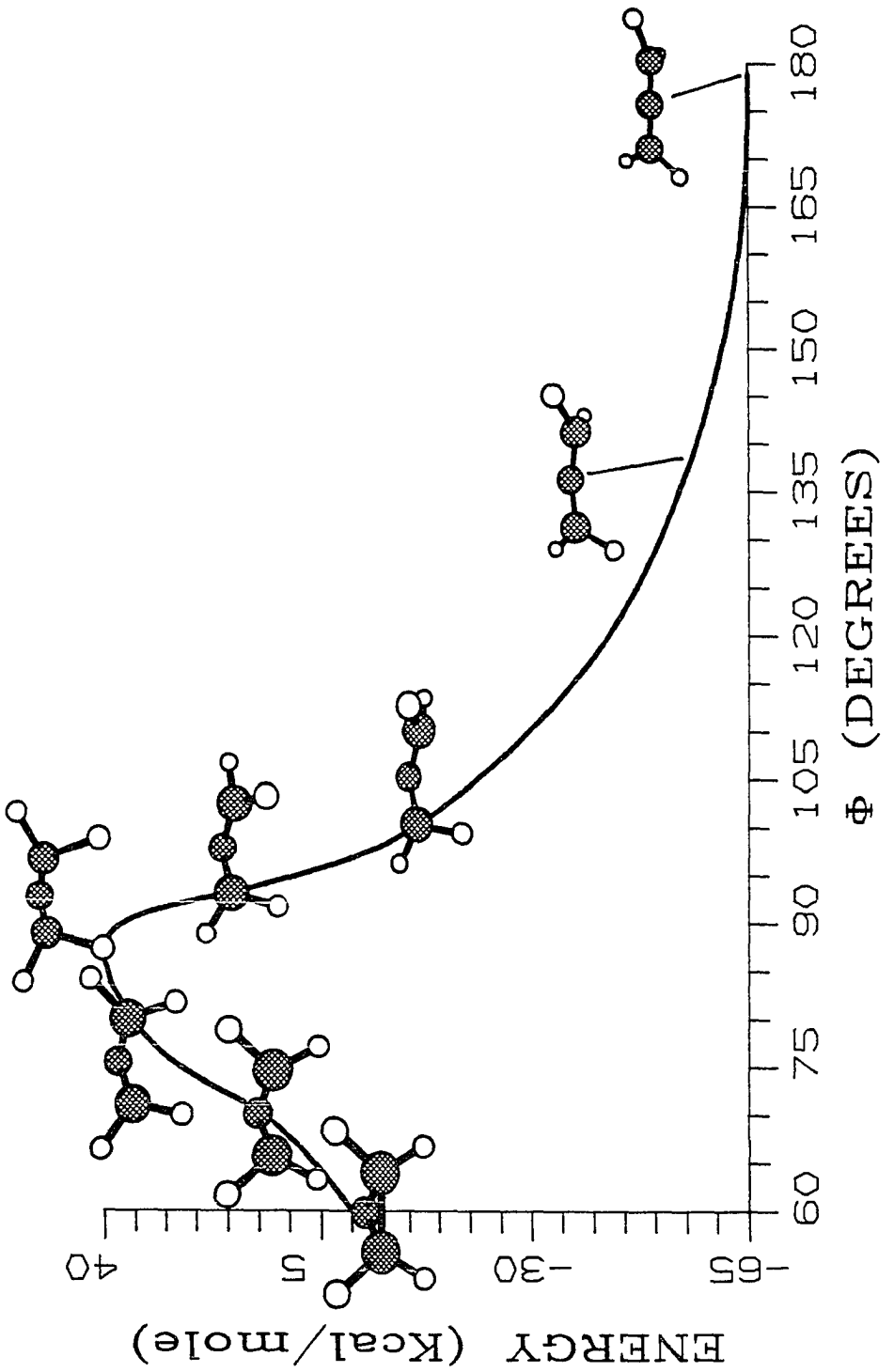
ENERGY (Kcal/mole)
40
5
-30
-65
60
75
90
105
120
135
150
165
180
Φ (DEGREES)

Table 3.1. Geometries (in terms of the 15 internal coordinates defined in Figure 3.2) and energies (in Hartree) of the most important species along the reaction path. Lengths are in A and angles are in degrees

Species	Φ	δ_1	δ_2	Length C-C	Length C_2-H_4 C_3-H_6	Length C_2-H_5 C_3-H_7
1[a]	59.5	90.0	90.0	1.5323	1.0811	1.0811
2[b]	84.0	50.0	130.0	1.4456	1.0881	1.0830
3[c]	133.3	0.0	0.0	1.3918	1.0810	1.0822
4[d]	180.0	0.0	90.0	1.3196	1.0826	1.0826

[a] Cyclopropylidene.

[b] Ring-opening transition state.

[c] Allene stereoisomerization transition state.

[d] Allene.

Bend C_1-C_2-H_4	Bend C_1-C_2-H_5	Bend C_1-C_2- H_4-H_5	Bend C_1-C_3- H_6-H_7	Energy
117.1	117.1	33.1	-33.1	-114.3956
118.5	127.1	3.1	-3.1	-114.3332
121.1	121.7	0.0	0.0	-114.4322
121.8	121.8	0.0	0.0	-114.4993

of some characteristic points on the Φ=const. panels are shown in Table 2.2.

We have shown the following: (i) cyclopropylidene is clearly a minimum on the surface (in direct contradiction to the results of Dillon and Underwood (1977)), (ii) initially it opens up in a nonrotatory fashion, i.e. the two CH_2 planes stay perpendicular to the C-C-C plane during the first few degrees of the ring opening; (iii) after a Φ angle of about 75^{o}, the two hydrogen planes start to move in a disrotatory fashion, i.e. the two top hydrogens start getting closer together while the two bottom ones start getting farther apart (or vice versa). All the while, the molecule keeps moving up towards the transition region; (iv) this region is situated at a Φ angle of about 84.2^{o} (as opposed to $90\text{-}94.5^{o}$ proposed by Pasto et al. (1978)). (v) The transition region has C_s symmetry, and as the reaction path reaches it, it bifurcates. This seemingly simple fact has implications reaching well beyond this particular reaction, and they will be discussed in detail in the next chapter.

(vi) The bifurcation is completely symmetric and this fact implies that the reaction has no inherent stereospecificity. Thus, once more, we are led to point out that all experimental evidence to the contrary must be due to steric and possibly weak electrostatic effects, including the case quoted by Jones and Krause (1971). This conclusion we

Table 3.2. Energies (in Hartree) and nature of some key points on Φ=const. panels. "Min." denotes a minimum, "Max." a maximum, "Sad." a saddle point, and "Val." a valley. Position is expressed in terms of δ_1 and δ_2

	(δ_1=90°/δ_2=90°)		(δ_1= 0°/δ_2= 0°)		(δ_1= 0°/δ_2=90°)[a]		Minimum on δ=90° line		
Φ	Energy	Nature	Energy	Nature	Energy	Nature	Energy	Nature	Position
50°	-114.3645	Min.	-114.0990	Max.	-114.3015	Sad.	-114.3645	Min.	90°/90°
60°	-114.3956	Min.	-114.1020	Max.	-114.2835	Sad.	-114.3956	Min.	90°/90°
70°	-114.3725	Min.	-114.2142	Sad.	-114.2901	Sad.	-114.3725	Min.	90°/90°
75°	-114.3512	Min.	-114.2449	Max.	-114.2993	Sad.	-114.3512	Min.	90°/90°
80°	-114.3311	Sad.	-114.2758	Max.	-114.3179	Sad.	-114.3387	Min.	120°/60°
82°	-114.3215	Sad.	-114.2860	Max.	-114.3281	Sad.	-114.3355	Min.	125°/55°
83°	-114.3186	Sad.	-114.2906	Max.	-114.3331	Min.	-114.3341	Min.	130°/50°
84°	-114.3155	Sad.	-114.2952	Max.	-114.3381	Min.	-114.3322	Min.	130°/50°
85°	-114.3129	Sad.	-114.3001	Max.	-114.3435	Min.	-114.3329	Sad.	130°/50°
86°	-114.3102	Sad.	-114.3079	Max.	-114.3486	Min.	-114.3315	Sad.	130°/50°
87°	-114.3079	Sad.	-114.3153	Max.	-114.3541	Min.	-114.3331	Sad.	135°/45°
88°	-114.3057	Sad.	-114.3226	Max.	-114.3596	Min.	-114.3348	Sad.	135°/45°
90°	-114.3016	Max.	-114.3361	Max.	-114.3701	Min.	-114.3404	Sad.	140°/40°
95°	-114.3008	Max.	-114.3482	Max.	-114.3928	Min.	-114.3655	Sad.	155°/25°

100^{o}	-114.3412	Max.	-114.3862	Sad.	-114.4121	Min.	-114.3862	Sad.	180^{o}/ 0^{o}
120^{o}	-114.3858	Max.	-114.4281	Sad.	-114.4615	Min.	-114.4281	Sad.	180^{o}/ 0^{o}
140^{o}	-114.4057	Max.	-114.4324	Sad.	-114.4848	Min.	-114.4324	Sad.	180^{o}/ 0^{o}
160^{o}	-114.4128	Max.	-114.4220	Sad.	-114.4965	Min.	-114.4220	Sad.	180^{o}/ 0^{o}
179^{o}	-114.4136	Max.	-114.4142	Sad.	-114.4992	Val.	-114.4142	Sad.	180^{o}/ 0^{o}

---

[a] Due to the existence of valleys instead of clear minima at Φ values greater than 85^{o}, the exact location of the minimum might vary from ($\delta_1=0^{o}$,$\delta_2=90^{o}$) on these panels. However, this minimum geometry would still produce D_{2d} allene if the angle Φ were to be opened in a nonrotatory fashion.

shall try to support further later on.

(vii) From the bifurcating transition region the molecule moves downhill towards either of two allene stereoisomers. The motion of the CH_2 planes now becomes more or less conrotatory. (viii) After an opening angle Φ of about 100^{o}, the molecule reaches the slopes of long isoenergetic valleys and will find itself in a state of free synchronized cogwheel-like rotations of the CH_2 planes. (ix) This rotation will degenerate into a rigid body rotation about the C-C-C axis once allene is reached.

(x) Finally, the internal rotation of allene involves bending of the molecule, a result which is consistent with the best previous calculations on that subject.

There is little doubt that the results presented here are qualitatively valid. The characteristics of the surfaces studied are too consistent and the trends observed too regular not to be physically significant. Quantitatively there is however considerable room for improvement. As an example we should cite the reaction barrier whose value of around 40 kcal/mole is clearly too high. Preliminary calculations with larger basis sets at various selected points show that the STO-3G geometries are very reliable and, based on this fact, we shall, later on improve the energetics of the reaction.

IV. BIFURCATIONS AND TRANSITION STATES ON REACTION SURFACES WITH C_s SYMMETRY

A. Introduction

In the preceding section it has been found that the ring-opening of cyclopropylidene has a bifurcation which practically coincides with the transition state. This result in in contradiction to a widely held belief that fundamental theoretical principles forbid pathways of chemical reactions to bifurcate near transition states. Murrell and Laidler (1968) have noted that it is impossible for three or more valleys to join at a transition state on a reaction surface as long as the matrix of second derivatives does not vanish. Murrell and Pratt (1970) as well as Stanton and McIver (1975) have furthermore pointed out that the transition state is completely determined by the requirement that all first derivatives vanish, and that it would be "an unlikely numerical accident" for all second derivatives to vanish as well at this very same point. This limitation is also adopted in a paper by Pechukas (1976). All of these investigations are mainly concerned with the conservation of nuclear symmetry during chemical reactions. In some quarters, these discussions appear to have led to the notion that reaction paths tend to avoid bifurcation in the

neighborhood of transition states.

A simple example of an "unlikely" bifurcating transition state is the "monkey saddle" given by the energy surface

$$E(x,y) = \frac{1}{3} ax^3 - xy^2, \quad a > 0 \qquad (4.A.1)$$

Contours of such a surface are shown in Figure 4.1. The figure also contains some of its orthogonal trajectories, which are given by the equation

$$[(2 + a)x^2 - y^2]y^a = \text{Constant} \qquad (4.A.2)$$

The orthogonal trajectory for Constant = 0 consists of the three straight lines

$$y = 0 , \quad y = x\sqrt{2 + a} , \quad y = -x\sqrt{2 + a} , \qquad (4.A.3)$$

which intersect at the origin. Each of them changes from a valley floor to a ridge crest at the origin. Thus, if a system following the "least energy path" comes up from one of these valley floors, it will encounter the incipient ridge at the origin. It will then change directions and descend into a valley along one or the other of the other two trajectories. The "bifurcation" of the reaction path is thus a consequence of a valley trajectory changing into a ridge

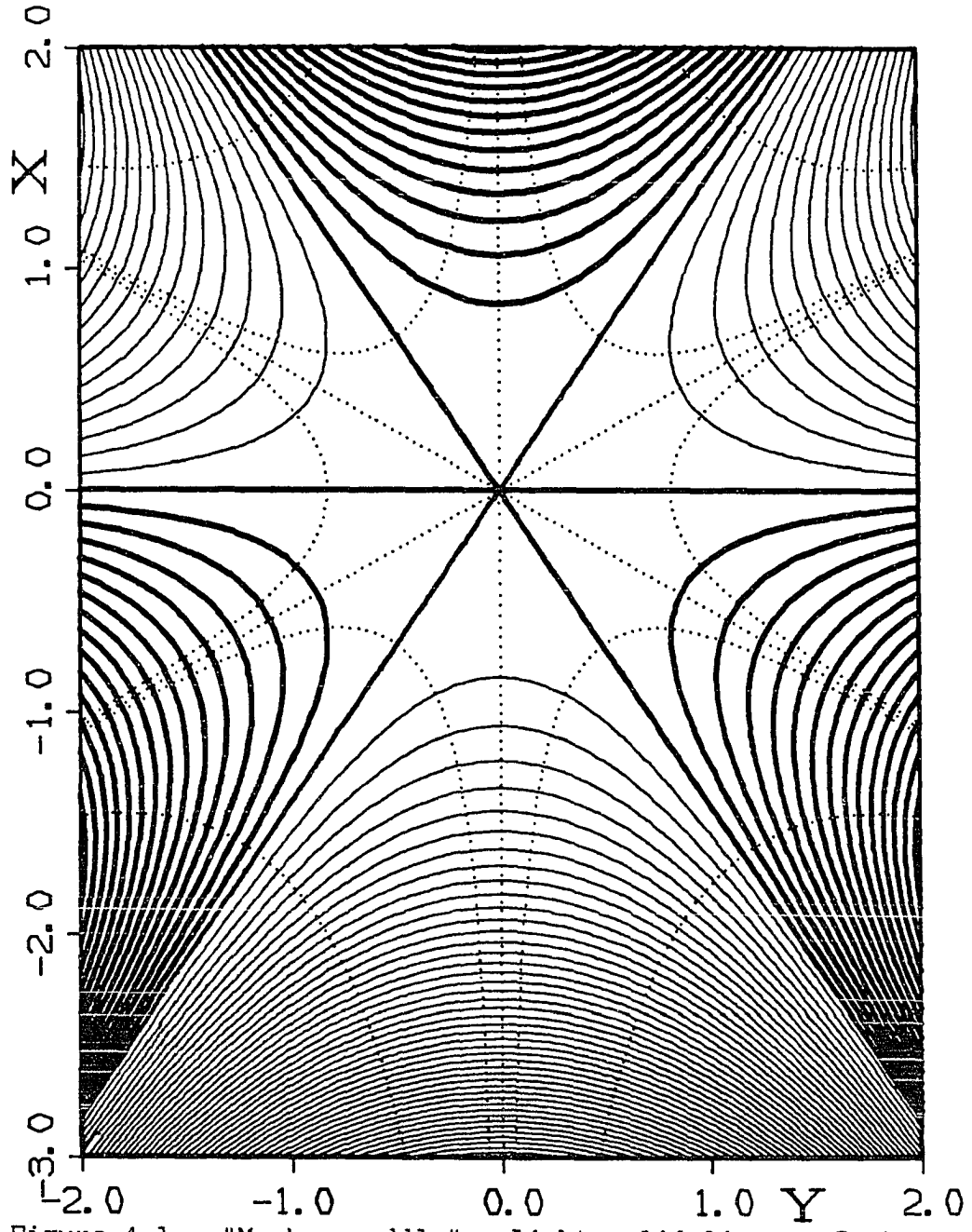

Figure 4.1. "Monkey saddle". Light solid lines: Contours for E < 0. Heavy solid lines: Contours for E > 0. Lowest heavy contour: E = 0. Increment between adjacent contours: 0.3. Dotted lines: Selected orthogonal trajectories

trajectory.

What can be taken as the general characteristic of a bifurcation? For the purpose of the present investigation, the following definition appears useful. If the path of a reaction at first follows the floor of a valley on the reaction surface and then comes to a point where the valley floor turns into a ridge, then the reaction path can be expected to bifurcate near that point (in this investigation we shall not distinguish between a valley and a cirque, nor between a ridge and a cliff). The reason is simple. Whereas the valley floor is a "stable path" in the sense that there exists a restoring force which tends to drive the trajectories of the system back to the floor, the crest of a ridge is an unstable path in as much as the slightest deviation of the system's trajectories will lead to their veering away further and further. If the ridge is approximately evenly sloped on both sides, then there exists a comparable likelihood for the trajectories to fall off the ridge on either side. Bifurcations are thus expected near valley-ridge inflection points. Such points, which we shall call VRI points, can occur of course at places which are not transition states. The condition that a valley change into a ridge is that the second derivative in the direction perpendicular to the orthogonal trajectory marking the valley floor vanishes, i.e.,

$$(\vec{e}\cdot\vec{\nabla})(\vec{e}\cdot\vec{\nabla})E(x,y) = 0 \ , \qquad (4.A.4)$$

where $\vec{e}$ is the direction perpendicular to the valley floor trajectory at the VRI point. This condition implies the equation

$$E_{xx}(E_y)^2 - 2E_{xy}E_xE_y + E_{yy}(E_x)^2 = 0 \ , \qquad (4.A.5)$$

which determines a line in the (x,y) plane. The intersection of this line with the valley floor trajectory uniquely determines the VRI point. It may be noted that on many surfaces the transition from a valley to a ridge is rather gradual, so that it is more realistic to talk about a bifurcation region than about a bifurcation point. Such a region surrounds a VRI point.

In the present section we examine whether VRI points can occur so close to transition points that one has in fact a "bifurcating transition region" in which the energy changes very little or whether such regions are "unlikely" in the sense mentioned in the first paragraph. For simplicity we limit the analysis to reaction surfaces that have C_s symmetry. Such surfaces are not uncommon and the results have general implications. It will be seen that bifurcating transition regions of this kind are in fact not unlikely to

occur and the findings for the cyclopropylidene ring-opening represent a concrete example for this general conclusion. The shapes of surfaces that represent such possible bifurcating transition regions will be analyzed in some detail. They can look fairly different from the aforementioned "monkey saddle". In particular, the exit channels may not have the usual appearance of valleys.

For the experimental chemist, the implication of the present analysis is that there exist no theoretical reasons to avoid the concept of a bifurcating transition state region, when making conjectures about reaction paths and reaction mechanisms.

B. Energy Surface in the Neighborhood of a Valley-Ridge Inflection Point

Consider a reaction surface in terms of two internal coordinates, $E = E(x,y)$, which has C_s symmetry. When the system point lies on the line of symmetry, then the molecular system itself has C_s symmetry. If the system point does not lie on this line, then the molecule does not have C_s symmetry, but there then exists another system point, related to the first by the C_s reflection, which corresponds to the molecular geometry which is the mirror image of the previous one.

If the x-axis is chosen to be identical with the trace of the C_s symmetry plane in the x-y plane, then one has $E(x,-y) = E(x,y)$ and the surface can be expressed in the form

$$E(x,y) = F(x,y^2) \qquad (4.B.1)$$

On the C_s plane, i.e. for $y = 0$, one has then

$$\partial E/\partial y = 0 \qquad (4.B.2)$$

$$\partial^2 E/(\partial y)^2 = 2\ \partial F/\partial(y^2) \qquad (4.B.3)$$

From Eq. (4.B.2) it is apparent that the surface is a valley or a ridge along the x-axis. Specifically,

$$\text{the x-axis is a valley, if } \partial F/\partial(y^2) > 0 \qquad (4.B.4)$$

$$\text{the x-axis is a ridge, if } \partial F/\partial(y^2) < 0 \qquad (4.B.5)$$

We are interested in the neighborhood of those points where a valley changes into a ridge, i.e. where

$$\partial F/\partial(y^2) = 0\ , \qquad (4.B.6)$$

which we called valley-ridge inflection (VRI) points.

Without loss of generality, the origin, where $x = 0$, may be placed at the VRI point whose neighborhood is of interest.

Furthermore, by adding an appropriate constant to E the zero of the energy surface can be shifted to the origin. Thus the conditions

$$F(x,y^2) = 0 \ , \ \partial F/\partial(y^2) = 0 \qquad (4.B.7)$$

are valid at the origin $x = y = 0$ and, hence, the expansion of F up to second order in x and y^2 around the origin has the form

$$F(x,y^2) = A_1x + A_2x^2 + A_3xy^2 + A_4y^4$$

In order to avoid "unlikely situations" in the sense of Section A, we assume that A_2, A_3, A_4 are nonzero. It is then expedient to write this Taylor expansion in the form

$$\bar{E}(x,y) = F(x,y^2) = Ax - B(x + C_1y^2)(x + C_2y^2) \qquad (4.B.8)$$

The first and second derivatives of this function are

$$E_x = A - B[2x + (C_1+C_2)y^2] \ , \qquad (4.B.9a)$$

$$E_y = -2By[(C_1+C_2)x + 2C_1C_2y^2] \ , \qquad (4.B.9b)$$

$$E_{xx} = -2B \ , \qquad (4.B.9c)$$

$$E_{yy} = -2B[(C_1+C_2)x + 6C_1C_2y^2] \ , \qquad (4.B.9d)$$

$$E_{xy} = -2B(C_1+C_2)y \ . \qquad (4.B.9e)$$

In the present context we are interested in transition states and this corresponds to the case that on the x-axis, where $E = Ax - Bx^2$, the surface has a maximum, implying that the value of B is positive. We further assume that for large negative x-values we start in a valley on the x-axis. In view of the choice of the origin, this implies that the x-axis is a valley for $x < 0$ and a ridge for $x > 0$. Since, according to Eq. (4.B.9d) one has $E_{yy} = -2B(C_1+C_2)x$ on the x-axis, it follows furthermore that the value of (C_1+C_2) is positive. There exist therefore two cases for the values of C_1 and C_2: Both are positive or the two have opposite signs, the positive being the larger one in absolute value. The maximum on the x-axis occurs for

$$x_m = A/2B \ , \qquad (4.B.10)$$

at which point the energy surface assumes the value

$$E_m = A^2/4B > 0 \ . \qquad (4.B.11)$$

If A is positive, then the point $(x_m, 0)$ lies on the ridge part of the x-axis and is a true (relative) maximum of the surface since, according to Eqs. (4.B.9c,d,e) one has $E_{xx} < 0$, $E_{yy} < 0$, $E_{xy} = 0$ at this point. On the other hand,

if A is negative, then this point lies in the valley part of the x-axis and it is a saddle point, since Eqs. (4.B.9c,d,e) now yield $E_{xx} < 0$, $E_{yy} > 0$, $E_{xy} = 0$. If the value of A vanishes, then the point $(x_m, 0)$ lies at the origin and is a higher order point, a kind of saddle where, however, the valley changes into a ridge.

For the purpose of discussing the contours of the energy surface, it is useful to note that the function of Eq. (4.B.8) can also be expressed in the factored form

$$E = E_0 - B(x + c_1y^2 - x_1)(x + c_2y^2 - x_2) , \quad (4.B.12)$$

where the constants E_0, x_1, x_2 are defined by

$$E_0 = (1-\gamma^2)E_m , \; x_1 = (1+\gamma)x_m , \; x_2 = (1-\gamma)x_m , \quad (4.B.13)$$

with E_m and x_m being the quantities given by Eqs. (4.B.10), (4.B.11) and γ being defined by

$$\gamma = (c_1 + c_2)/(c_1 - c_2) \quad (4.B.14)$$

It is apparent that the contour corresponding to the energy value $E = E_0$ consists of the union of the two parabolas

$$x = x_1 - c_1 y^2 \quad \text{and} \quad x = x_2 - c_2 y^2 \ . \qquad (4.B.15)$$

In order to gain further insight in these surfaces, it is necessary to discuss the various possible choices for A, B, C_1, C_2 separately.

C. First Case (A = 0)

Whereas it was no loss of generality to place the origin at the VRI point, it cannot be expected in general that one has also $E_x(x=0,y=0) = A = 0$ at this same point, i.e. that the origin is a stationary point as well as a VRI point. In the spirit of the arguments quoted in Section A such a coincidence would be considered as "unlikely". Nonetheless it is of interest to discuss this case first, before considering the general (and <u>not</u> "unlikely") case of nonvanishing A. If A vanishes then we can, with no loss of generality, consider the prototype function

$$E(x,y) = - (x + c_1 y^2)(x + c_2 y^2) \ . \qquad (4.C.1)$$

On the x-axis, the maximum occurs at the origin, where E = 0. It is apparent that the contours going through the origin are given by the two parabolas

$$(x + c_1 y^2) = 0 \text{ and } (x + c_2 y^2) = 0 \ . \qquad (4.C.2)$$

Figure 4.2 displays the contours for Case (1a), i.e. when c_1 and c_2 are both positive, together with some typical orthogonal trajectories. The -x axis is seen to be the bottom of a valley which ascends to the origin. The descent into the +x direction is along a ridge. The contours that go through the origin, i.e. E(x,y) = 0, are the two parabolas of Eq. (4.C.2) that touch at the origin. The surface ascends in all directions that lie between these two parabolas. The origin has thus the character of a transition state. Since the descent into the +x direction is along a ridge, a reacting system that has come up the valley from the -x direction, will fall off this ridge soon after passing through the transition state. It would however seem artificial to associate its descent with any particular orthogonal trajectory. The origin is therefore a bifurcating transition state where only the entrance channel is a valley in the usual sense.

In the special case where $c_1 = c_2$, the two parabolic contours that pass through the transition state coincide and the ridges going uphill from the transition state disappear. The contours and some orthogonal trajectories are shown in Figure 4.3. They are all parabolas $(x + c_1 y^2) = \text{const}$. It is to be noted however, that all contours have $E < 0$. The

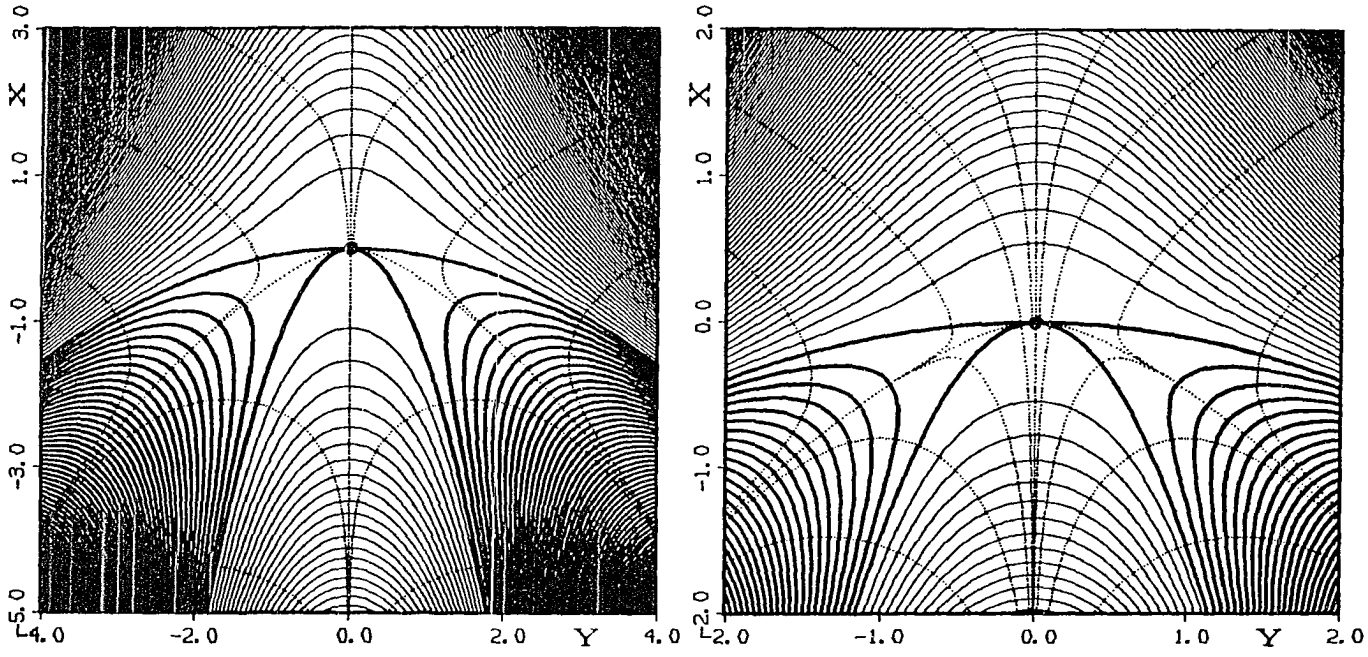

Figure 4.2. The surface $E = -(x+1.5y^2)(x+0.1y^2)$. The right panel is an enlargement of the area near the VRI point which is identified by a heavy dot. Light solid lines: Contours for $E < 0$. Heavy solid lines: Contours for $E > 0$. Lowest heavy contour: $E = 0$. Increment between adjacent contours: 1.2 on left panel, 0.3 on right panel. Dotted lines: selected orthogonal trajectories

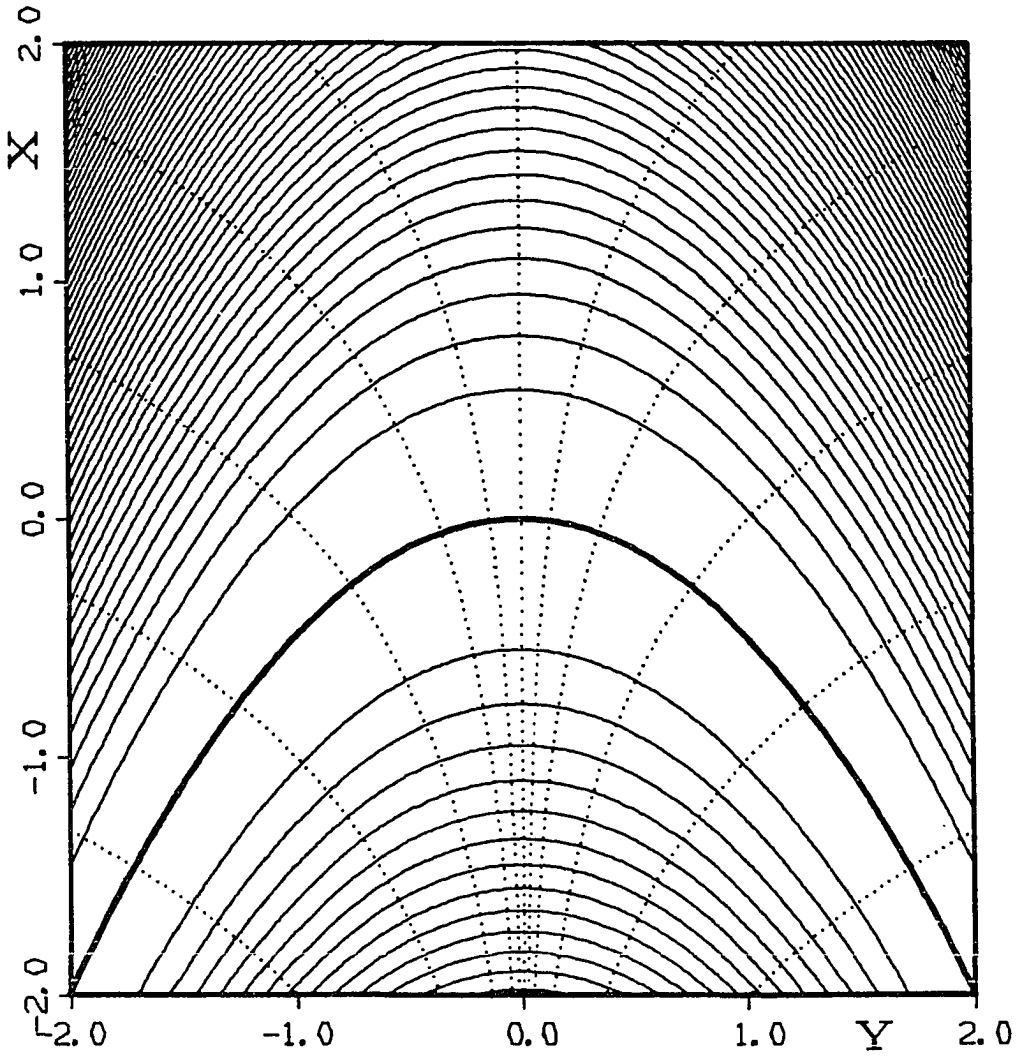

Figure 4.3. The surface $E = -(x+0.5y^2)^2$. Light solid lines: Contours for $E < 0$. Heavy solid line: Contour for $E = 0$. Increment between adjacent contours: 0.3. Dotted lines: Selected orthogonal trajectories

value of E decreases in both the +x and -x directions. We still have a valley on the -x axis and a ridge on the +x axis.

Figure 4.4 displays the contours and some orthogonal trajectories for Case (1b) i.e. when c_1 and c_2 have opposite signs such that $c_1 + c_2 > 0$. The main difference from Figure 4.2 is that one of the parabolic contours going through the transition state has reversed its curvature. It is the one corresponding to $c_2 < 0$. As before the surface ascends uphill from the transition state in all directions between the two transition state parabolas. As before the -x direction is an ascending valley. As before the +x axis is a descending ridge, so that the origin is again a bifurcation point. It is seen however that, now, two valley-like formations have developed on both sides of the +x axis ridge. In this case, the origin is a bifurcating transition state where the exit channels have somewhat the character of valleys.

For the special case where $c_1 = -c_2$ the contours and orthogonal trajectories are those shown in Figure 4.5. The ridge on the +x axis has disappeared in agreement with the fact that now $E_{yy} = 0$ everywhere on the x-axis (see Eq. 4.B.9d). The surface has now the simple form

$$E(x,y) = -x^2 + c_1^2 y^4 \ , \qquad (4.C.3)$$

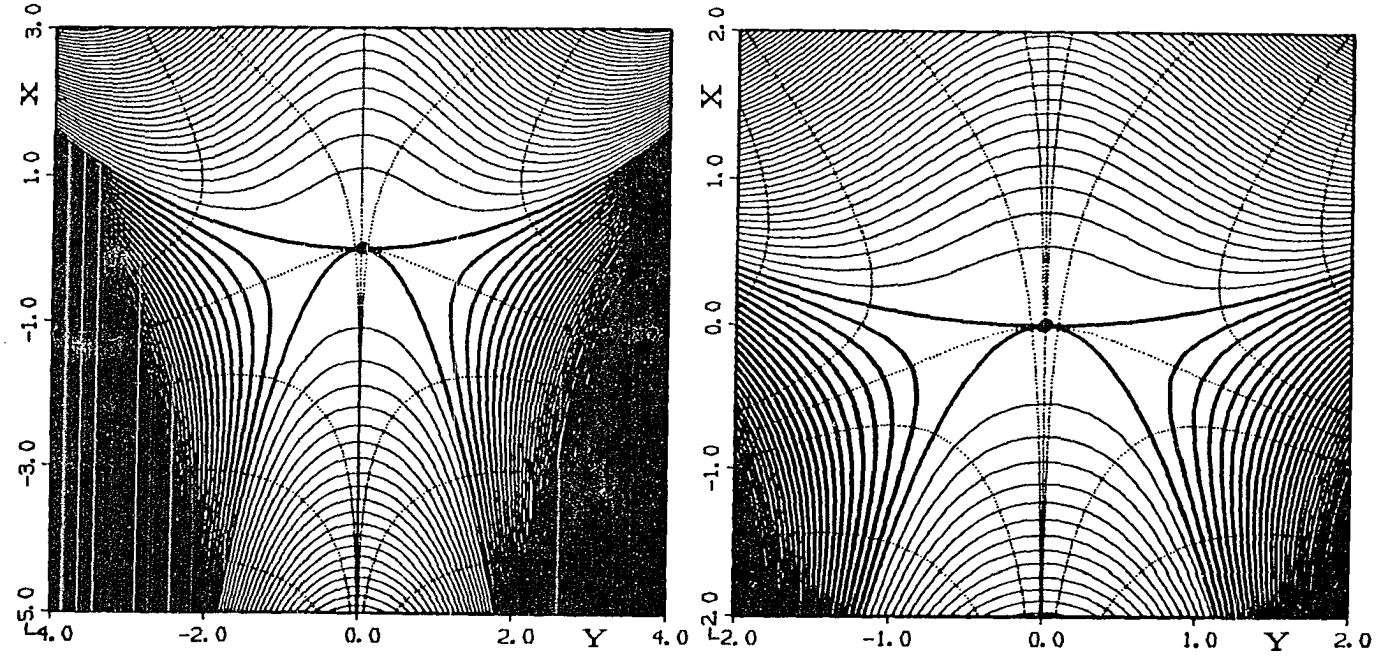

Figure 4.4. The surface $E = -(x+1.5y^2)(x-0.1y^2)$. The right panel is an enlargement of the area near the VRI point which is identified by a heavy dot. Light solid lines: Contours for $E < 0$. Heavy solid lines: Contours for $E > 0$. Lowest heavy contour: $E = 0$. Increment between adjacent contours: 1.2 on the left panel, 0.3 on the right panel. Dotted lines: Selected orthogonal trajectories

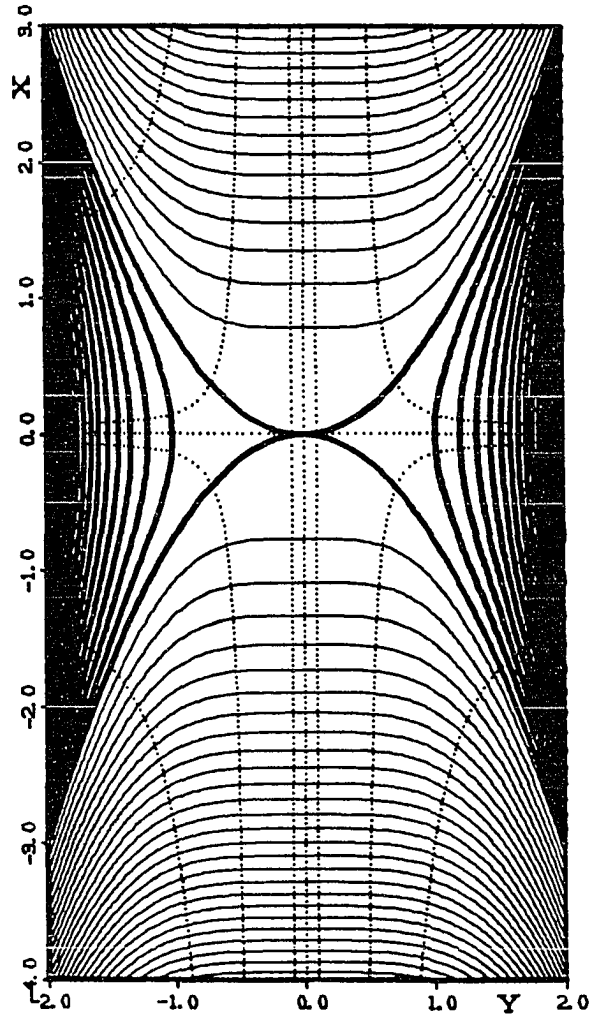

Figure 4.5. The surface $E = -(x+0.75y^2)(x-0.75y^2)$. Light solid lines: Contours for $E < 0$. Heavy solid lines: Contours for $E > 0$. Lowest heavy contour: $E = 0$. Increment between adjacent contours: 0.6. Dotted lines: Selected orthogonal trajectories

and the origin is similar to an ordinary saddlepoint that lies at the intersection of two orthogonal trajectories, one connecting two valleys, the other connecting two ridges. But in contrast to a second-order saddlepoint, the contours passing through the saddle are tangent to each other rather than intersecting with a finite angle.

D. Second Case (A < 0)

As discussed in the text after Eq. (4.B.11), there exists a saddlepoint on the negative x-axis when A is negative. It is now expedient to choose the distance of this saddlepoint from the origin [$|x_m| = -A/2B$, see Eq. (4.B.10)] as unit of length and the value of E at the saddle point [$A^2/4B$, see Eq. (4.B.11)] as unit of energy. Through this choice of units the general expression (4.B.8) becomes

$$E(x,y) = -2x - (x + c_1y^2)(x + c_2y^2) \ , \qquad (4.D.1)$$

where $c_1 = |A/2B|C_1$, $c_2 = |A/2B|C_2$.

Figure 4.6 exhibits the contours and orthogonal trajectories for Case (2a) where c_1 and c_2 are both positive. The difference from Case (1a), where A = 0 is that the transition state has separated from the VRI point at the origin. The transition state is the saddlepoint at x = -1.

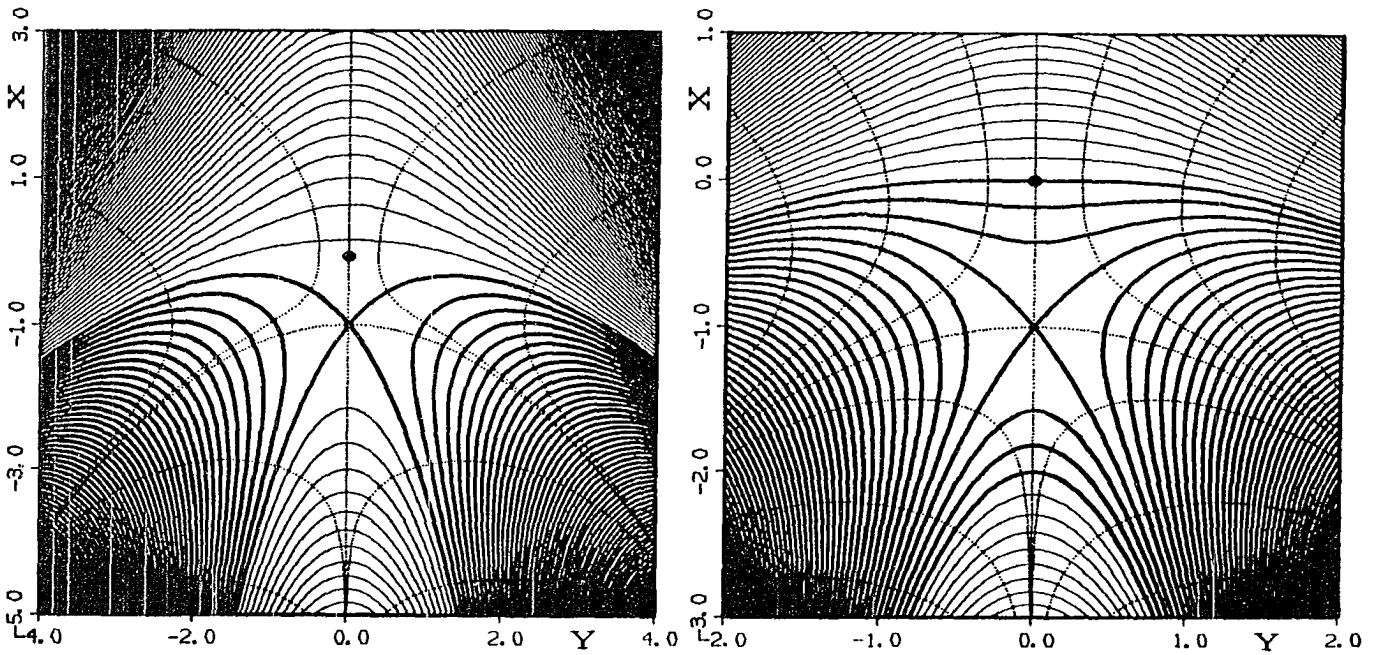

Figure 4.6. The surface $E = -2x-(x+1.5y^2)(x+0.1y^2)$. The right panel is an enlargement of the region near the VRI point which is identified by a heavy dot. Light solid lines: Contours for $E < 0$. Heavy solid lines: Contours for $E > 0$. Lowest heavy contour: $E = 0$. Increment between adjacent contours: 1.333 on the left panel, 0.333 on the right panel. Dotted lines: Selected orthogonal trajectories

Coming up the valley from -x, the reaction path reaches this saddlepoint and then descends in a short valley towards the origin, where the valley turns into a ridge. The reaction path will then bifurcate towards the left or the right of this ridge. The exit channels do not have the character of valleys.

Figure 4.7 shows the contours and orthogonal trajectories for Case (2b) where c_1 and c_2 have opposite signs. The differences in the contours between Figures 4.6 and 4.7 is similar to that between Figures 4.2 and 4.4. Everything that has been said for Figure 4.6 also applies to Figure 4.7. The main difference is that the exit channels have somewhat the character of valleys.

If the distance between the saddlepoint and the valley ridge inflection point, on either of these surfaces, is short compared to the overall length of the reaction path and if, in addition, the energy difference between these two places on the surface is small compared to their elevation over the reactant and product energies, then it is justified to consider the region encompassing both the saddlepoint and the valley ridge inflection point, as a <u>bifurcating transition state region</u>. For all intents and purposes, the bifurcation of the reaction path occurs immediately after passing through the saddle.

In the special case where $c_1 = -c_2$, one has again

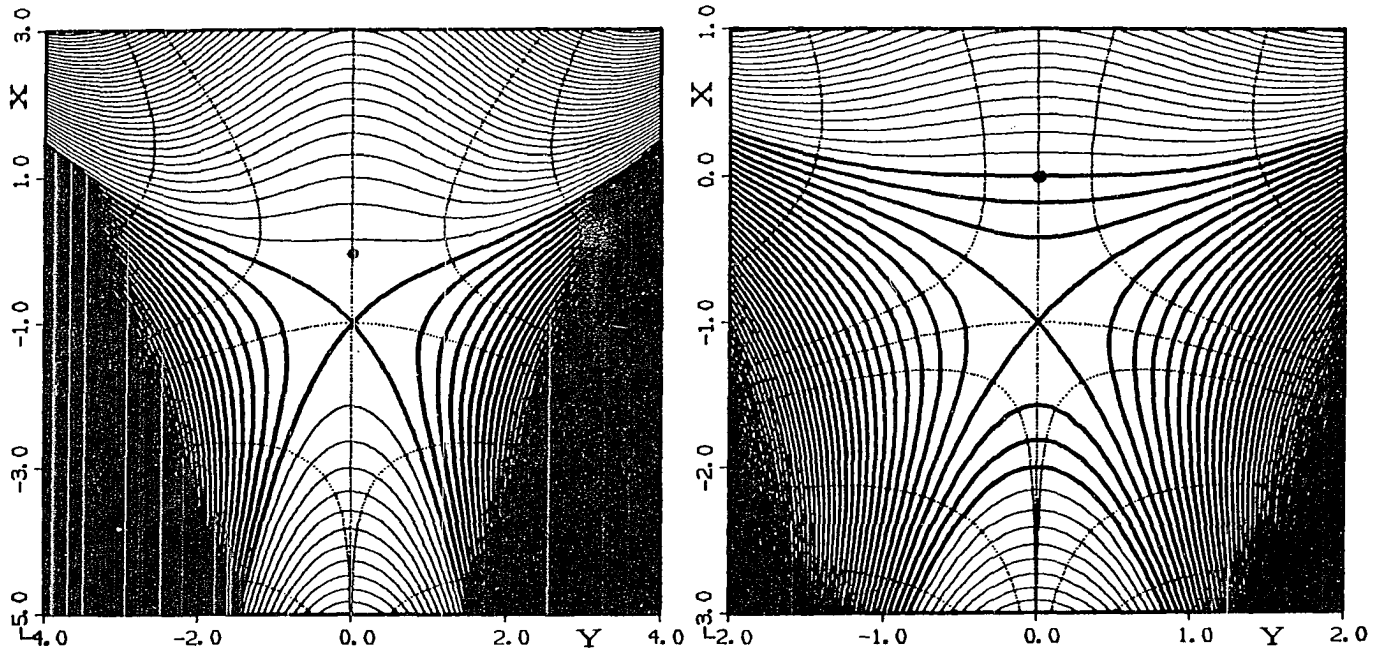

Figure 4.7. The surface $E = -2x-(x+1.5y^2)(x-0.1y^2)$. The right panel is an enlargement of the region near the VRI point which is identified by a heavy dot. Light solid lines: Contours for $E < 0$. Heavy solid lines: Contours for $E > 0$. Lowest heavy contour: $E = 0$. Increment between adjacent contours: 1.333 on the left panel, 0.333 on the right panel. Dotted lines: Selected orthogonal trajectories

$E_{yy} = 0$ on the entire x axis (See Eq. 4.B.9d). The resulting surface

$$E = -2x - x^2 + c_1^2 y^4 \qquad (4.D.2)$$

differs from that of Eq. (4.C.3) only by the shift of the maximum to x = -1. The contours can therefore be obtained from those of Figure 4.5 by a corresponding shift along the x-axis and increasing all contour values by adding 1.0.

E. Third Case (A > 0)

As discussed in the text after Eq. (4.B.12), the maximum on the x-axis occurs for a positive x value when A is positive. It is furthermore a relative maximum in every direction. As in the preceding section, it is expedient to use its distance from the origin [$x_m = A/2B$, Eq. (4.B.10)] as unit of length and to choose the energy difference between the maximum and the origin [$A^2/4B$, Eq. (4.B.11)] as unit of energy. Thereby the energy surface becomes

$$E(x,y) = 2x - (x + c_1 y^2)(x + c_2 y^2) \; . \qquad (4.E.1)$$

Figure 4.8 displays the contours and orthogonal trajectories of a surface of Case (3a) corresponding to Eq.

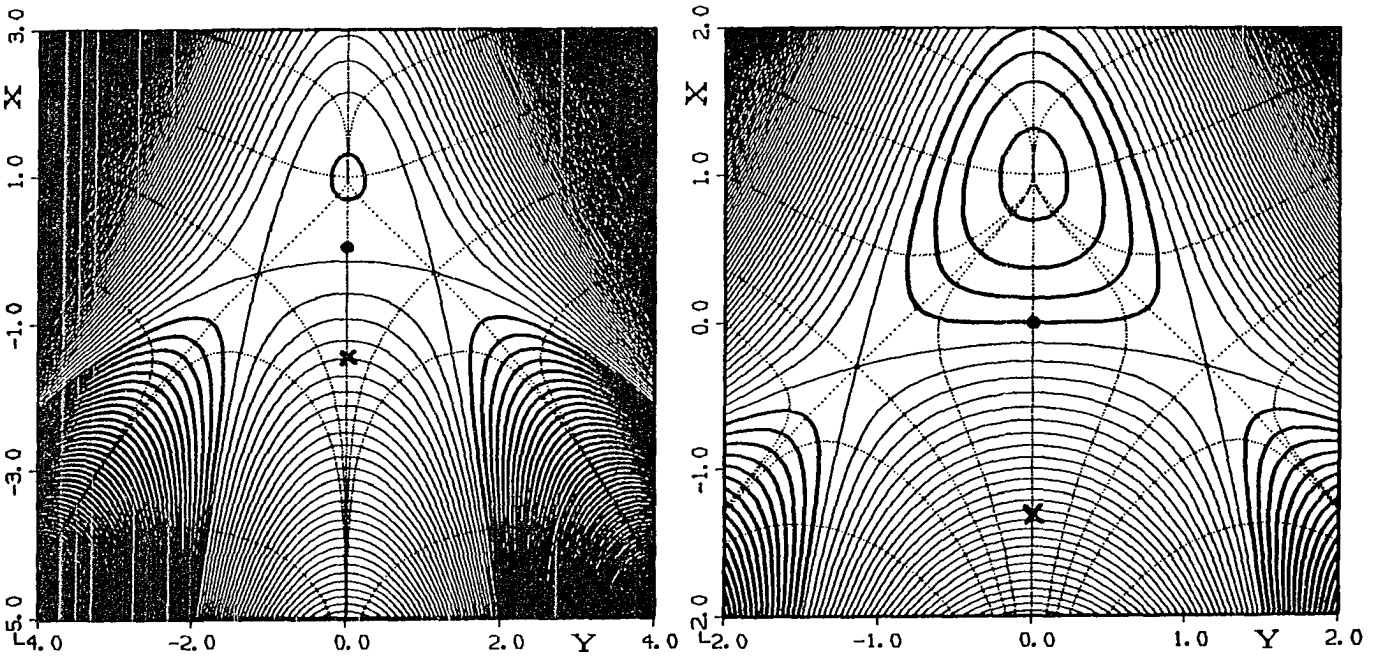

Figure 4.8. The surface $E = 2x-(x+1.87706y^2)(x+0.12294y^2)$. The right panel is an enlargement of the region near the VRI point which is identified by a heavy dot. Light solid lines: Contours for $E < 0$. Heavy solid lines: Contours for $E > 0$. Lowest heavy contour: $E = 0$. Increment between adjacent contours: 1.2 on the left panel, 0.3 on the right panel. Dotted lines: Selected orthogonal trajectories

(4.E.1) with $c_1 > 0$, $c_2 > 0$, $c_1 > c_2$. Figure 4.9 displays the contours and orthogonal trajectories for Case (3b) corresponding to Eq. (4.E.1) with $c_1 > 0$, $c_2 < 0$, $c_1 > |c_2|$. It is seen that, in both cases, the surface has two saddlepoints off the x-axis. The positions of these saddlepoints are obtained by using, in the stationary condition $E_x = E_y = 0$, the derivative expressions (4.B.9a), (4.B.9b) in conjunction with the surface of Eq. (4.E.1). Assuming that y does not vanish, one thereby obtains the equation set

$$2x + (c_1+c_2)y^2 = 1 \ , \qquad (4.E.2a)$$

$$(c_1+c_2)x + 2c_1c_2y^2 = 0 \ , \qquad (4.E.2b)$$

which has the solution

$$x_s = 1 - \gamma^2 \ , \quad y_s^2 = \gamma^2/c \ , \qquad (4.E.3)$$

where

$$\gamma = (c_1 + c_2)/(c_1 - c_2) \ , \ c = (c_1 + c_2)/2 \qquad (4.E.4)$$

It should be noted that both γ and c are positive in all cases. Hence, one has indeed two real stationary points, corresponding to $y_s = \pm \gamma/\sqrt{c}$. For c_1 and c_2 both positive,

one has $\gamma > 1$ and hence $x_s < 0$; for $c_1 > 0$, $c_2 < 0$ (but $c_1 > |c_2|$), one has $\gamma < 1$ and hence $x_s > 0$, in agreement with Figures 4.8 and 4.9. The value of the surface at the saddlepoints is found to be

$$E_s = 1 - \gamma^2 \ . \qquad (4.E.5)$$

The contour which passes through the saddlepoint intersects the x-axis for

$$x' = 1+\gamma \quad \text{and} \quad x'' = 1-\gamma \qquad (4.E.6)$$

According to Eqs. (4.B.12-14) the surface of Eq. (4.E.1) can also be expressed in the factored form

$$E(x,y) = (1-\gamma^2) - [x + c_1y^2 - (1+\gamma)][x + c_2y^2 - (1-\gamma)] \ , \qquad (4.E.7)$$

from which, in conjunction with Eq. (4.E.5), it is apparent that the contours passing through the saddlepoints are the parabolas given by

$$x = (1+\gamma) - c_1y^2 \ , \quad x = (1-\gamma) - c_2y^2 \ . \qquad (4.E.8)$$

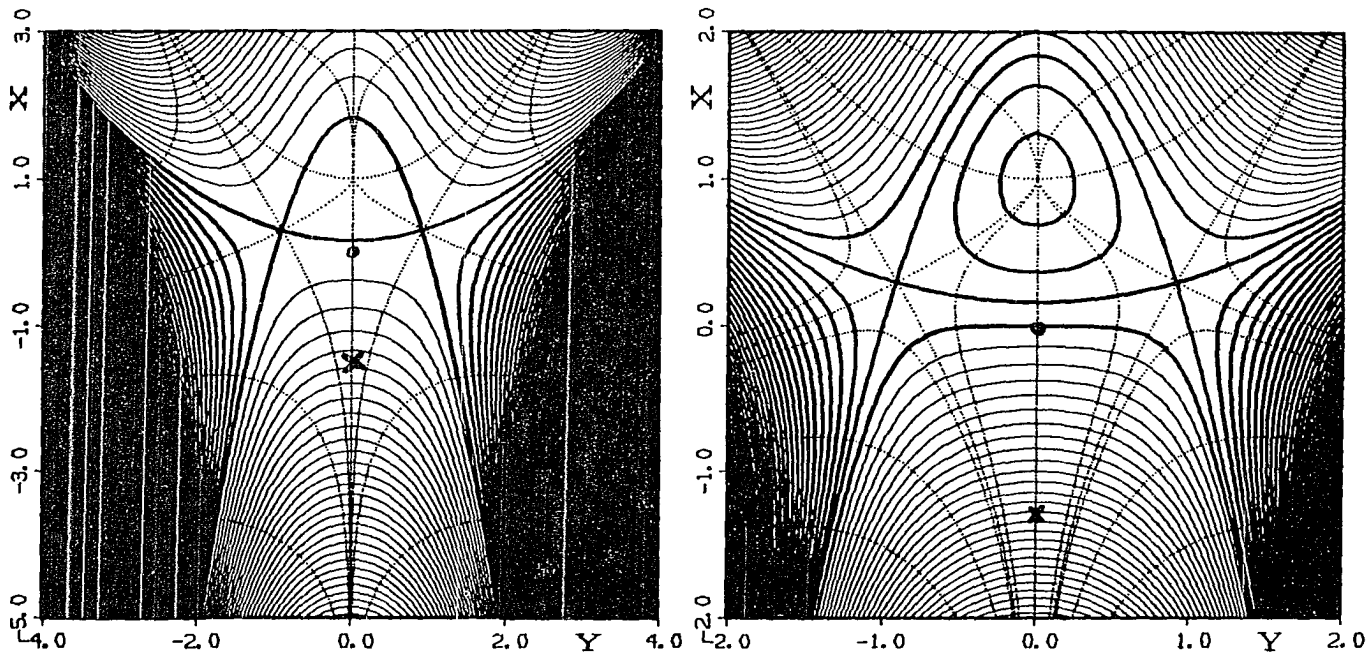

Figure 4.9. The surface $E = 2x-(x+1.83666y^2)(x-0.16334y^2)$. The right panel is an enlargement of the region near the VRI point which is identified by a heavy dot. Light solid lines: Contours for $E < 0$. Heavy solid lines: Contours for $E > 0$. Lowest heavy contour: $E = 0$. Increment between adjacent contours: 1.2 on the left panel, 0.3 on the right panel. Dotted lines: Selected orthogonal trajectories

(It may be noted that, for the surfaces discussed in the preceding section, see Eq. (4.D.1), the first stationary condition, analogous to Eq. (4.E.2a), has the value (-1) on the right hand side. This leads to the solution $y_s^2 = -\gamma^2/c$ instead of Eq. (4.E.3). Since c is positive, it follows that there is no real saddlepoint off the x-axis, in agreement with the discussion in section D.)

The present case is interesting as regards the concept of bifurcation. For large negative x values, there is nothing peculiar about the entrance valley. If the system would follow a reaction path along the valley floor trajectory, it would encounter the incipient ridge at the VRI point x = 0. It would discover a bit late, so it seems, that it would have been better off to veer earlier toward one of the saddlepoints. On the other hand, if the value of $|E_s|$ is small compared to $|E_R|$, with E_R being the energy of the reactant, and if y_s is small compared to $|x_R|$, the distance of the reactant from the origin, then it would be unphysical to consider the beginning of the bifurcation at the location of the reactant. A reasonable choice for the bifurcation point in this case would seem to be the intersection of the two straight lines which are tangent to the downhill trajectories at the two saddle points and which intersect on the x-axis. It is apparent that each of these straight lines

is the bisectrix of the tangents to the two intersecting contours at the respective saddle point. These contours are given by Eq. (4.E.8) and, at the saddle points, their tangential slopes are

$$m_1 = \pm 2(\gamma+1)\sqrt{c} \ , \quad m_2 = \pm 2(\gamma-1)\sqrt{c} \ , \qquad (4.E.9)$$

where the positive signs apply when y_s is negative and the negative signs apply when ys is positive. The slopes of the downhill trajectories at the saddle points are then given by $\pm m$ where m is

$$m = (1 - M_1 M_2)/(M_1 + M_2) \qquad (4.E.10)$$

with

$$M_k = (1 + \sqrt{1+m_k^2})/m_k \ , \quad k = 1,2 \ . \qquad (4.E.11)$$

It may be noted that m is positive when y_s is positive, and that m is negative when y_s is negative. From these slopes and the saddlepoint coordinates [Eq. (4.E.3)] the x-coordinate of the bifurcation point is found to be

$$x_B = 1 - \gamma^2 - |m|\gamma/\sqrt{c} \ . \qquad (4.E.12)$$

It is indicated in Figures 4.8 and 4.9 by cross marks.

In the case $c_1 = -c_2$ the surface simplifies to

$$E = 2x - x^2 + c_1^2 y^2 \qquad (4.E.13)$$

which is similar to the surface of Eq. (4.C.3) shown in Figure 4.5. It differs from it only by a shift of the maximum onto the +x axis.

F. Applications to the Cyclopropylidene-Allene Case

The preceding discussion can be applied directly to the cyclopropylidene-allene ring-opening reaction energy surface, in particular in the form exhibited in Figure 4.6. All the ingredients appear to be present for the existence of one of the previously discussed cases, most probably case (3c). We note the existence of the ascending valley which turns into a ridge at at valley-ridge inflection (VRI) point, and the valley-like character of the exit channels. These features are even more apparent in Figure 4.10a, which exhibits an enlargement of a small area around the transition region. The small inscribed rectangle delineates the area where the curvature of the lines is such that a reasonable analytic fit of the type discussed in the preceding sections can be

Figure 4.10. The reaction surface for the ring opening described by Eq. (4.5.1). The coordinates x and y are defined in the text. Top panel (a): Contours of the actual surface; the increment is 0.5 millihartree. Middle panel (b): Contours of the analytical least mean squares fit $F = A_0 + B_1x + B_2y^2 + C_1x^2 + C_2y^4 + C_3xy^2$ of the area inside the inscribed rectangle. Bottom panel (c): Same as top panel except inscribed rectangle points are now replaced by the ones from fit in (b)

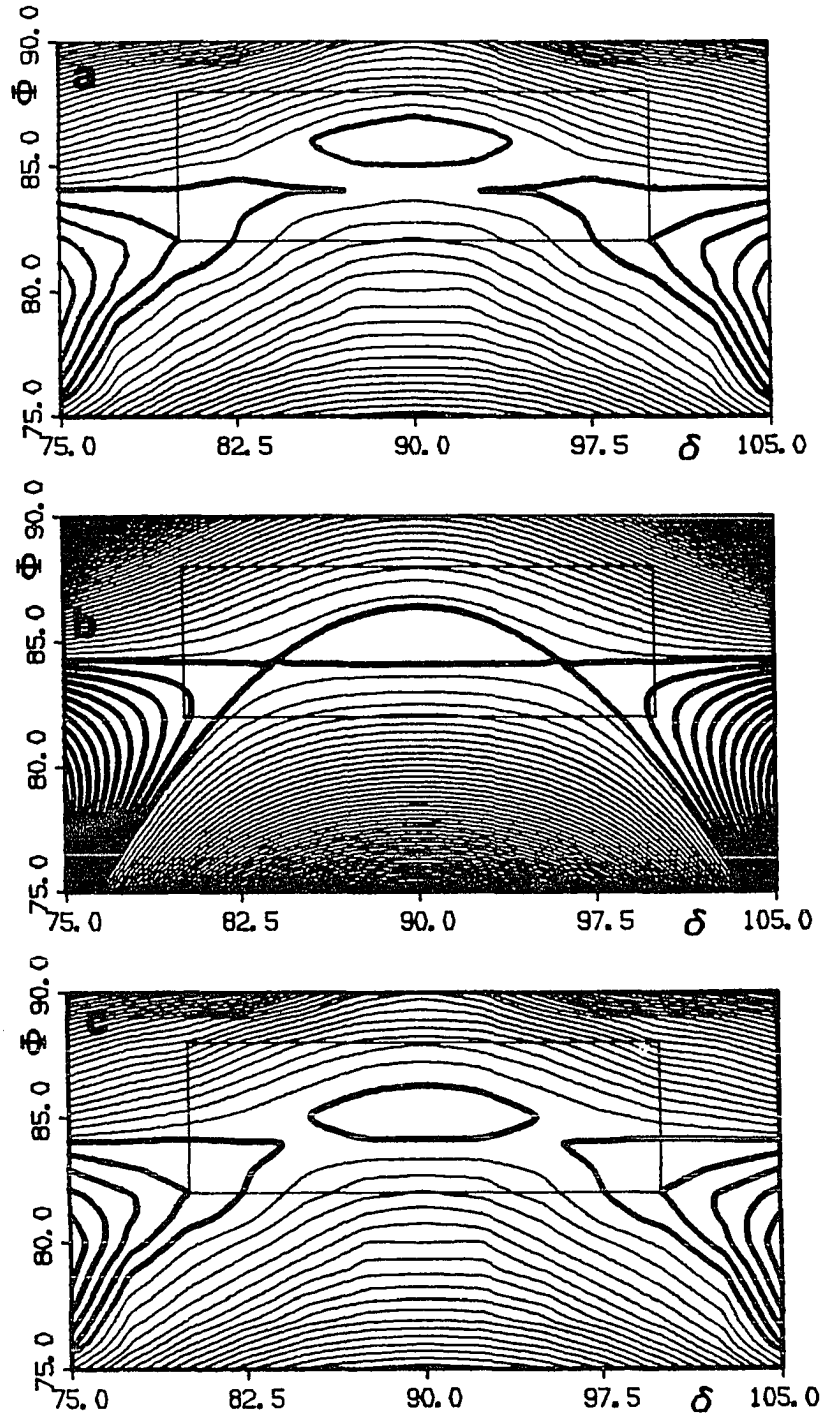
a
b
c
Φ
90.0
85.0
80.0
75.0
75.0
82.5
90.0
97.5
105.0
δ

expected. Outside this rectangle the contours change slope rather sharply, a feature that would tend to mask the real behavior in the interesting area near the VRI point, if it were included in the analytical fit.

An expression of the type shown in Eq. (4.B.8) was fitted to the theoretically calculated points within the inscribed rectangle of Figure 4.10a. The parameters of the fit turned out to be:

$$A = 7.78085 \times 10^{-2}$$

$$B = -3.30738 \times 10^{-1}$$

$$C_1 = 1.52592 \times 10^{-1}$$

$$C_2 = -2.05250 \times 10^{-3}$$

with a standard deviation of 4.06%. The resulting analytical surface, extrapolated to cover the same area as Figure 4.10a, is shown in Figure 4.10b. The fit is noticeably good within the fitted area (within the inscribed rectangle), but deviates outside of it, as one would expect in such a case.

Figure 4.10c is a combination of Figures 4.10a and 4.10b. The points within the inscribed rectangle have been substituted with points from the analytically fitted surface, while the rest of the area is left as originally calculated.

We believe that Figure 4.10c is a more accurate rendition of the true surface around the transition region

than Figure 4.10a. The reason for this belief is that to create contours to fit random data, the appropriate computer program interpolates in order to get enough points to produce smooth contours. This interpolation is, in general, good, but in this particular case, where the characteristics of the function are known, a general interpolation algorithm cannot be expected to produce results that are as accurate as those produced by an interpolation tailored to the problem at hand.

G. Conclusions

The difference between the present analysis and previous approaches lies in the choice of the valley-ridge inflection point as the basic concept for the discussion of bifurcations, and in the explicit examination of a higher-than-second-order Taylor expansion around such points. This analysis has led to the following conclusions:

(i) The nature of bifurcations on analytical surfaces, near transition states or otherwise, is such that it is more reasonable to associate them with small regions rather than with single points.

(ii) There exists a finite domain for the values of the Taylor expansion coefficients, such that the neighborhood of a VRI point acquires the character of a bifurcating transition region if the coefficients fall

in this domain. Such regions are therefore no oddities. They can occur in particular when a reaction leads to products of lower symmetry.

(iii) Even if the entrance channel is a valley, the exit channels may have appearances which are different from valleys in the usual sense.

(iv) If the bifurating transition region of a reaction is small enough, then it may be useful to use the corresponding "unlikely" Case 1 surface (A = 0) as a simplified mathematical model for certain discussions.

The reaction surface which was obtained for the cyclopropylidene-allene ring-opening demonstrates that bifurcating transition regions do occur in practice.

V. EXTENDED BASIS SET CALCULATIONS

A. Introduction

Although there is little doubt that the results obtained in Chapter III are qualitatively valid, there is certainly room for quantitative improvement in the calculated energy differences. The STO-3G minimal basis set, although usually giving good geometries, cannot be reasonably expected to reproduce consistently correct energy barriers. Moreover, some of the values obtained differ from the data inferred from experiments, e.g. the ring-opening activation energy of 40 kcal/mole is probably too high.

In order to obtain reliable energetics it was therefore judged to be imperative to repeat the calculations for the key regions of the reaction surface using a substantially improved extended basis set. Preliminary tests showed that some symmetry constraints were necessary in order to keep the problem within the limits of feasibility of the available programs. We were therefore limited to those points on the energy curve which exhibit symmetry higher than C_1, effectively excluding all points between the transition state and the final product. Similarly, the reoptimization of the geometries for a given set of (Φ,δ_1,δ_2) values with the extended basis set exceeded the capabilities of the GAMESS

program. However, extended basis set calculations for some STO-3G geometries were compared to such calculations at other optimized geometries (for example the 3-21G geometries of Angus, Schmidt and Johnson (1985)). In all cases, the STO-3G geometries yielded lower energies. Moreover, the STO-3G geometry for allene (the only species in the course of the reaction for which an experimental geometry is available) differs from the experimental one (as given by Herzberg (1966)) by only 0.011 A for the C=C bond lengths, 0.004 A for the C-H bond lengths and 0.9^{o} for the C=C-H bond angles. It is therefore to be expected that the geometries obtained by reoptimizing the remaining 12 internal coordinates would differ only little from those obtained in the last section.

B. Calculational Details

The basis sets used in these calculations were even-tempered Gaussian bases of double-zeta quality (for a discussion of even-tempered basis sets see Feller and Ruedenberg (1979) and Schmidt and Ruedenberg (1979)), contracted in the way first suggested by Raffenetti (1973). The Carbon (14s7p/3s2p) and the Hydrogen (6s/2s) bases were taken from Schmidt and Ruedenberg (1979), with the Hydrogen exponents scaled by 1.2. One d polarization function was added to each Carbon with the exponent taken from Dunning and

Hay (1977). This choice yields a total of 147 primitive atomic orbitals contracted to 53 quantitative basis orbitals. Calculations with a somewhat smaller basis set, namely the Dunning-Hay basis consisting of the segmented contractions (9s5p/3s2p) on Carbon and (4s/2s) on Hydrogen without polarization functions, gave unsatisfactory results.

Calculations were performed starting with cyclopropylidene for increasing Φ values maintaining C_s symmetry, i.e. keeping $\delta_1+\delta_2=180^o$. For each value of Φ, enough calculations were performed along the disrotatory line ($\delta=\{(\delta_1+\delta_2)/2\}=90^o$) to determine the minimum on that line. These calculations determined the uphill portion of the reaction path. The calculations were discontinued after a value of Φ was reached for which the energy started to decrease, indicating that the transition state had been passed. Furthermore, the energies for allene and for the transition state of the internal rotation of allene were also calculated with the extended basis set.

All calculations were performed using the ALIS system of programs, developed by Elbert, Cheung and Ruedenberg (1980).

C. Results

Table 5.1 lists the results obtained by these calculations. Each row corresponds to a particular Φ value,

Table 5.1. Extended basis set [Carbon: (14s7pld/3s2pld), Hydrogen: (6s/2s)] calculations along the line $\delta_1+\delta_2=180^{o}$ for various values of Φ. (Energies in Hartrees)

	δ_1,δ_2					
Φ	90,90	80,100	70,110	60,120	50,130	40,140
59.5	-115.82693					
70.0	-115.81352	-115.81369	-115.81242			
75.0	-115.80167	-115.80347	-115.80653	-115.80680	-115.80428	
80.0			-115.79837	-115.80422	-115.80346	
82.0				-115.80295	-115.80451	-115.79888
84.0				-115.80343	-115.80547	-115.80385

Allene: -115.93060

Allene stereoisomerization transition state: -115.86369

while each column corresponds to a position on the line $\delta=90^{o}$, identified by the corresponding pair of dihedral angles (δ_1,δ_2). Unfilled entries indicate that a calculation for that geometry was considered unnecessary. At the bottom of the table, the energies for allene and its internal rotation transition state are shown.

The STO-3G calculation results implied that the hydrogen pairs begin their disrotatory motion only when Φ has reached a value of about 80^{o}. By contrast, with the extended basis set, this disrotatory motion (i.e. the first bifurcation) on the reaction path occurs already before $\Phi=70^{o}$. It is also apparent that the transition state occurs "earlier" than for the STO-3G basis. In the latter case it happened for a Φ value of 84.2^{o}. Now this second bifurcation occurs for $\Phi=80.7^{o}$. Moreover, the hydrogen atoms have rotated slightly less at the transition state ($\delta_1=55^{o},\delta_2=125^{o}$ instead of $\delta_1=50^{o},\delta_2=130^{o}$).

From the results presented in Table 5.1, the critical energies of the reaction, namely the ring-opening barrier, the ring-opening reaction exothermicity and the allene stereoisomerization barrier, can be easily deduced. They are listed in the right-hand column of Figure 5.1. The left-hand column shows the values obtained with the STO-3G basis set. It is seen that two of the three critical energies are correctly obtained with the latter basis, but use of the

CRITICAL ENERGIES (Kcal/mole)

	Minimal Basis (STO-3G)	Extended Basis C:(9S5P/3S2P) H:(4S/2S)	Extended Basis C:(14S7P1D/3S2P1D) H:(6S/2S)
Ring Opening Reaction Energy	65	82	65
Ring Opening Barrier	40	13.5	14
Stereoisomerization Barrier of Allene*	42	38	42

* Occurring for a 133.3° bend

Figure 5.1. Critical energies of the cyclopropylidene allene system

extended basis has decreased the ring-opening barrier by about 65%! The middle column shows the results of some calculations performed with the intermediate basis set mentioned in the previous section. It can be seen that this basis set gives a slightly lower ring-opening barrier, a considerably higher exothermicity and a somewhat lower allene stereoisomerization barrier.

As a final aid to comparison with the STO-3G calculation, the energy curve for the extended basis set is depicted in Figure 5.2 as a bold line. The corresponding minimal basis set curve is shown as a thin line.

D. Discussion and Conclusions

It is instructive to compare these results to the best literature values. The best values for the ring-opening barrier and the reaction exothermicity must be considered those of Honjou, Pacansky and Yoshimine (HPY) (1984), due to the high level of sophistication of their calculations carried out at IBM. Their values are 11 kcal/mole for the barrier and 62.6 kcal/mole for the exothermicity. Our extended basis set values are 14 and 65 kcal/mole respectively. HPY state that they believe their energies to be correct to within 3 kcal/mole and our values certainly lie within these limits. We believe that our values for both the

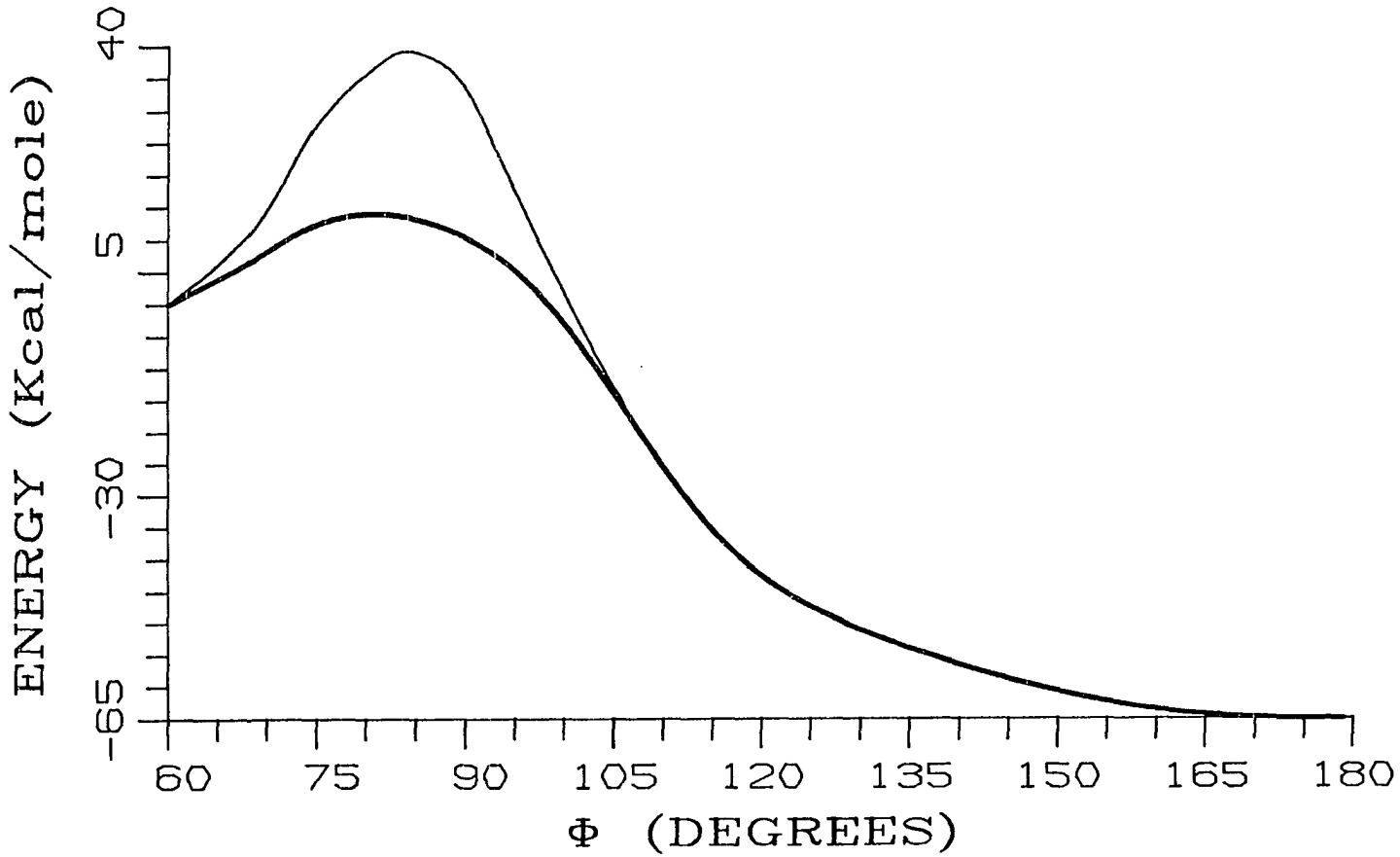

Figure 5.2. Energy curve for the cyclopropylidene-allene ring-opening reaction. The bold line corresponds to the extended basis set calculation, while the thin line corresponds to the STO-3G calculation

barrier and the reaction exothermicity may be accurate.

There is, unfortunately, no clearly established value for the allene stereoisomerization barrier. A consensus seemed to exist that the actual barrier is around 50 kcal/mole. This value is an estimate based on the experimental value for the dimethyl-substituted species and on certain previous calculations of rather low sophistication and accuracy. By contrast, a recent calculation by Johnson (1985) using 3-21G basis sets and optimized geometries has yielded a value of around 44 kcal/mole. This is rather close to our value of 42 kcal/mole. There can be two explanations for the discrepancy from the value of 50 kcal/mole: (i) the basis set and the FORS-MCSCF approximation (also used by Johnson) fail to completely accurately model this particular rotation barrier or (ii) the previous consensus is wrong and the barrier is a little lower than previously thought. It is quite possible that the substituted allene bends sufficiently less during isomerization due to the steric hindrance caused by the two methyl groups in the planar transition state. In fact, we shall find such a trend in the next chapter where the transition state of the substituted allene is shown to occur at around 145^{o} instead of at 133^{o} for the unsubstituted species. Keeping in mind the fact that this figure shows qualitative trends rather than quantitative differences, it is possible that this difference in bending could be even

bigger. We consider 42 kcal/mole the best substantiated value for the allene isomerization at this time.

With respect to the differences between the basis sets employed the following observations can be made. Since the results from the extended basis set with polarization functions are the most accurate ones, the other two basis sets are seen to succeed in some things and fail in others. The STO-3G set correctly predicts the reaction exothermicity and the allene stereoisomerization barrier, but overestimates the ring-opening barrier by about 65%. The extended Dunning-Hay basis set without polarization functions, on the other hand, does a reasonably good job on the ring-opening barrier but underestimates the one for the internal rotation of allene and overestimates the reaction exothermicity by 25%. This shows two things : (i) if a basis set correctly models one part of a reaction, this does not imply that other parts will be correctly modeled as well; (ii) the results obtained from using "intermediate" basis sets are not necessarily more reliable than those from corresponding minimal basis set calculations just because the basis set used is a little better. To obtain reliable energies one must, in most cases, use very good basis sets. Anything less must be suspect (unless compared to experimental or reliable theoretical results), irrespective of the amount of basis set flexibility given up.

It is also interesting to note that the present calculations do not support the widely held belief that STO-3G basis sets tend to disfavor π bonding. It may be that this is due to the fact that our calculations are MCSCF calculations and that the inclusion of correlation may correct the tendency observed for SCF calculations.

VI. THE SUBSTITUTED REACTION

A. Introduction

The results obtained in the preceding chapters for the unsubstituted ring-opening reaction imply that there exists no inherent electronic reasons for the reaction to be stereospecific. Consequently, it seems likely that observed stereospecificities are caused by steric and/or weak electrostatic effects of the substituents. To investigate this conjecture, it was decided to add such effects to the calculated surface and to determine whether their influence can in fact explain the experimentally observed phenomena.

While a recalculation of the surface with substituents introduced in place of one or more hydrogens would be an obvious route to follow, it suffers from two serious drawbacks: First, such a calculation would be prohibitively expensive and time-consuming, involving computations orders of magnitude larger than the ones already performed, even with the knowledge already gained as a guide to certain simplifications. Second, without an extensive analysis of the bonding and other effects, the results of such a calculation would not reveal whether the introduction of substituents merely added steric hindrances or whether they changed the covalent bonding.

It was therefore felt, that a more useful approach would be to add the necessary effects to the already calculated unsubstituted energy surface, and to see whether such additive corrections were sufficient to explain the experimentally available data. This approach contains of course certain inherent shortcomings regarding the geometries involved. However, since the main goal is to observe qualitative rather than quantitative agreement or disagreement with experiment, it was felt that the results would nonetheless be significant. If they would qualitatively explain the observed facts, then the fundamental point will have been made.

Three different substituted cyclopropylidenes will be investigated, namely HCH_3C-C-$CHCH_3$, HCH_3C-C-CH_2 and HCH_3C-C-CHBr, in order to focus on different features in the different cases.

B. The Corrective Potential

Happily, the tools for adding nonbonded interaction effects to the calculated surface, exist in the field of molecular mechanics. Burkert and Allinger (1982) give an excellent account of the methods usually employed and of the reliable results obtained by many workers in the field. In the present case, there exist two kinds of interactions,

namely the steric effects, due to the size and nature of the substituents and the electrostatic effects, if any, due to the polarization of bonds already present.

Neutral, nonpolar parts of a molecule interact at large distances through induced electric moments, giving rise to London dispersion forces. This interaction is attractive and, according to Burkert and Allinger (1982), its general form is:

$$V_{disp} = -c_6 r^{-6} - c_8 r^{-8} - c_{10} r^{-10} - \ldots \qquad (6.B.1)$$

Usually only the r^{-6} term is kept, with the coefficient slightly adjusted to account for the neglected higher order terms.

At sufficiently small distances, a repulsive interaction due to Pauli exclusion prevails. Its exact form is usually based on expediency.

The most common general form of the total potential for neutral, nonpolar atoms or molecules, which is called van der Waals interaction, is that given by Lennard-Jones (1924):

$$V_{VDW} = \frac{n\varepsilon}{n-m} \left[\frac{m}{n} \left(\frac{r_0}{r} \right)^n - \left(\frac{r_0}{r} \right)^m \right] \qquad (6.B.2)$$

where ε is the depth of the potential and r_0 the position of

this minimum. The latter is usually taken equal to twice the van der Waals radius. For the case of two interacting moieties X and Y, the combination rule commonly used is $\varepsilon^{XY}=(\varepsilon^{X}\varepsilon^{Y})^{1/2}$ and $r_0^{XY}=(r_0^{X}+r_0^{Y})/2$. The exponent of the attractive potential, m, is usually set to 6 for the reasons outlined above, but there is no compelling theoretical reason to choose any specific value for n, the exponent of the repulsive potential, as long as it is greater than 6. When n is set to 12, the equation assumes the particularly simple form:

$$V_{VDW} = \varepsilon \left[\left(\frac{r_0}{r}\right)^{12} - 2 \left(\frac{r_0}{r}\right)^{6} \right] \qquad (6.B.3)$$

This so-called 6-12 form of the Lennard-Jones potential fits the data for rare gases very well and has been the most used form of the potential for many years. More recently, however, it was shown by, among others, Warshel and Lifson (1970), that this potential is, in fact, too hard for hydrocarbons and they have proposed the use of a softer repulsive part. Such a 6-9 potential is given by Hagler, Huler and Lifson (1974):

$$V_{6\text{-}9} = \epsilon \left[2 \left(\frac{r_0}{r}\right)^9 - 3 \left(\frac{r_0}{r}\right)^6 \right] \qquad (6.B.4)$$

In the case of noncharged <u>polar</u> molecules, or fragments thereof, the prevailing term is a dipole/dipole interaction term, calculated by the so called Jeans' formula (as given by Lehn and Ourisson (1963)), where D is the (effective) dielectric constant, χ is the angle between the two dipoles μ_i and μ_j, and the αs are the angles that the dipoles form with the vector connecting the positions of the two dipoles:

$$V_{dipol} = \frac{\mu_i \mu_j}{D r_{ij}^3} (\cos\chi - 3\cos\alpha_i \cos\alpha_j) \qquad (6.B.5)$$

For the purposes of the present investigation where interactions between hydrogens and substituents such as CH_3 and Br are of interest, the inclusion of both the nonpolar and the polar terms is appropriate. While polar terms are negligible in the case of hydrocarbons and are therefore usually neglected, neglecting them in the case of fragments such as C-Br, which exhibit substantial polarization, would falsify the results. Since these terms will therefore be included in some cases, it seems appropriate to include them in all, leaving those which are negligible to effectively zero themselves out.

Within the spirit of the present approach as oulined in the preceding section it seems moreover appropriate to take into account only the nonpolar interactions between the pairs of substituents 1-2, 1-2', 1'-2 and 1'-2', where the numbers represent the positions of the hydrogens in the unsubstituted species as given in Figure 3.1. The interaction between pairs 1-1' and 2-2' are omitted, since they remain essentially constant throughout the reaction because the C-H bond lengths and the H-C-H angles remain almost unchanged, as was documented in Chapter III, Section B.4. For the same reasons the dipole/dipole interactions between the pairs of bonds (1-1)-(2-2), (1-1)-(2-2'), (1-1')-(2-2) and (1-1')-(2-2') are included and those between the pairs (1-1)-(1-1') and (2-2)-(2-2') are omitted. The dipoles are assumed to be located at the bond center. The additive potential, which represents the corrections due to the non-bonded interactions, is then obtained by calculating and summing up all these individual interactions and subtracting from them the sum of all interactions which would be present if all substituents were hydrogens, since the latter are included in the original FORS-MCSCF calculation.

As regards the actual parameters used in the calculations they are as follows. The values of ϵ and r_0 for H were taken from Hagler, Huler and Lifson (1974), Wertz and Allinger (1974) and Pauling (1960) as 0.08 kcal/mole and 3.0

A respectively, as were the same parameters for CH_3 as 0.1 kcal/mole and 4.0 A respectively. The dipole moment for C-H is taken as 0.55 Debye with a polarity of C^--H^+ as calculated by Wiberg and Wendoloski (1976). That for C-CH_3 is taken from Wodarczyk and Wilson (1972) as being 0.06 Debye with a polarity of C^--C^+H_3. The ε and r_0 parameters for Br as well as the C-Br dipole moment were taken from Meyer and Allinger (1975) and Pauling (1960) as being 0.395 kcal/mole, 3.9 A and 2.15 Debye respectively, with an obvious polarity of C^+-Br^-.

C. The Dimethyl Species

1. The reaction surface in the Φ,δ_1,δ_2 space

As in Chapter III, Section B.2, we represent this reaction surface through a series of contour diagrams in terms of the variables δ_1 and δ_2, for fixed values of Φ. The shading scheme is the same as that used previously and illustrated in Figure 3.4. However very high energy areas are left blank and no contours are drawn within this unshaded area because the nonbonded interactions between the two methyl groups can become quite large, reducing the contours to a mass of black, indistiguishable lines. Moreover the areas of high energy are of little interest compared to those of low energy.

Figures 6.1.1 to 6.1.18 show the Φ=constant panels for

the ring opening of 2,3-dimethylcyclopropylidene to 2,3-dimethylallene. Note that both the cis as well as the trans stereoisomers appear on each panel, thus allowing an easy comparison between the two distinct species.

a. $\Phi=59.5^{o}$ (Fig. 6.1.1) The four distinct minima that were observed in Fig. 3.5.1 are no longer equivalent. The two that are situated on the diagonal lines $\delta_1+\delta_2=0$ and $\delta_1+\delta_2=180^{o}$ correspond to the cis case and are denoted by C. The other two, located on the lines $\delta_1+\delta_2=\pm 90^{o}$, correspond to the trans case and are denoted by T. The first thing that one observes is that the trans compound is about 10 kcal/mole lower in energy that the cis compound. This is probably intuitively obvious due to increased steric hindrance from the bulk of the methyl substituents in the cis case. Also probably intuitively obvious is the observed asymmetry of the cis species in the disrotatory direction, i.e. along the line $\delta_1+\delta_2=0^{o}$. The energy goes up much faster if we try to bring the two methyl groups closer together than if we try to bring them farther part. The two trans species exhibit no such assymetry, since the two opposing disrotatory motions are, for them, completely equivalent. One should note that, while the two cis compounds are mirror images of one another, they are completely equivalent in every respect and indistinguishable except by numbering the substituents. The

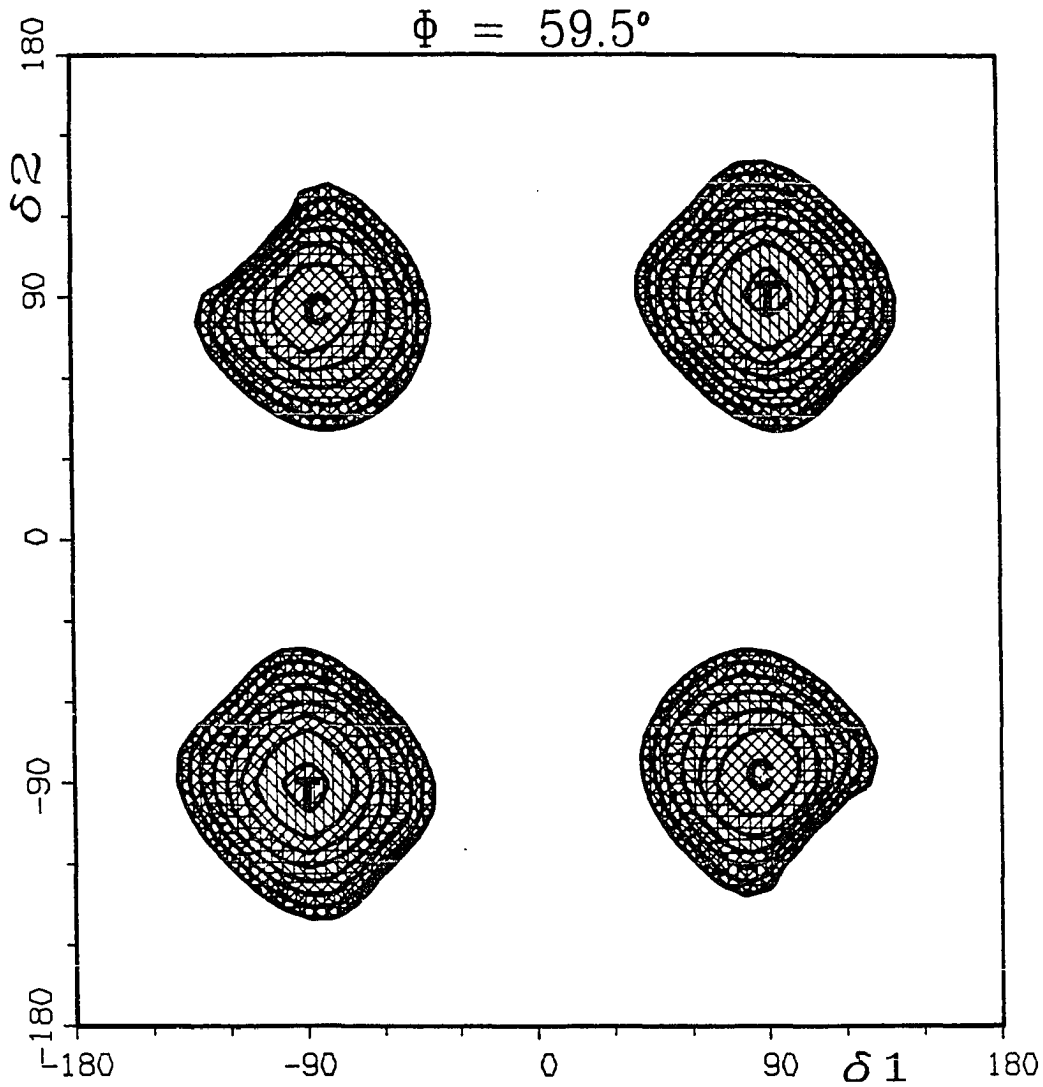

Figure 6.1.1. Energy surface over dihedral angle plane for Φ=59.5^{o} (2,3-dimethylcyclopropylidene). Note the two equivalent trans positions (T) which are symmetric, and the two equivalent cis positions (C), which are not

same, of course, holds true for the two trans species.

As in the case of the unsubstituted compound, all minima are, in this case also, situated at the points which correspond to the CH_3-C-H planes being perpendicular to the C-C-C plane.

b. $\Phi=70^{o}$ (Fig. 6.1.2) As in the case of the unsubstituted compound, one observes the elongation of the area around the minima, which are still situated so that the CH_3-C-H planes are perpendicular to the C-C-C plane. As in the preceding panel, and for the same reasons, the trans minimum area is symmetric along the disrotatory direction, while the cis is not. Moreover, one notes that the trans regions (T) are less elongated than in the unsubstituted case (again due to steric hindrances), while the cis regions (C) are as elongated in the favorable direction as the unsubstituted species was, and not at all in the other. This is because there is no steric hindrance to the two methyl groups moving farther apart from one another, while the molecule will strongly resist their being brought closer together. The trans minimum is again significantly lower in energy than the cis minimum.

The energies of all minima have of course increased since the molecule is moving uphill towards the transition state.

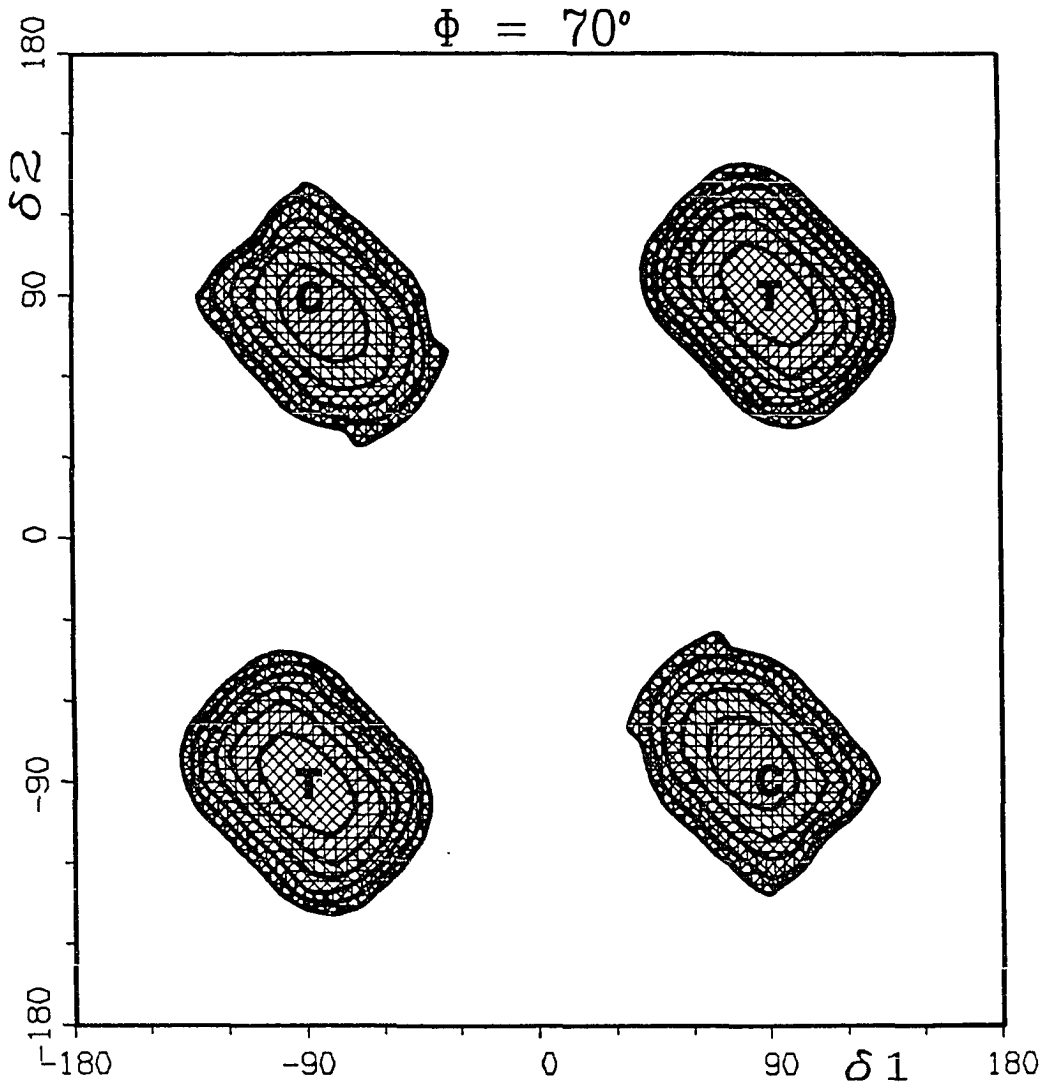

Figure 6.1.2. Energy surface over dihedral angle plane for $\Phi=70^{\circ}$. The **cis** minima (C) are elongated only in one direction while the **trans** minima (T) are less elongated but symmetrically in both directions

c. $\Phi=75^{o}$ (Fig. 6.1.3) As in the preceding panel, the minimum areas for the trans compound (T), are elongated along the disrotatory direction, but less so than in the case of the unsubstituted species. The minimum areas for the cis compound (C), however, are not at all elongated in one direction, while in the other direction they behave exactly like the unsubstituted molecule. The trans species is once more lower in energy than the cis, while both are higher than the corresponding values found for $\Phi=70^{o}$.

d. $\Phi=80^{o}$ (Fig. 6.1.4) As in the unsubstituted system, the ring-opening has reached the point of the first bifurcation in the reaction path. This is true, however, only for the trans species. The cis species can, as we have seen, move in only one direction, the other being sterically obstructed. The behavior of the surface in the allowed direction of the cis ring-opening is remarkably similar to that for the unsubstituted compound. The behavior of the trans compound is becoming increasingly similar to that of the unsubstituted compound because, as the opening angle increases, so does the distance between the methyl groups and hence the steric hindrance decreases. The difference in energy between the trans species (T), which is still lower, and the cis (C) species is less than before, which is due to

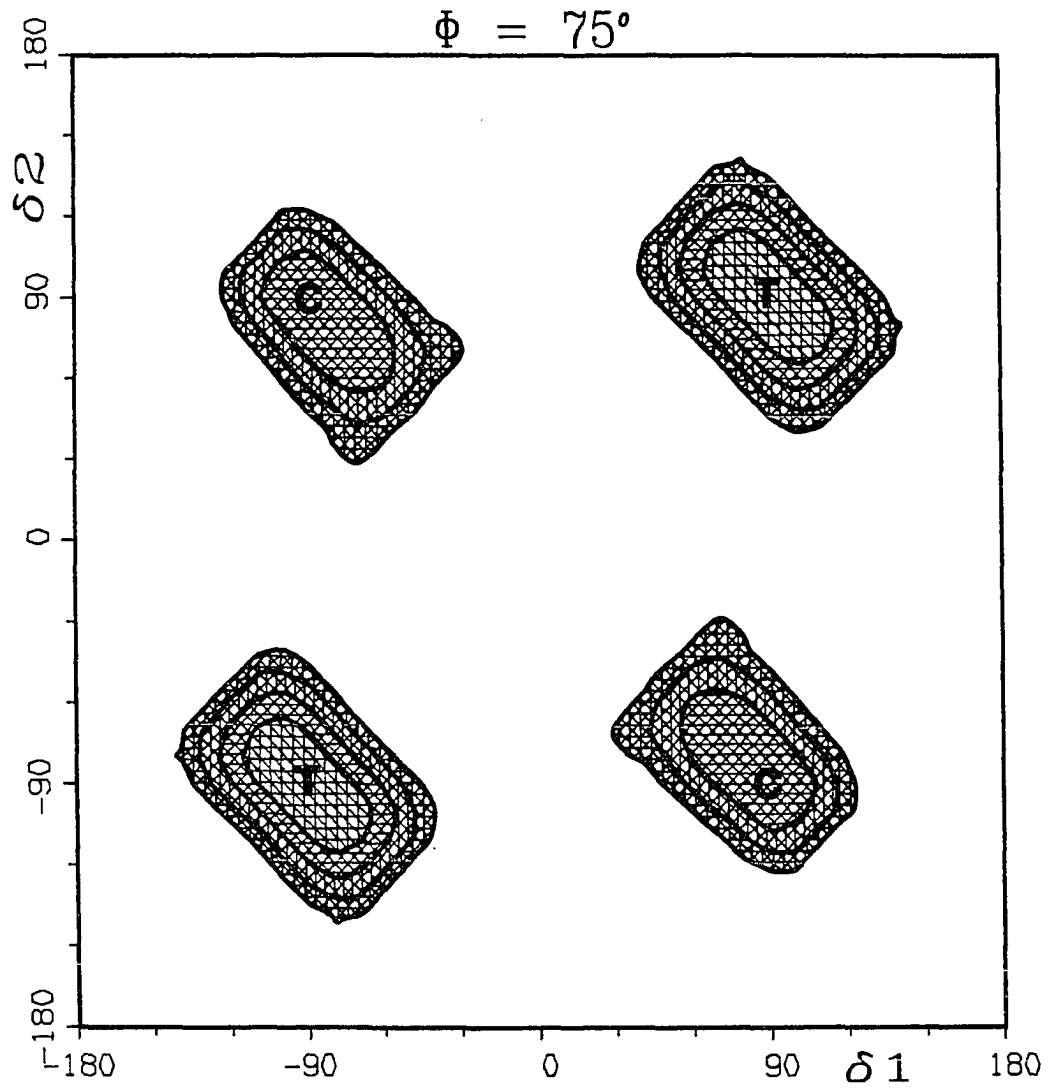

Figure 6.1.3. Energy surface over dihedral angle plane for $\Phi=75^{o}$. There is increased elongation around the minima. The cis compound (C) is still elongated in one direction only, while the trans (T) is still symmetric

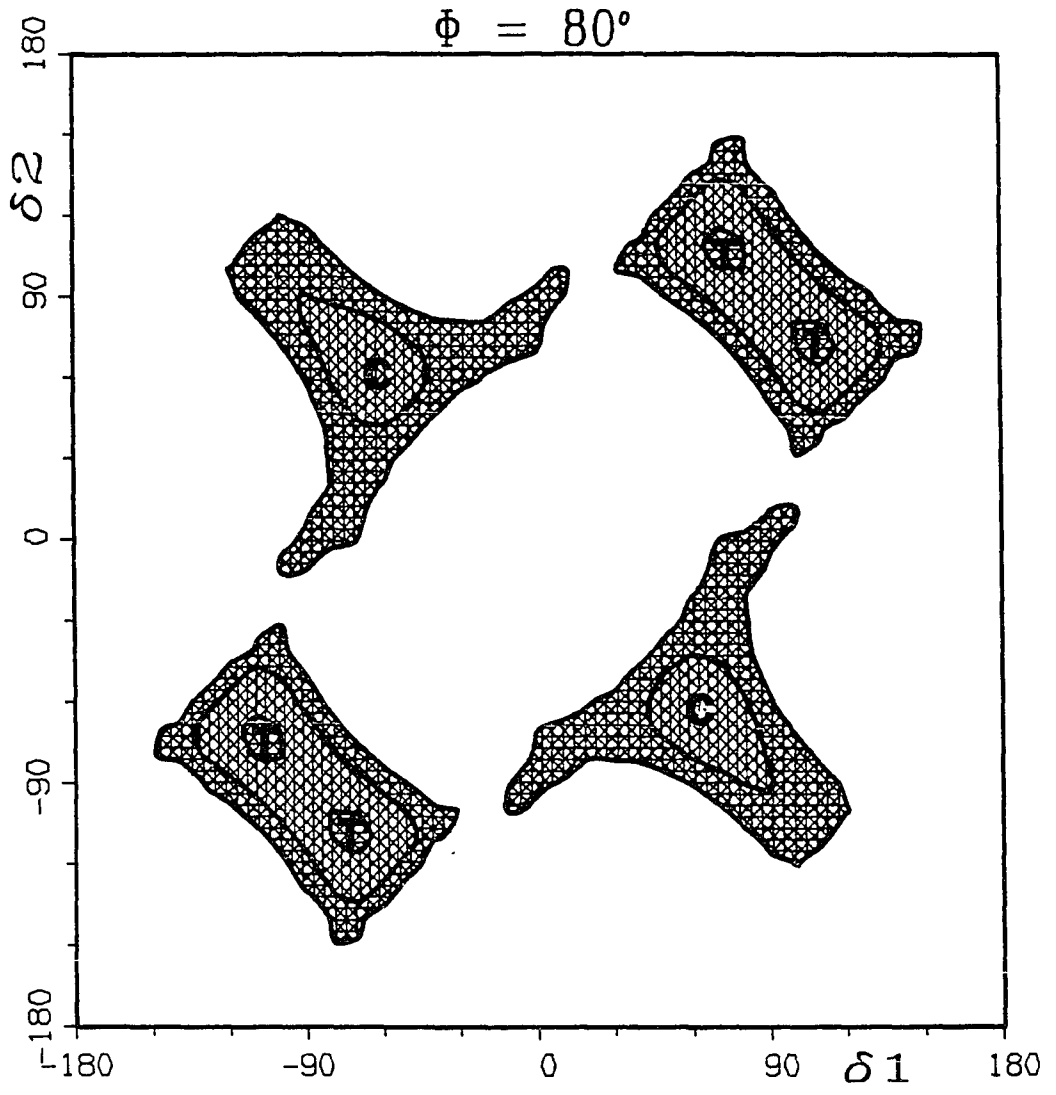

Figure 6.1.4. Energy surface over dihedral angle plane for $\Phi=80^{o}$. First bifurcation for the trans species, whose minimum has separated in two. No bifurcation for the cis, which can only move in one direction

the lessening role of the steric hindrances. Both the trans and the cis molecules are still moving uphill on their reaction paths towards their respective transition states.

e. $\Phi=82^{o}$ (Fig. 6.1.5) There is little difference between this panel and the previous one, except for the fact that the cis and trans isomers are now almost the same in energy. One can still observe that the disrotatory motion of the cis molecule is greater than that of the trans molecule, and that the energy of both has increased with respect to that of the previous panel. The new alternate minima (m) at ($\delta_1=0^{o},\delta_2=90^{o}$), which for the unsubstituted species appeared at $\Phi=83^{o}$, have already appeared here, although the molecule cannot move to them due to the existence, as before of saddle points (S) separating them.

f. $\Phi=83^{o}$ (Fig. 6.1.6) One immediately sees that the saddle point separating the cis species disrotatory minimum (C) from the new alternate minimum (m) at ($\delta_1=0^{o},\delta_2=90^{o}$) has disappeared, leaving the molecule free to move downhill. This means that the cis compound reached its transition point somewhere between a Φ angle of 82 and 83^{o}. This transition state has all the characteristics of the one of the unsubstituted species, i.e. it is a bifurcating one in the sense that the cis molecule is equally likely to move

down to either of two valleys, representing two stereoisomers. It should be noted here that while, in the unsubstituted compound, these two stereoisomers were different for theoretical purposes only (due to the numbering of the atoms), in the present case they are nonsuperimposable and experimentally distinguishable.

The trans compound (T), on the other hand, is still hindered by saddle points (S) from reaching the alternate minimum. It has, therefore, not yet reached its transition state. We have, in effect, an interesting case here where, even though the trans configuration for $\Phi=83^{\circ}$ is slightly lower in energy than the equivalent cis configuration for the same Φ, the cis molecule will actually have moved to a lower energy because it has passed its transition state, while the trans molecule has not.

g. $\Phi=84^{\circ}$ (Fig. 6.1.7) The cis molecule is well on its way downhill on the energy curve, while the trans still remains in its disrotatory minimum (T), not having yet reached its transition state. The two saddle points (S_1 and S_2), however, that separate this minimum from the lower energy valleys, are no longer equivalent: The S_1 barrier is clearly higher than the S_2 barrier, i.e the $\delta_1+\delta_2=0$ line containing the two trans minima no longer has C_s symmetry. This is due to the fact that to move in the direction of the

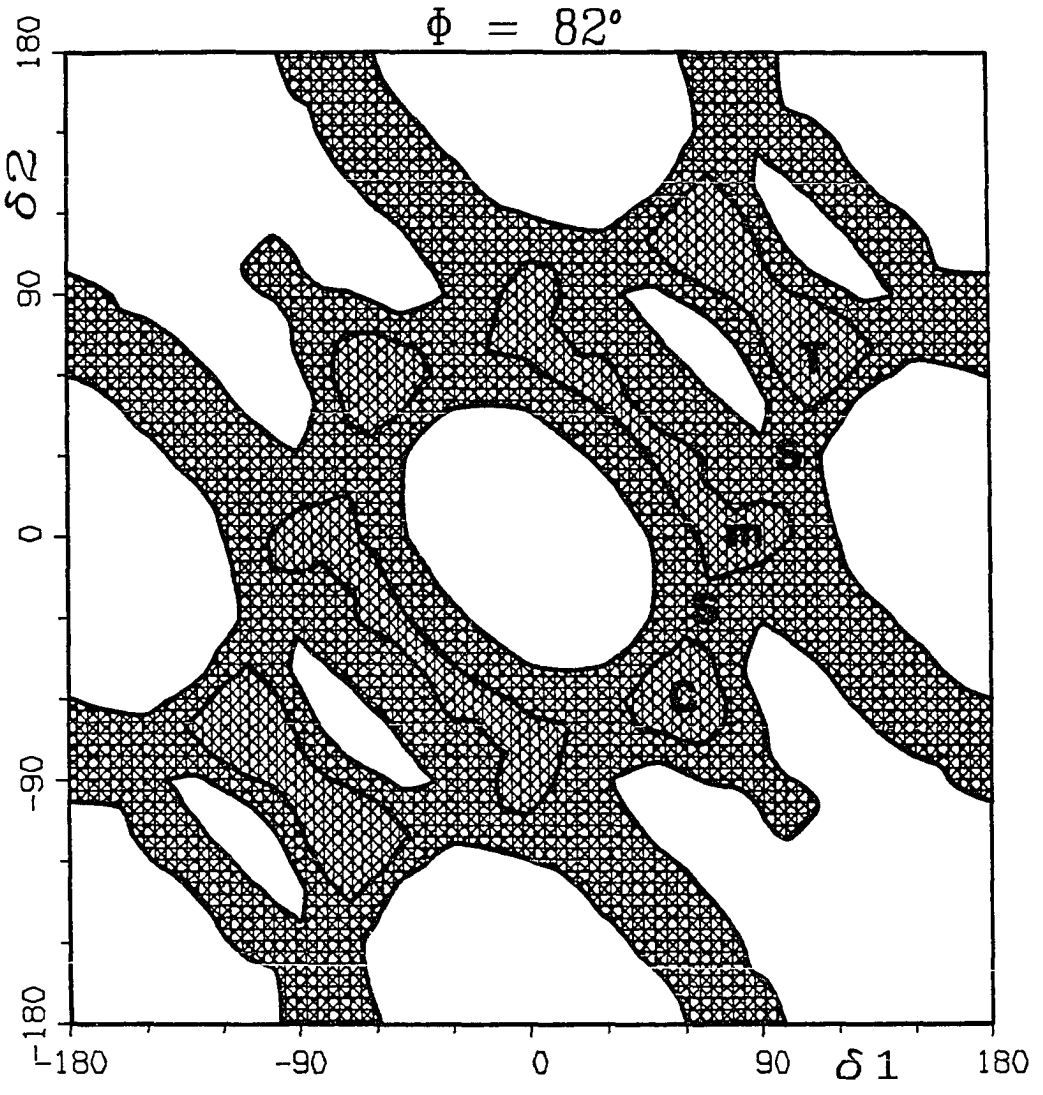

Figure 6.1.5. Energy surface over dihedral angle plane for $\Phi=82^{o}$. The alternate minima (m) have appeared at ($\delta_1=0^{o},\delta_2=90^{o}$), but are separated from the cis (C) and trans (T) minima by saddle points (S)

S_1 barrier, the molecule would have to go through a geometry where a methyl group would be situated between carbons 1 and 2, while in the other case the equivalent methyl group would lie outside the three-carbon ring.

h. $\Phi=85^{\circ}$ (Fig. 6.1.8) There is very little to be said, anymore, about the cis species, since from this point on it behaves essentially like the unsubstituted compound. The trans species, however, has just reached its own transition state, and it is not stereospecific. Indeed, one can clearly see that there is a barrierless path from the disrotatory minimum (T) to one of the minimum valleys below (V_1), while there is still a barrier (S) in the way towards the other one (V_2), for the same reasons as those outlined for the preceding panel. This barrier is only of the order of a few kcal/mole, but it is enough to direct the molecule preferentially towards one stereoisomer rather than the other. As was the case for the cis compound, the two stereoisomers V_1 and V_2 are experimentally distinguishable.

i. $\Phi=86^{\circ}$ (Fig. 6.1.9) There is very little difference between this panel and the one for $\Phi=85^{\circ}$, except that the trans barrier (S) towards one of the two valleys is becoming smaller and is about to disappear too.

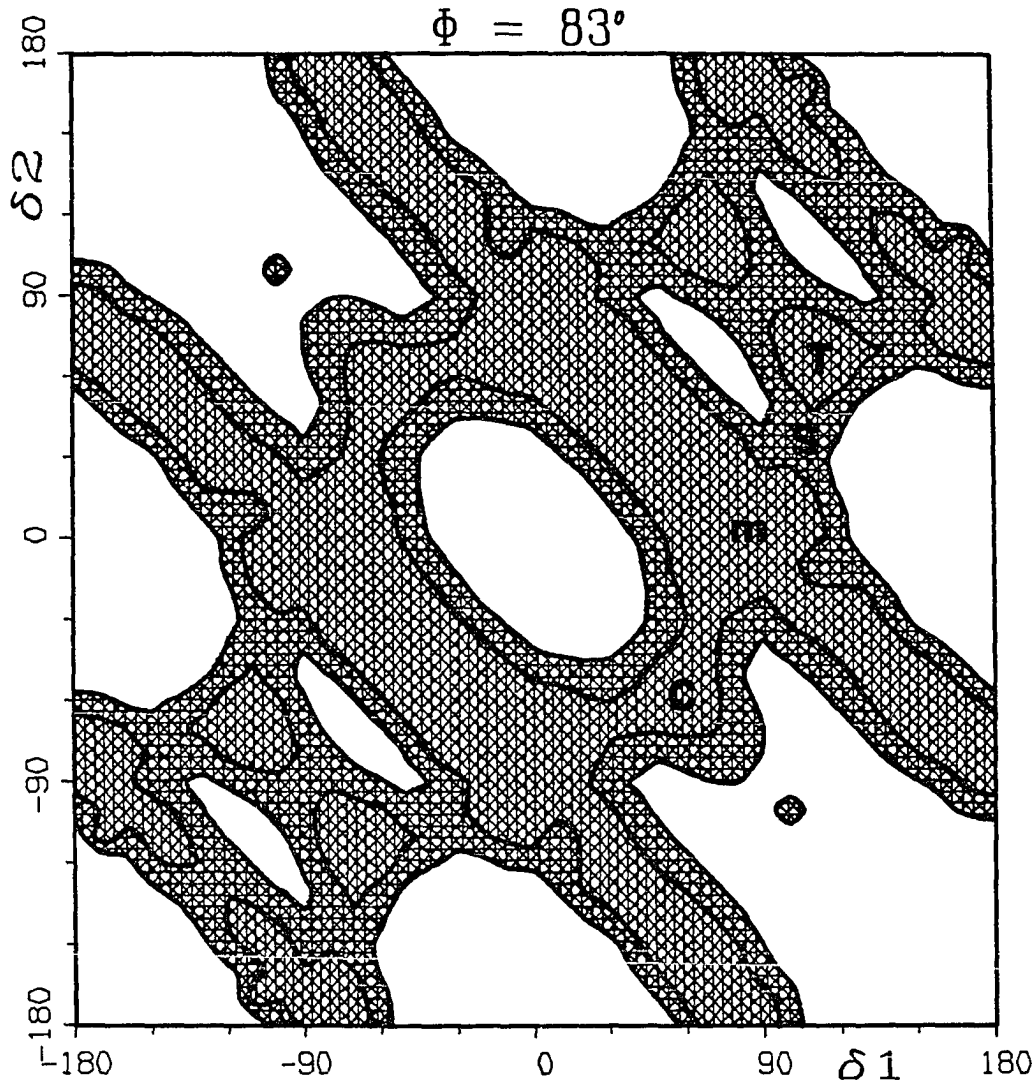

Figure 6.1.6. Energy surface over dihedral angle plane for $\Phi=83^{o}$. Note that the cis compound has passed its transition state, while the trans (T) is still prevented by a saddle point (S) from reaching the minimum energy valley

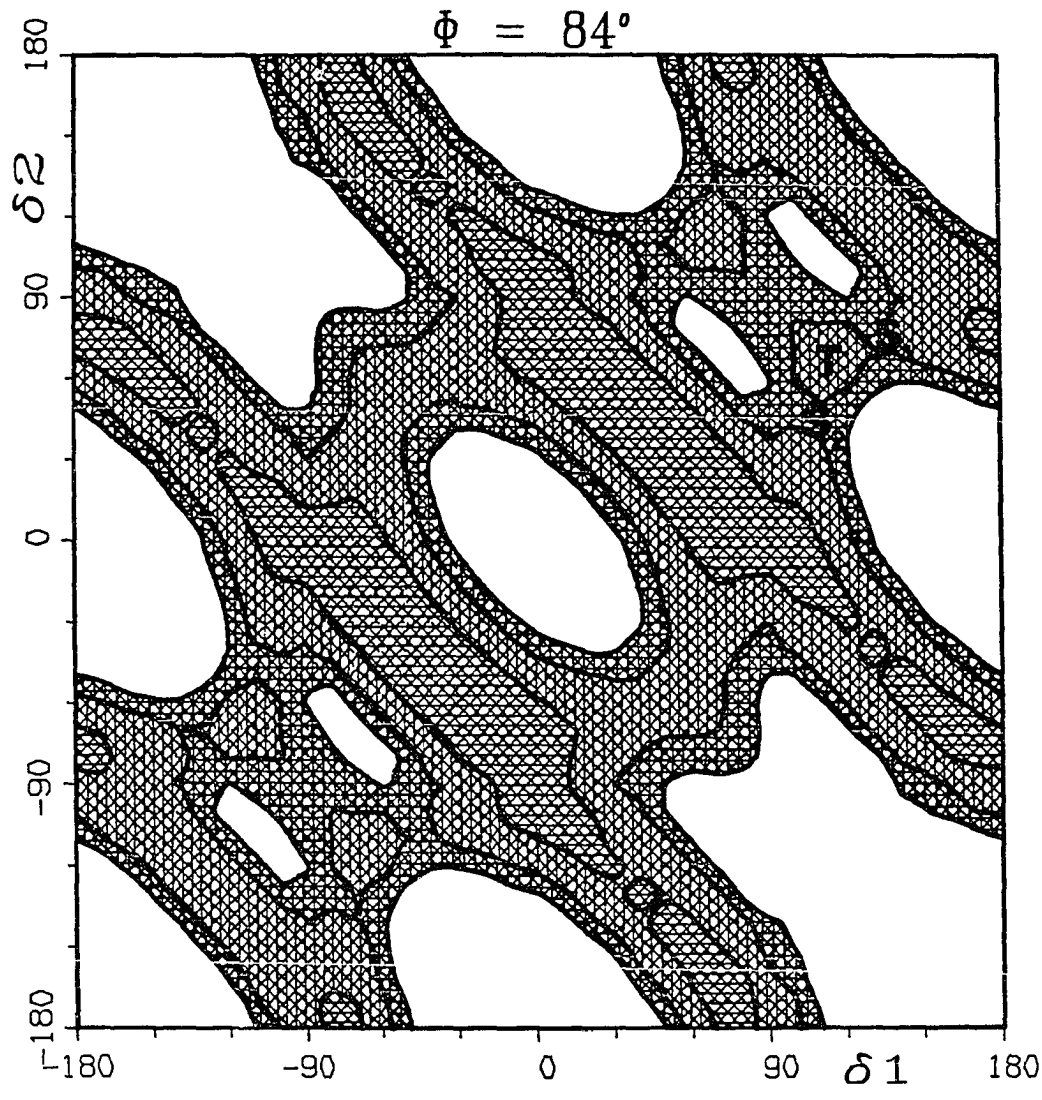

Figure 6.1.7. Energy surface over dihedral angle plane for $\Phi=84^{o}$. Note that the two saddle points (S_1 and S_2), on either side of the trans geometry are no longer equivalent

j. $\Phi=87^{o}$ to 160^{o} (Figs. 6.1.10 - 6.1.17) Both the trans and the cis species are now moving downhill towards the final products, in much the same way as for the unsubstituted compound. The only noteworthy feature is the gradual restoration of the C_s symmetry about and along the axis $\delta_1+\delta_2=0^{o}$, as the Φ angle increases. By the time $\Phi=160^{o}$ is reached, this symmetry is almost completely restored. The reason for this symmetry restoration is, of course, the fact that as the opening angle Φ increases, the distance between the methyl groups increases also, and the corresponding nonbonded interactions decrease.

k. $\Phi=179^{o}$ (Allene, Fig. 6.1.18) As in the case of the unsubstituted allene, we again have a series of nearly perfectly straight valleys and ridges. The only differences are that the valleys are a little narrower (again steric effects, albeit weak ones, come into play when the D_{2d} symmetry is broken), the height of the ridges with respect to the valleys is a little higher, and, more importantly, the ridge situated at $\delta_1+\delta_2=90^{o}$ is slightly higher than the ridge at $\delta_1+\delta_2=0^{o}$, showing that allene would prefer to internally rotate in one direction rather than the other. The reasons are once more steric, i.e. rotation in one direction brings the two methyl groups closer together while rotation in the opposite direction brings them farther apart.

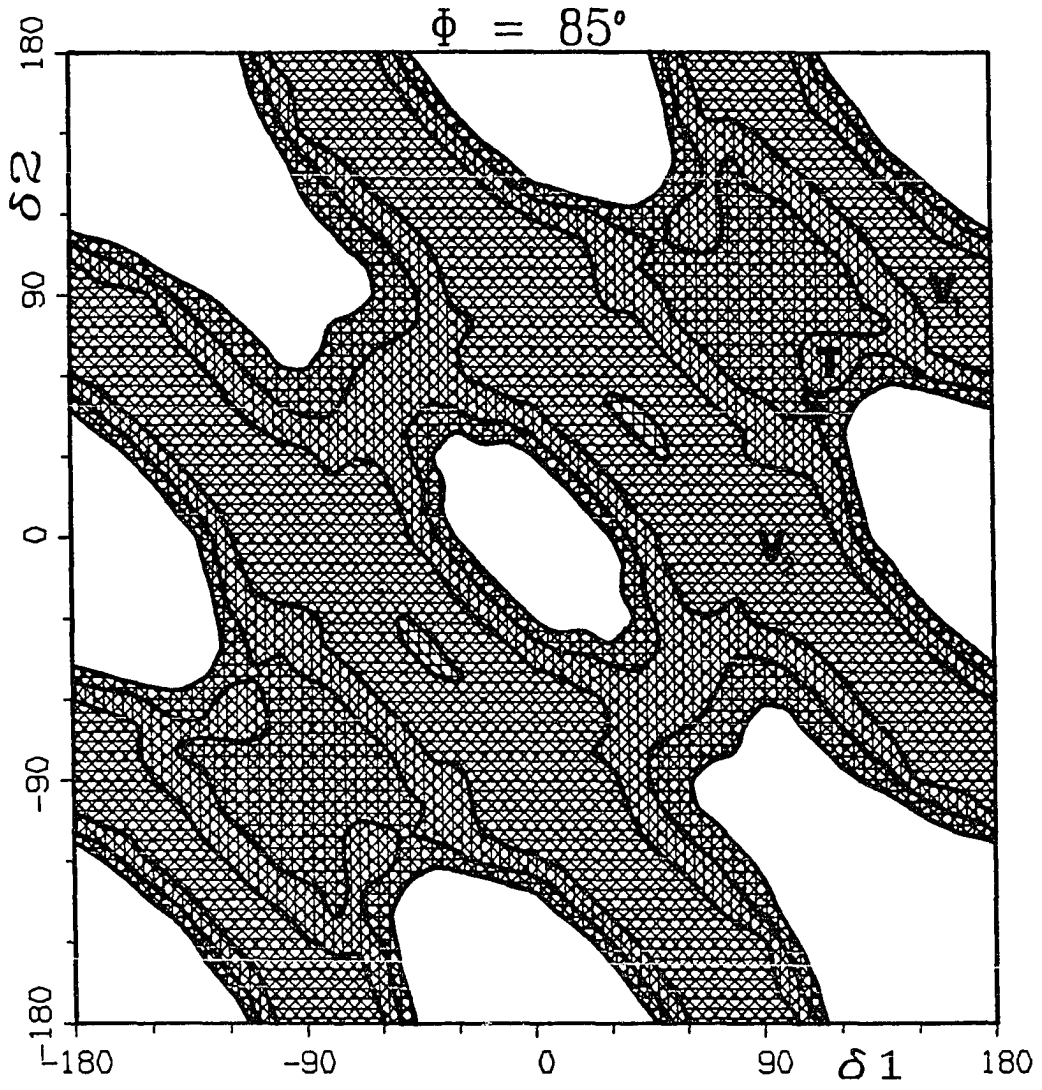

Figure 6.1.8. Energy surface over dihedral angle plane for $\Phi=85^{o}$. The trans transition state has been reached. There is no longer a barrier towards one of the valleys (V_1), while a saddle point (S) bars the way towards the other one (V_2)

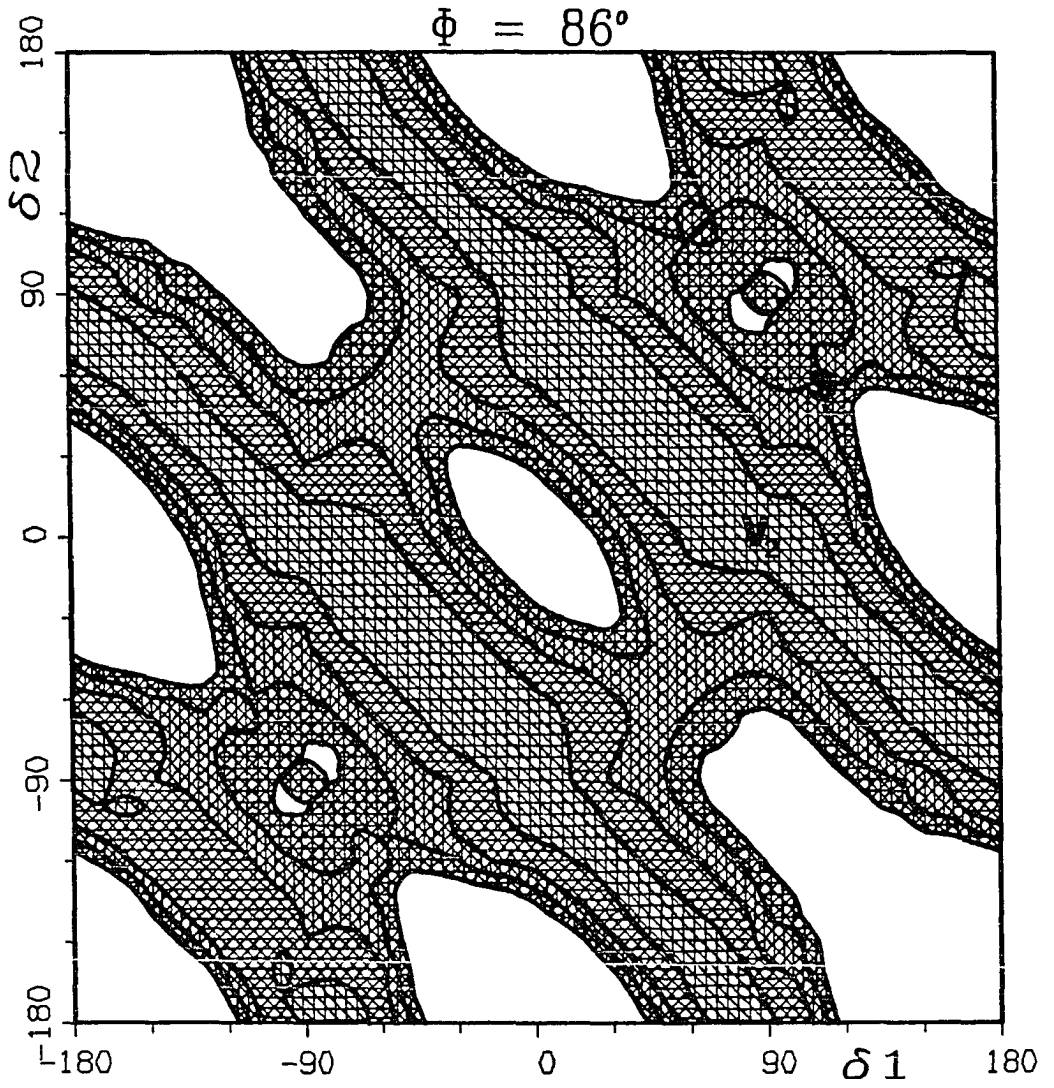

Figure 6.1.9. Energy surface over dihedral angle plane for $\Phi=86^{o}$. The remaining barrier (S) towards valley V_2 is decreasing in height

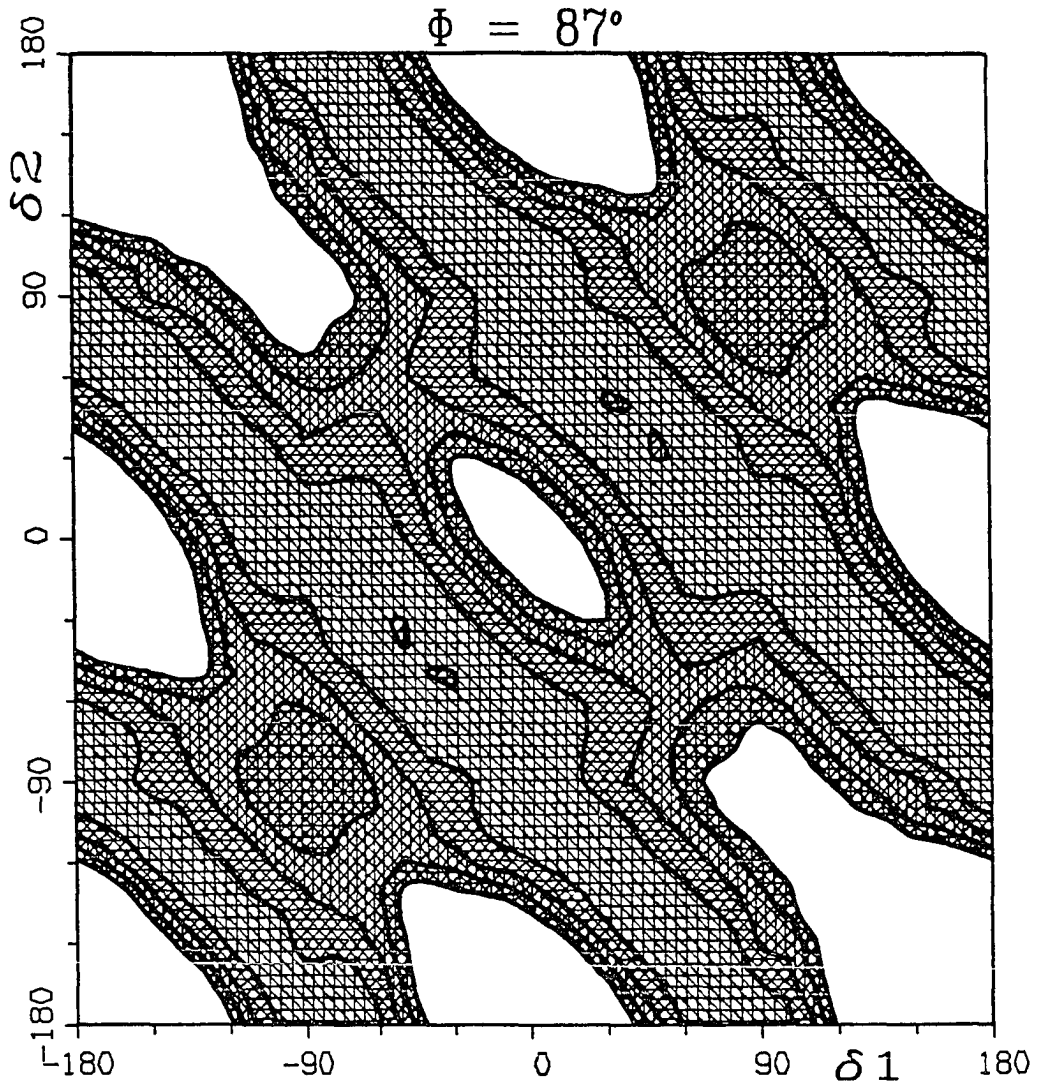

Figure 6.1.10. Energy surface over dihedral angle plane for $\Phi=87^{o}$. Note the beginning of the restoration of symmetry for the trans compound

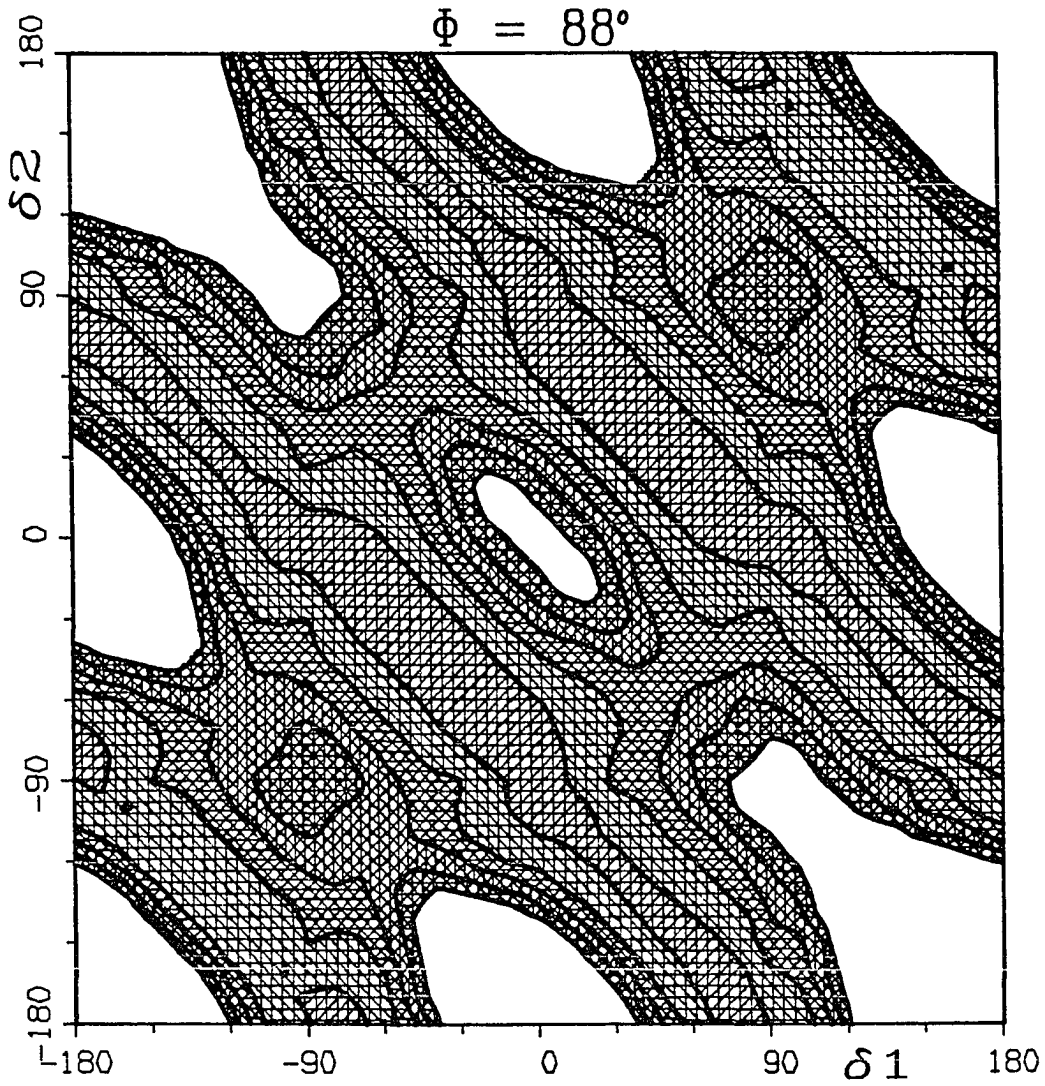

Figure 6.1.11. Energy surface over dihedral angle plane for $\Phi=88^{o}$. The surface is becoming more and more symmetric about the line $\delta_1+\delta_2=0^{o}$

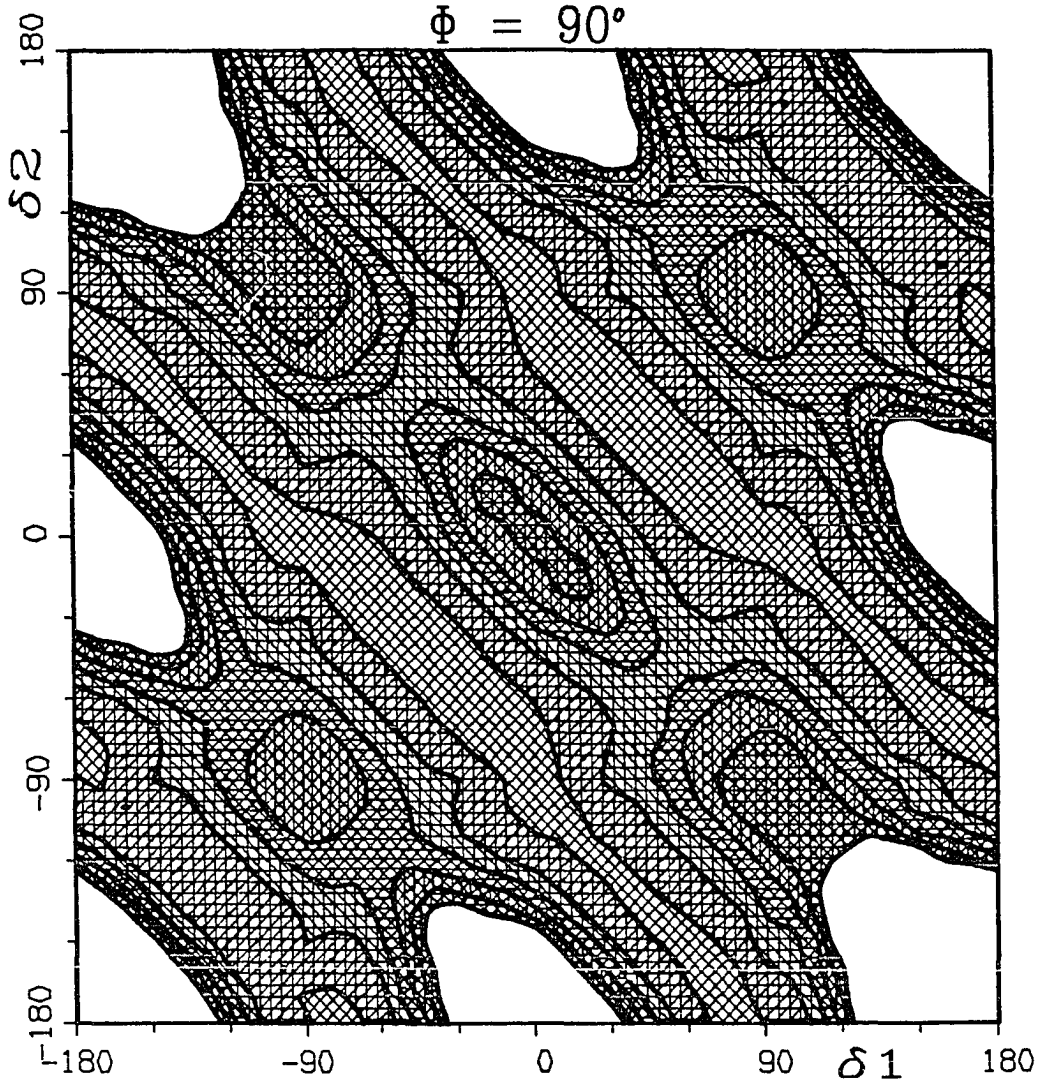

Figure 6.1.12. Energy surface over dihedral angle plane for $\Phi=90^{o}$. This panel is very similar to the one for $\Phi=88^{o}$, except that all the energies are getting lower

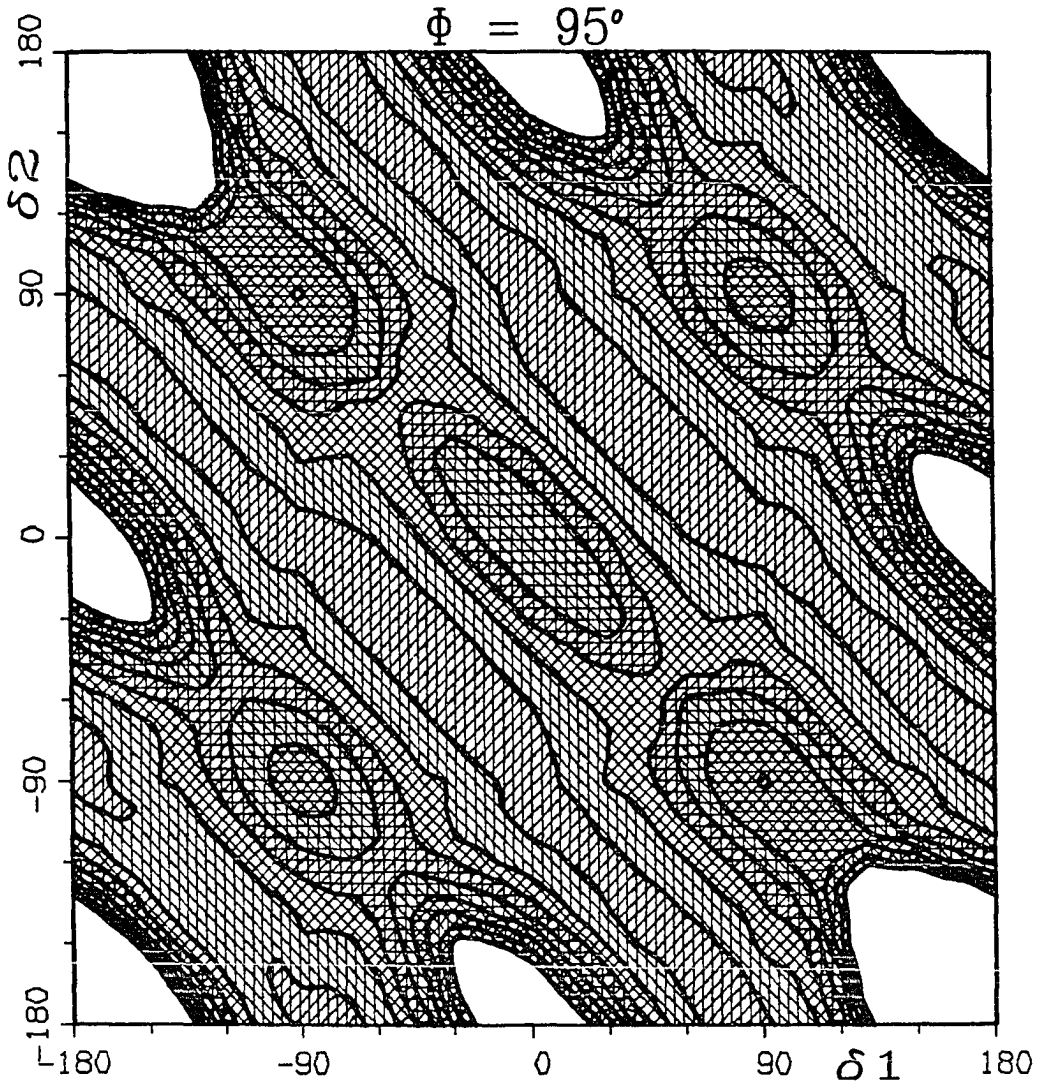

Figure 6.1.13. Energy surface over dihedral angle plane for $\Phi=95^{o}$. Similar to the panel for $\Phi=90^{o}$, with lowering of all energies. Note the gradual diminishing of the area of high energy on the two ends of the **cis** disrotatory line $\delta_1+\delta_2=0^{o}$

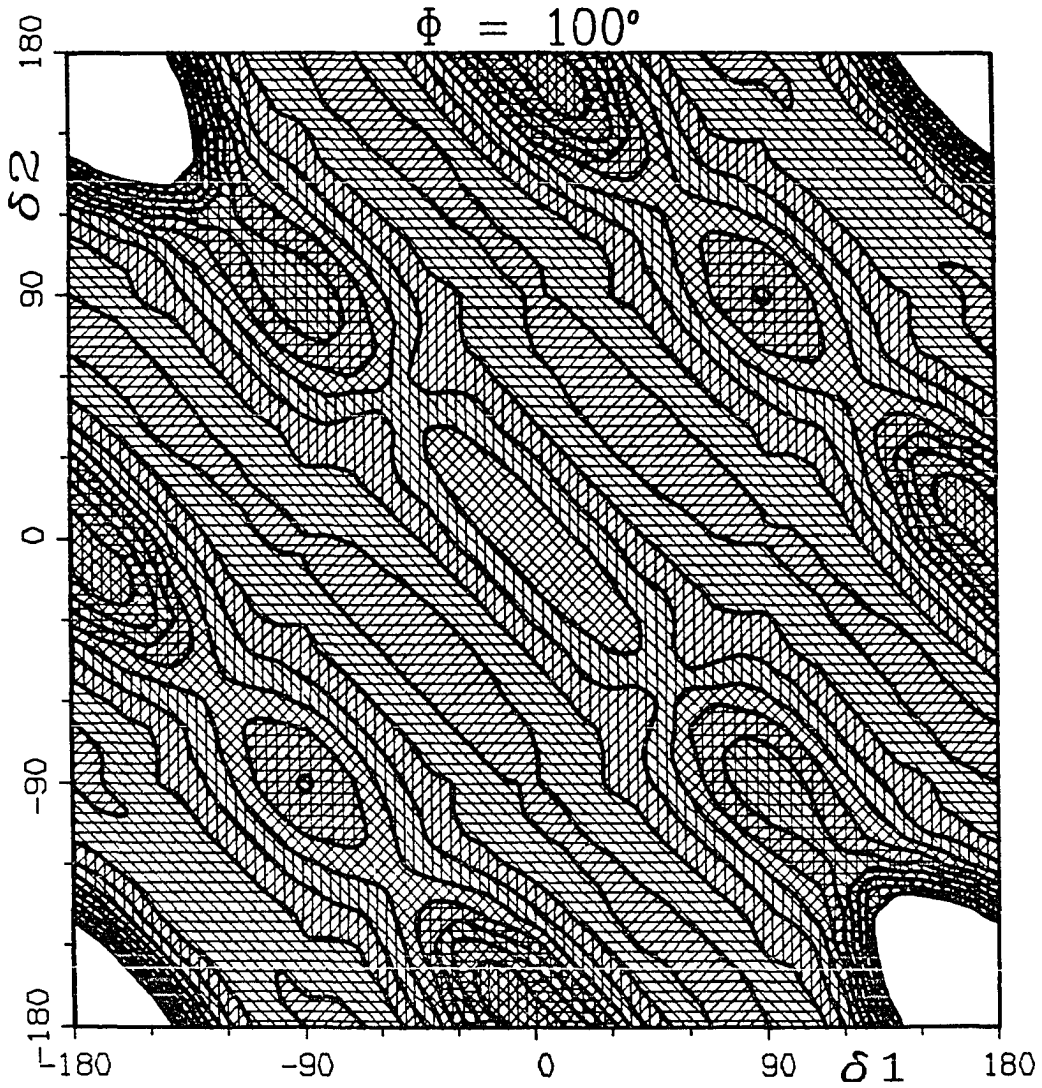

Figure 6.1.14. Energy surface over dihedral angle plane for Φ=100°. Very similar to the panel for Φ=95°. The symmetry about the line $\delta_1+\delta_2=0^\circ$ is almost completely restored

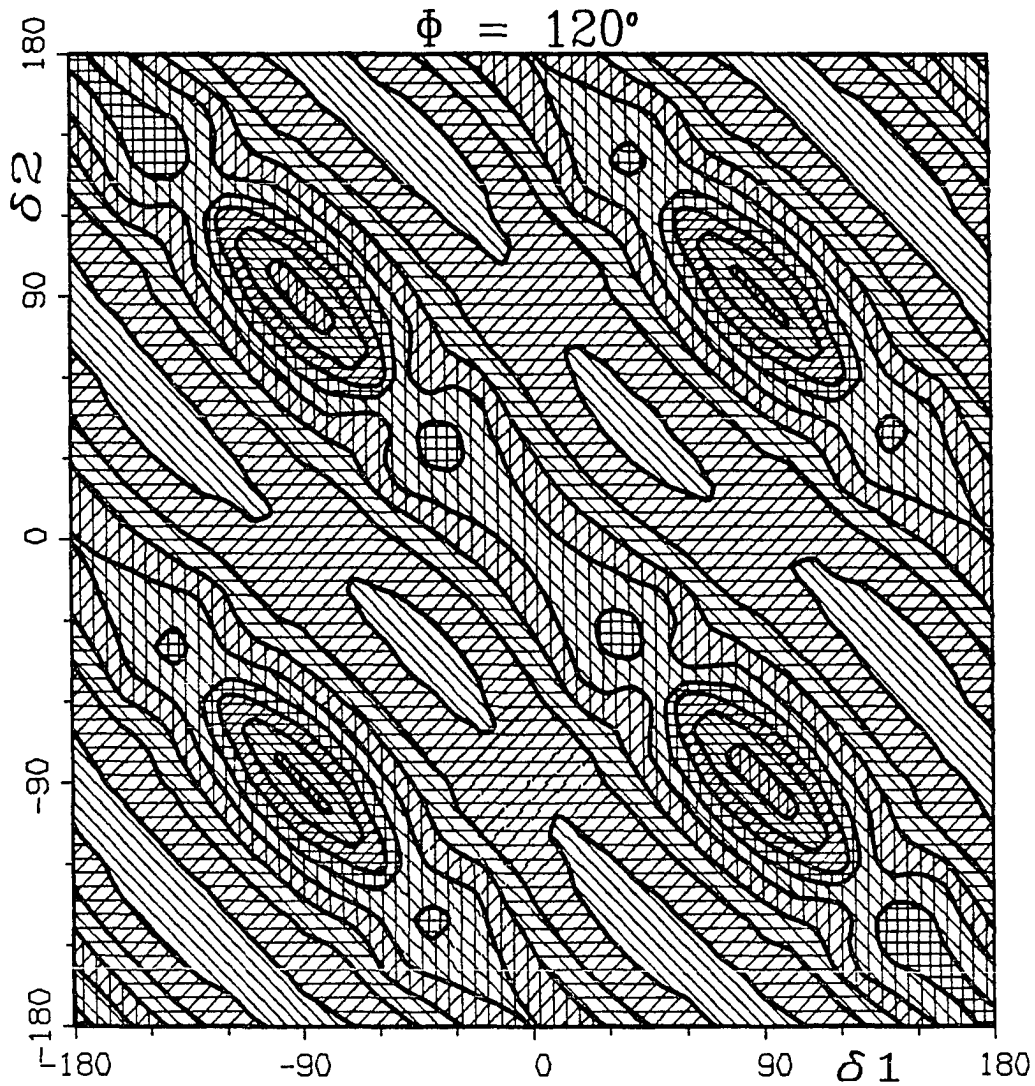

Figure 6.1.15. Energy surface over dihedral angle plane for $\Phi=120^{o}$. The high energy areas associated with the cis species have disappeared. Dissimilarities between cis and trans are slowly disappearing, too

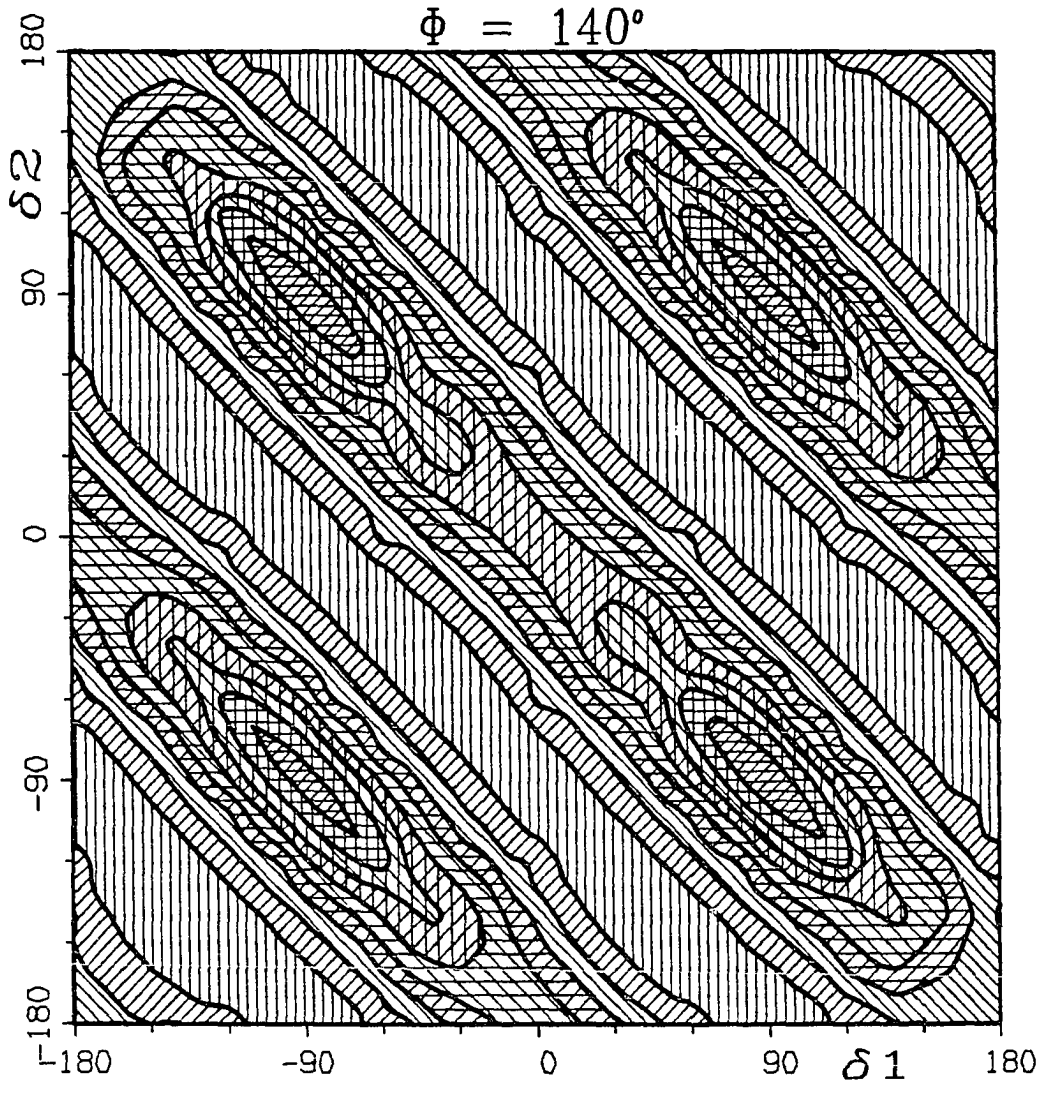

Figure 6.1.16. Energy surface over dihedral angle plane for Φ=140°. Total symmetry of the surface is slowly being restored

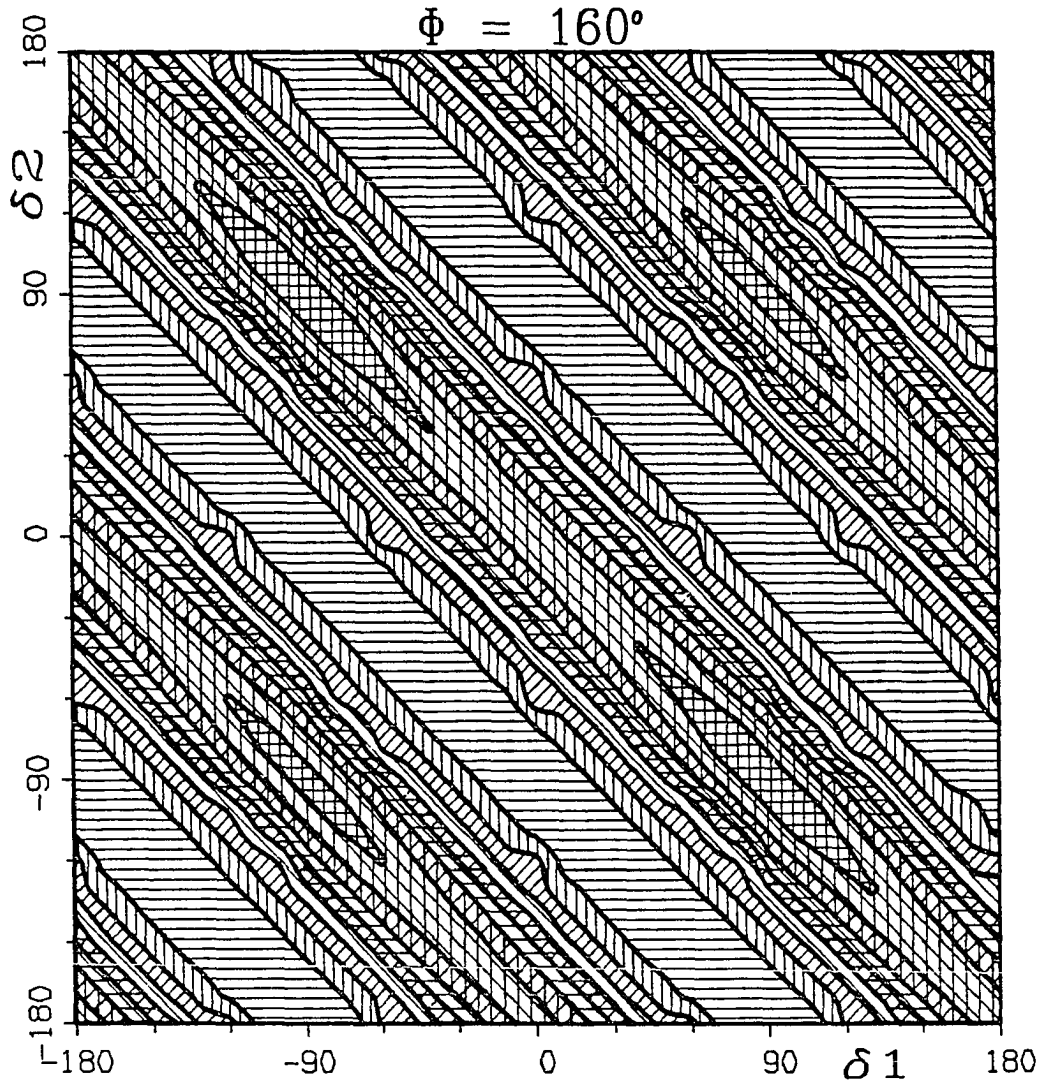

Figure 6.1.17. Energy surface over dihedral angle plane for $\Phi=160^{\circ}$. The surface has now regained almost all of the symmetry found in the unsubstituted reaction

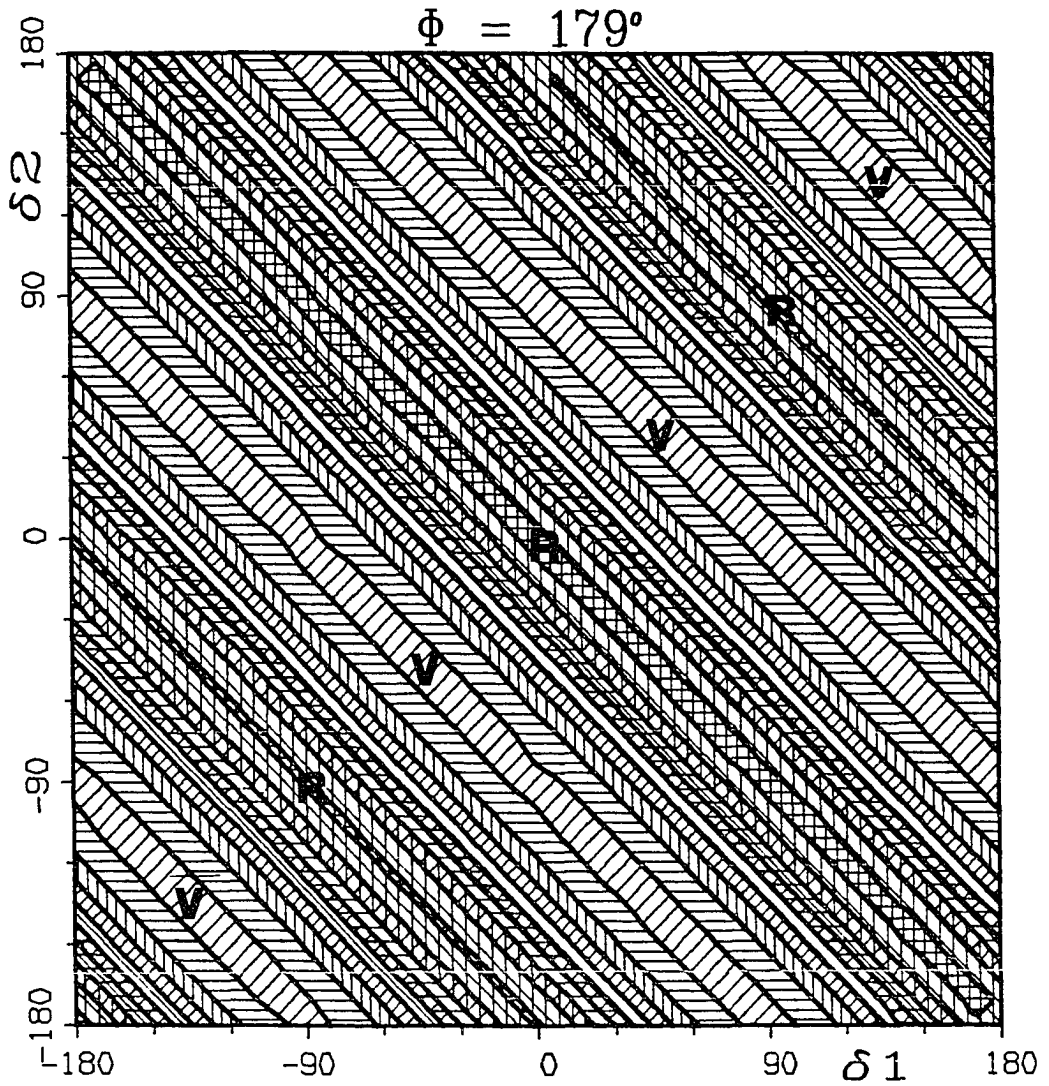

Figure 6.1.18. Energy surface over dihedral angle plane for Φ=179^{o} (2,3-dimethylallene). Note the similarity to the unsubstituted reaction surface for the same Φ. The valleys (V) are narrower and the ridges (R) slightly higher. Note that the ridge at δ=0^{o} is slightly higher than the other two

This is also an appropriate place to note that the isoenergetic valleys of free synchronized disrotatory rotation of the two CH_3-C-H planes, that we first observed in the unsubstituted compound, still exist in the present case and go as far back as the respective **trans** and **cis** transition states.

In summary, we conclude that the analysis of the various Φ=constant panels, shows clearly that the addition of substituents other than hydrogen to the parent compound recovers the experimentally observed stereospecificity.

2. The reduced reaction surface in the Φ,δ space

In order to get a more complete picture, it is again helpful to reduce the 4-dimensional surface (Φ,δ_1,δ_2) to a 3-dimensional one, as was done for the case of the unsubstituted molecule. This condensation is accomplished by the same method as that employed in Chapter III, Section B.3, with the following difference: In order to obtain reaction paths which are continuous in the sense that no discontinuities with respect to the optimized internal coordinates in general and $\delta_-=(\delta_1-\delta_2)/2$ in particular exist, we restrict the search for the minimum along the $\delta=(\delta_1+\delta_2)/2$=constant lines to the area enclosed by the lines $\delta_-=90^o$ and $\delta_-=-90^o$, thus effectively separating the cis from

the trans cases. The new surface will again be a plot of the energy as a function of $\delta=(\delta_1+\delta_2)/2$ and Φ.

The results are shown in Figure 6.2. In contrast to the corresponding plot for the unsubstituted system we now display a wider range of δ values in order to cover the areas corresponding to the various isomeric species. It is apparent that the surface possesses translational symmetry in the δ direction with a period of 360°. It is also apparent that the surface exhibits reflection symmetry with respect to the lines $\delta=0^{\circ},180^{\circ}$, but <u>not</u> with respect to the lines $\delta=-90^{\circ},90^{\circ}$. Points on the plot which are mirror images with respect to the lines $\delta=0^{\circ},180^{\circ}$ correspond to molecular geometries which are chiral images of each other and are distinguished by their optical activities. Molecular geometries corresponding to the points <u>on</u> the lines $\delta=0^{\circ},180^{\circ}$ etc. show no such activity, because they are their own mirror image.

For $\Phi=59.5^{\circ}$ we have the cyclopropylidene isomers. The trans isomers occur for $\delta=-90^{\circ},90^{\circ}$. Although the energy at these points is the same, the isomers at 90° and -90° are each others chiral images and experimentally distinguishable by their optical activities. The cis isomers occur for $\delta=0^{\circ},180^{\circ}$. The energies at these points are the same (and different from the trans isomers) and the isomers at 0° and 180° differ from each other merely by a rotation of the whole

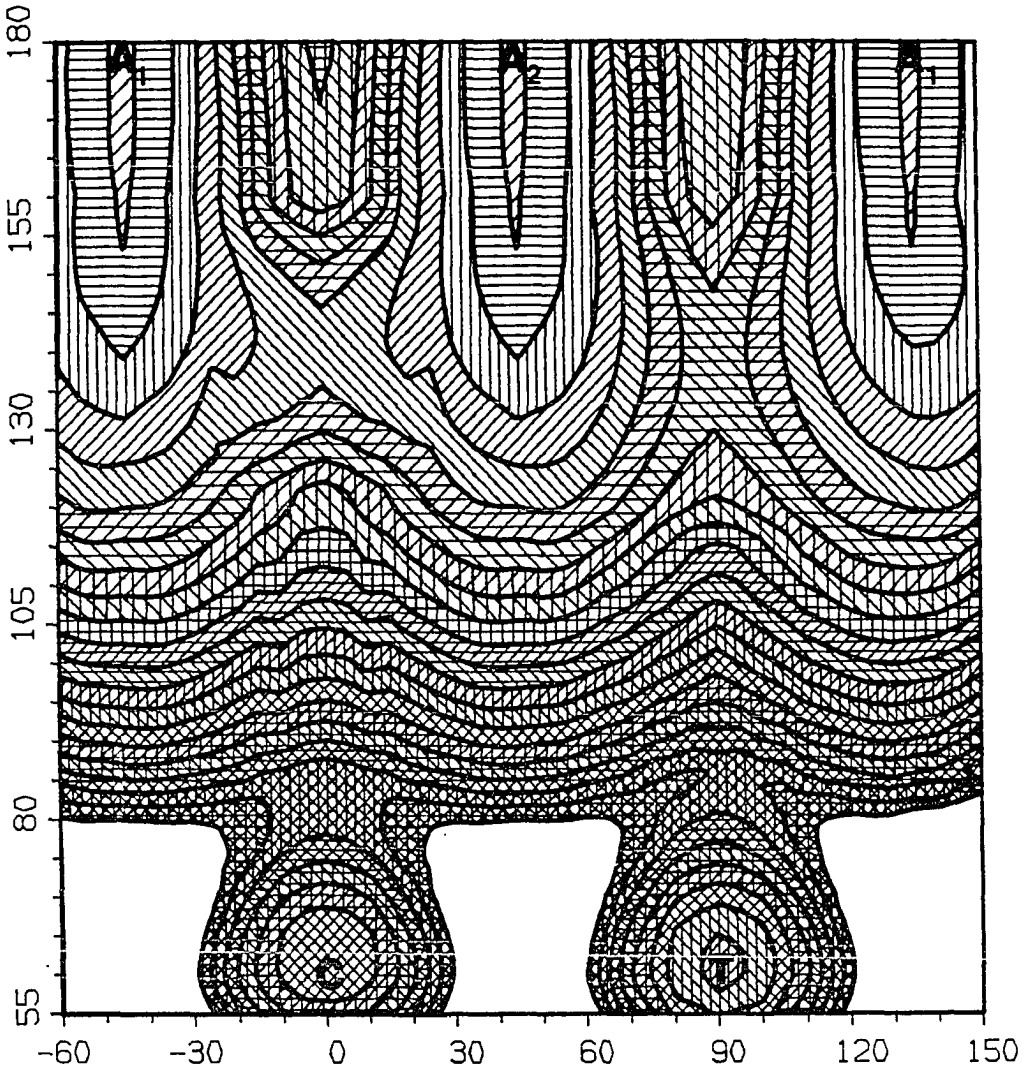

Figure 6.2. Contour plot of the energy as a function of Φ and δ. Note the minima for cis (C) and trans (T) 2,3-dimethylcyclopropylidene, the minima (A_1, A_2 and A_3) for 2,3-dimethylallene and the saddle points (S_1 and S_2) for the internal rotation of the allenes. Also note the asymmetry of the trans transition region

molecule. They are thus experimentally indistinguishable. The surfaces around these points, although locally symmetric, differ from each other at large distances, corresponding to two different paths from cis to trans.

For $\Phi=180^{o}$ we have the allene isomers A_1 and A_2 all of which have the same energy. The isomer A_1 occurs for $\delta=-45^{o},135^{o}$ etc., whereas the isomer A_2 occurs for $\delta=-135^{o},45^{o}$ etc. The isomers A_1 and A_2 are each others mirror images and chiral isomers.

The first thing we observe is that the trans dimethylcyclopropylidene species is lower in energy than the cis molecule. As the C_2-C_3 bond breaks and the ring starts to open, the molecules (cis and trans) move upwards towards their respective transition states. The cis species continues to be higher in energy than the trans all through this ascent. It will, however, reach its transition state first (at a Φ angle of around 82.5^{o}). The trans species does not reach its transition state until about 84.5^{o}. As soon, therefore, as the cis molecule arrives at the top of its own energy curve, it will start descending towards the final products and, for a while at least, it will be lower in energy than the trans compound with the same Φ ring-opening angle. But there is a more important difference between the two transition states. While the cis transition state is quite similar to that of the unsubstituted species, viz., a

perfectly symmetrical, valley-into-ridge bifurcation region, leading to two distinct allene stereoisomers with exactly equal probability, the **trans** transition state is obviously asymmetrical. One can clearly see that when the molecule reaches the transition region, it will find it energetically advantageous to move to the right instead of to the left. And while this advantage is only of the order of a few kcal/mole, it is enough to bias the reaction in one direction rather than the other, i.e. to make it, at least partially, stereospecific.

It is also of interest to note that there exists no reasonable path that leads from cis-dimethyl-cyclopropylidene to the trans molecule, or vice versa. At first glance, this may seem to be intuitively obvious because of the fact that, to achieve the internal rotation necessary for the stereo-isomerization, one has to first break the C_1-C_2 bond. However a closer look reveals that it is independent of the bond-breaking. In other words, even though at, e.g., $\Phi=80^{o}$, the bond has long since broken, there is still no orthogonal trajectory from the **cis** to the **trans** compound, or vice-versa. Moreover, this feature is not a consequence of having the methyl substituents, but existed already for the unsubstituted species (see Figure 3.6). There, however, it was impossible to experimentally distinguish between the **cis** and the **trans** isomers.

With the molecules now moving past their respective transition states towards the final products, one notes that the ridge following the trans transition region is steeper, with the valleys on either side more pronounced that the respective cis valleys. This will have the effect of further enhancing the stereospecificity, because once the molecule starts falling down one side of the ridge, there is less possibility that it will recover and go the other way.

When analyzing the Φ=constant panels in the preceding section, it was noted that it was more favorable for the allene stereoisomers to internally rotate one way rather than the other in order to produce the other stereoisomer, due to steric reasons. From the surface on Figure 6.2 one confirms this observation by noting that the barrier separating the isomers is higher at ($\delta=0^{o},\Phi=180^{o}$) than at ($\delta=90^{o},\Phi=180^{o}$). As in the case of the unsubstituted species, however, it is evident that here, too, it is energetically advantageous for allene to bend in order to stereoisomerize. It is also interesting to note that the saddle point corresponding to the energetically less favorable linear internal rotation <u>is considerably lower in energy</u> than the one corresponding to the more favorable linear rotation. This is so because, although this particular linear rotation brings the two methyl substituents closer together than the other one, the simultaneous bending brings them as far apart as it is

possible and thereby lowers the energy significantly.

D. The Asymmetrically Disubstituted Species

The study of 2,3-dimethylcyclopropylidene and its conversion to 2,3-dimethylallene has given satisfactory explanations of all experimentally observations in terms of purely nonbonded interactions.

There remains however one unresolved question. This is the case, mentioned in Chapter II, where Jones and Krause (1971) observed that cis-2-p-bromophenyl-3-p-methylphenyl-cyclopropylidene gave an allene of higher optical activity and the same relative configuration as cis-2-phenyl-3-p-methylphenylcyclopropylidene, even though bromine is larger than hydrogen, so that purely steric arguments would tend to predict the opposite result. Based on these results, the authors go on to argue that the substituents must therefore be able to promote or retard the rotation of one group relative to the other during the ring-opening process by electronic effects. They use Borden's (1967) suggested mechanism (where only one CX_2 group is supposed to rotate, with the other remaining fixed) in their arguments and suggest that the relative electron-donating or electron withdrawing potential of the two groups will determine which of the two will, in fact, rotate.

These arguments seem a little far-fetched. First of all, in light of the results presented in Chapter III, Borden's mechanism does not seem to be the correct one. Moreover, the suggestion that a bromine substituent on the phenyl substituent of one of the carbons connected to the carbene carbon would have an electronic effect on the carbene center sufficient to influence the outcome of the reaction seems somewhat difficult to imagine.

A much simpler possibility (not considered by Jones and Krause) is that the observed changes are due to the fact that the C-Br bond is highly polar and it can therefore be expected to interact via nonbonded dipole-dipole interactions with such bonds as C-H. Although the latter are considerably less polar, the interactions may nevertheless be sufficiently strong to be nonnegligible. In view of the opposing polarity of the C-Br and C-H bonds this dipole-dipole interaction is in most cases attractive. If it is greater than the corresponding nonpolar steric repulsion, then it might explain the results observed by Jones and Krause, without recourse to arguments about electronic effects. It should be pointed out that covalent electronic effects are "short range" because they are related to exponentially decaying overlap integrals. Dipole-dipole interactions are by contrast "long range" effects, as shown by Eq. (6.B.5).

In order to test the validity of this conjecture, the

method used in the previous section to simulate the nonbonded effects of methyl groups substituting for two of the hydrogens will be used again. This time, however, two separate cases will be considered and compared: First, the case where only one hydrogen is substituted by a methyl group, and second, the case where a bromine atom is placed cis to the methyl group in place of a second hydrogen. In the first case, the methyl group will be considered to be cis to a hydrogen. Obviously this will lead to products indistiguishable experimentally, but the numbering of the atoms allows them to be distinguished easily in the course of a theoretical calculation.

The general features of these cases are either identical or very similar to the case of the previously considered dimethyl compound, the main difference being in the fact that the cis species reaction now exhibits stereospecificity due to the dissimilarity of the two substituents. Moreover, these observed cis asymmetries in the reaction surface are considerably smaller than those observed earlier. It would, therefore, be meaningless to show the complete results for every Φ=constant panel. Instead we show an enlargement of the area around the intersection of the reaction path with the $\Phi=83^{\circ}$ panel, which in this case happens to be right around the transition state.

Figure 6.3 shows two such enlargements. The one on the

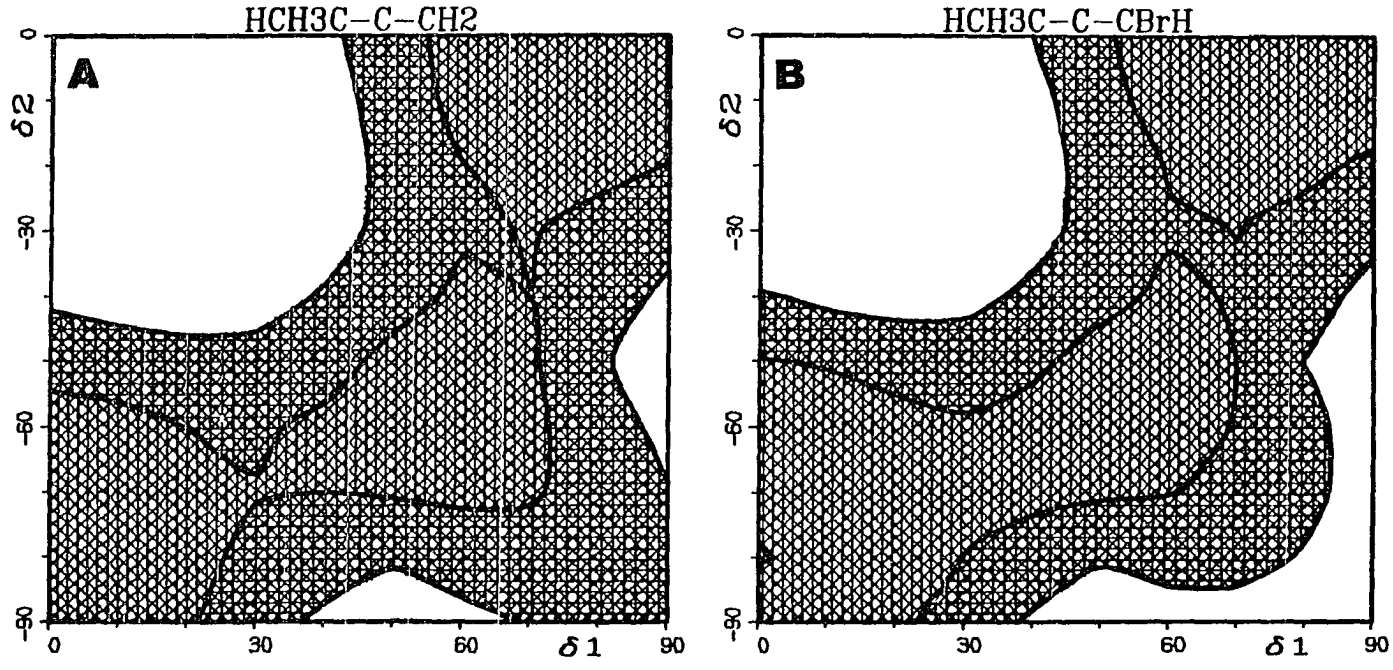

Figure 6.3. Enlargement of the area around the intersection of the reaction path with the $\Phi=83^{o}$ panel for 3-methylallene (A) and cis-2-bromo-3-methylallene (B). Note that B exhibits more stereospecificity than A, and in the same direction

left (A) corresponds to the 3-methyl species, while the one on the right (B) corresponds to the 2-bromo-3-methyl species. It should be noted that in both cases, movement from the transition state (located at around ($\delta_1=60^o, \delta_2=-60^o$)) towards the lower left hand corner corresponds to the methyl group moving outside the three-carbon ring, while movement towards the upper right hand corner corresponds to the methyl group moving inside the ring. The compound on the left shows a small bias towards moving to the left rather than to the right, in that on that side the way toward the minimum on the surface (m) is open while on the other side there exists a saddle point (S) barring the way. The height of the saddle point is no more than 1-2 kcal/mole, but the bias exists nonetheless. The compound on the right, on the other hand, exhibits a much larger and clearer bias towards the same side as the compound on the left, which is exactly what Jones and Krause thought should not happen, since, by purely steric arguments and in view of the fact that Br is as large or larger than CH_3, this figure should exhibit no bias or, possibly, a bias towards the right.

What Jones and Krause observed has therefore been reproduced by the simple expedient of taking into account long-range non-bonded dipole-dipole interactions. The postulate of changes in electronic covalent binding seems therefore unnecessary.

E. Conclusions

The detailed calculation of the complete reaction surface (Chapter III) led to inferences (Chapter IV) which left some of the observed experimental phenomena unexplained. In the present chapter we have shown that the results of the initial calculation applied to all cases when simply calculated nonbonded interactions simulating the introduction of substituents were added to the ab-initio reaction surface. With this correction all experimental observations were satisfactorily reproduced.

It was shown that the disubstituted **trans** species exhibits clear stereospecificity while the corresponding **cis** compound does not. Both results agree with experiment and with chemical intuition. Moreover, it was shown that dipole-dipole interactions are as important as steric effects in inducing stereospecificity and in determining the direction that this stereospecificity will take.

It is difficult to ascertain what quantitative conclusions, if any, can be drawn from the calculations of this section. There seems to exist considerable uncertainty in just how quantitatively stereospecific some reactions are and there is, therefore, little to compare the results against. The order of magnitude of the barriers, energy differences etc., however, seem to fall within the range

which one would expect from the experimental results.

We believe that the explanation of all experimental observations by the methods employed in this chapter, refutes all arguments regarding any covalent electronic nature of the stereospecificity-inducing effects. We therefore conclude that the ring-opening reaction of cyclopropylidene to give allene is inherently nonstereospecific and that all observed instances of stereospecificity are entirely due to nonbonded interactions between the introduced substituents.

VII. APPENDIX

Tables 7.1 through 7.17 show the changes of the 12 optimized internal coordinates with (Φ,δ_1,δ_2). The dihedral angle values of the intersection of each panel Φ=constant with the reaction path are highlighted in boldface. Deviations from the exact values of δ_1 and δ_2 are due to the nonlinearity of the cartesian to internal coordinate transformation during optimization. Energies are in Hartree (-114.0). The meanings of the symbols used are as follows:

↔ 01	C_0-C_1 bond length (in Å).
↔ 02	C_0-C_2 bond length (in Å).
↔ 11	C_1-H_1 bond length (in Å).
↔ 11′	C_1-H_1, bond length (in Å).
↔ 22	C_2-H_2 bond length (in Å).
↔ 22′	C_2-H_2, bond length (in (Å).
∢ 011	C_0-C_1-H_1 bond angle (in degrees).
∢ 011′	C_0-C_1-H_1, bond angle (in degrees).
∢ 022	C_0-C_2-H_2 bond angle (in degrees).
∢ 022′	C_0-C_2-H_2, bond angle (in degrees).
PB 1	C_0-$C_1H_1H_1$, out-of-plane bend (in degrees).
PB 2	C_0-$C_2H_2H_2$, out-of-plane bend (in degrees).

Table 7.1. Variation of the twelve remaining internal coordinates around the intersection of the reaction path for the panel $\Phi=60^{\circ}$

δ_1	80.9	90.0	85.5	85.0	90.2	89.2	95.0	94.5	99.1
δ_2	90.2	90.0	85.5	95.0	80.9	99.1	83.0	94.5	89.8
Energy	-.3902	-.3929	-.3913	-.3916	-.3902	-.3902	-.3916	-.3913	-.3902
↔ 01	1.533	1.532	1.532	1.532	1.533	1.533	1.532	1.532	1.533
↔ 02	1.533	1.532	1.532	1.532	1.533	1.533	1.532	1.532	1.533
↔ 11	1.083	1.081	1.082	1.081	1.082	1.079	1.081	1.080	1.080
↔ 11′	1.080	1.081	1.080	1.081	1.079	1.082	1.081	1.082	1.083
↔ 22	1.079	1.081	1.080	1.081	1.080	1.083	1.081	1.080	1.082
↔ 22′	1.082	1.081	1.082	1.081	1.083	1.080	1.081	1.082	1.079
∢ 011	111.5	117.0	113.1	114.5	114.6	119.5	119.7	121.1	123.0
∢ 011′	123.0	117.0	121.1	119.7	119.5	114.6	114.5	113.1	111.5
∢ 022	119.5	117.0	121.1	114.5	123.0	111.5	119.7	113.1	114.6
∢ 022′	114.6	117.0	113.1	119.7	111.5	123.0	114.5	121.1	119.5
PB 1	32.47	33.11	32.88	32.97	33.12	33.12	32.97	32.88	32.47
PB 2	-33.12	-33.11	-32.88	-32.97	-32.47	-32.47	-32.97	-32.88	-33.12

Table 7.2. Variation of the twelve remaining internal coordinates around the intersection of the reaction path for the panel $\Phi=70^{0}$

δ_1	80.8	90.0	85.3	85.0	90.0	90.0	95.0	94.7	99.4
δ_2	90.0	90.0	85.3	95.0	80.6	99.3	85.0	94.7	90.0
Energy	-.3687	-.3707	-.3690	-.3702	-.3686	-.3687	-.3702	-.3690	-.3686
↔ 01	1.481	1.481	1.480	1.481	1.481	1.480	1.481	1.481	1.480
↔ 02	1.479	1.481	1.481	1.481	1.480	1.480	1.481	1.480	1.481
↔ 11	1.084	1.080	1.081	1.079	1.080	1.079	1.079	1.078	1.076
↔ 11′	1.076	1.080	1.078	1.080	1.080	1.080	1.080	1.081	1.082
↔ 22	1.079	1.080	1.079	1.080	1.080	1.081	1.080	1.080	1.081
↔ 22′	1.079	1.080	1.080	1.080	1.079	1.078	1.080	1.079	1.081
∢ 011	113.8	118.0	114.8	115.9	116.3	120.0	120.2	121.3	123.0
∢ 011′	122.9	118.0	121.3	120.2	119.7	116.0	115.9	114.9	113.8
∢ 022	120.2	118.0	121.3	115.9	122.9	113.7	120.2	114.8	116.0
∢ 022′	116.0	118.0	114.9	120.2	113.8	122.9	115.9	121.2	119.7
PB 1	25.51	26.57	26.57	26.46	26.55	26.63	26.46	26.25	25.42
PB 2	-26.41	-26.51	-26.32	-26.40	-25.52	-25.57	-26.40	-26.54	-26.90

Table 7.3. Variation of the twelve remaining internal coordinates around the intersection of the reaction path for the panel $\Phi=75^{0}$

δ_1	90.9	95.3	95.0	99.7	100.0	100.0	104.2	105.0	108.5
δ_2	80.0	75.7	85.0	71.4	80.0	89.2	76.0	85.0	80.5
Energy	-.3499	-.3499	-.3514	-.3497	-.3514	-.3498	-.3512	-.3496	-.3497
↔ 01	1.472	1.470	1.472	1.467	1.472	1.475	1.468	1.472	1.471
↔ 02	1.474	1.471	1.472	1.467	1.472	1.474	1.467	1.472	1.467
↔ 11	1.080	1.080	1.078	1.082	1.078	1.078	1.082	1.078	1.077
↔ 11′	1.077	1.081	1.080	1.084	1.080	1.081	1.080	1.080	1.082
↔ 22	1.077	1.077	1.079	1.077	1.079	1.079	1.079	1.079	1.081
↔ 22′	1.084	1.084	1.080	1.083	1.080	1.075	1.082	1.080	1.080
∢ 011	116.2	116.8	119.0	117.5	120.8	123.1	120.8	122.7	124.7
∢ 011′	120.9	121.1	118.6	121.8	116.9	114.4	118.9	115.1	115.6
∢ 022	123.3	123.9	118.6	124.4	120.5	116.0	120.7	118.6	116.8
∢ 022′	114.6	114.6	119.0	114.9	117.2	121.3	117.9	119.0	121.3
PB 1	23.19	21.38	22.04	18.81	21.77	21.85	18.02	21.34	17.11
PB 2	-21.40	-20.86	-21.87	-20.01	-21.60	-21.94	-21.02	-21.87	-21.79

Table 7.4. Variation of the twelve remaining internal coordinates around the intersection of the reaction path for the panel $\Phi=80^{\circ}$

δ_1	110.0	115.0	115.0	120.0	120.0	120.0	125.0	125.0	130.0
δ_2	60.0	55.0	65.0	50.0	60.0	70.0	55.0	65.0	60.0
Energy	-.3371	-.3375	-.3382	-.3368	-.3388	-.3371	-.3377	-.3375	-.3368
↔ 01	1.454	1.452	1.452	1.448	1.452	1.455	1.452	1.452	1.452
↔ 02	1.455	1.452	1.452	1.452	1.452	1.454	1.452	1.452	1.449
↔ 11	1.082	1.080	1.080	1.082	1.080	1.080	1.080	1.080	1.082
↔ 11'	1.081	1.085	1.085	1.087	1.085	1.086	1.085	1.085	1.083
↔ 22	1.079	1.080	1.080	1.084	1.080	1.082	1.080	1.080	1.084
↔ 22'	1.085	1.085	1.085	1.084	1.085	1.080	1.085	1.085	1.088
< 011	124.3	125.7	125.7	124.6	126.5	128.2	127.1	127.1	128.1
< 011'	118.5	118.2	118.2	119.7	117.5	115.5	116.9	116.9	117.2
< 022	128.5	127.0	125.6	128.3	126.3	124.0	127.0	125.6	124.3
< 022'	115.4	117.0	118.3	117.0	117.6	118.8	117.0	118.3	119.8
PB 1	10.09	8.14	8.14	9.62	7.78	5.81	7.36	7.36	5.21
PB 2	-4.71	-7.30	-8.08	-4.91	-7.72	-10.47	-7.30	-8.08	-10.72

Table 7.5. Variation of the twelve remaining internal coordinates around the intersection of the reaction path for the panel $\Phi=82^{o}$

δ_1	115.7	120.0	120.0	124.9	125.0	124.9	130.0	130.0	134.2
δ_1	55.1	50.0	60.0	45.8	55.0	64.2	50.0	60.0	55.0
Energy	-.3346	-.3347	-.3355	-.3336	-.3358	-.3346	-.3342	-.3347	-.3336
↔ 01	1.447	1.448	1.448	1.445	1.448	1.451	1.448	1.448	1.451
↔ 02	1.450	1.448	1.448	1.451	1.448	1.447	1.448	1.448	1.445
↔ 11	1.083	1.082	1.082	1.082	1.082	1.082	1.082	1.082	1.086
↔ 11′	1.084	1.087	1.087	1.090	1.087	1.086	1.087	1.087	1.083
↔ 22	1.081	1.082	1.082	1.086	1.082	1.082	1.082	1.082	1.083
↔ 22′	1.085	1.087	1.087	1.084	1.087	1.083	1.087	1.087	1.090
∢ 011	125.5	126.6	126.6	125.4	127.0	128.7	127.4	127.4	128.3
∢ 011′	118.4	118.4	118.4	119.7	118.0	116.1	117.6	117.6	117.9
∢ 022	128.5	127.4	126.6	128.3	127.0	125.5	127.4	126.6	125.7
∢ 022′	116.2	117.6	118.4	117.9	118.0	118.5	117.6	118.4	119.7
PB 1	7.24	4.92	4.92	7.26	4.66	2.50	4.35	4.35	1.97
PB 2	-2.60	-4.46	-5.05	-2.24	-4.77	-6.95	-4.46	-5.05	-7.06

Table 7.6. Variation of the twelve remaining internal coordinates around the intersection of the reaction path for the panel $\Phi=84^{o}$

δ_1	130.1	130.0	125.0	135.0	120.2	139.8	125.0	135.0	129.8
δ_1^1	40.1	50.0	45.0	45.0	50.1	49.9	55.0	55.0	59.8
Energy	-.3309	-.3332	-.3325	-.3313	-.3328	-.3309	-.3335	-.3325	-.3328
↔ 01	1.443	1.446	1.446	1.446	1.444	1.452	1.446	1.446	1.448
↔ 02	1.452	1.446	1.446	1.446	1.448	1.443	1.446	1.446	1.444
↔ 11	1.085	1.083	1.083	1.083	1.085	1.084	1.083	1.083	1.081
↔ 11′	1.091	1.088	1.088	1.088	1.087	1.088	1.088	1.088	1.085
↔ 22	1.084	1.083	1.083	1.083	1.081	1.085	1.083	1.083	1.085
↔ 22′	1.089	1.088	1.088	1.088	1.086	1.090	1.088	1.088	1.086
∢ 011	127.0	127.1	126.8	127.4	125.8	128.1	126.8	127.4	127.5
∢ 011′	119.1	118.5	118.8	118.3	119.2	118.1	118.8	118.3	117.8
∢ 022	128.3	127.1	127.4	127.4	127.6	126.9	126.8	126.8	125.7
∢ 022′	118.0	118.5	118.3	118.3	117.7	119.2	118.8	118.8	119.3
PB 1	3.68	3.07	3.28	2.83	4.00	1.95	3.28	2.83	2.55
PB 2	-2.00	-3.08	-2.85	-2.85	-2.62	-3.66	-3.30	-3.30	-3.85

Table 7.7. Variation of the twelve remaining internal coordinates around the intersection of the reaction path for the panel $\Phi=86^{0}$

δ_1	135.0	120.0	140.0	125.0	135.0	130.0	130.0	125.0	130.0
δ_1	45.0	50.0	50.0	55.0	55.0	60.0	40.0	45.0	50.0
Energy	-.3312	-.3310	-.3316	-.3314	-.3319	-.3309	-.3317	-.3320	-.3321
↔ 01	1.445	1.440	1.455	1.445	1.450	1.448	1.435	1.437	1.445
↔ 02	1.445	1.449	1.435	1.445	1.438	1.441	1.457	1.451	1.445
↔ 11	1.084	1.085	1.085	1.084	1.083	1.082	1.086	1.086	1.084
↔ 11′	1.088	1.087	1.086	1.088	1.086	1.085	1.092	1.089	1.088
↔ 22	1.084	1.083	1.086	1.084	1.086	1.085	1.085	1.084	1.084
↔ 22′	1.088	1.086	1.091	1.088	1.088	1.086	1.088	1.086	1.088
∢ 011	127.3	126.6	127.6	127.2	127.5	127.4	127.5	127.0	127.3
∢ 011′	118.3	118.6	118.5	118.4	118.1	117.7	118.6	118.6	118.4
∢ 022	127.3	127.6	127.4	127.3	127.0	126.6	127.7	127.6	127.3
∢ 022′	118.3	117.6	118.7	118.3	118.7	118.6	118.4	118.0	118.3
PB 1	0.41	0.98	-0.77	0.48	-0.59	-0.44	1.84	1.31	0.45
PB 2	0.04	0.88	-1.45	0.05	-0.80	-0.36	1.21	1.02	0.04

Table 7.8. Variation of the twelve remaining internal coordinates around the intersection of the reaction path for the panel $\Phi=88^{o}$

δ_1	120.0	125.0	130.0	**130.0**	130.0	135.0	135.0	140.0	125.0
δ_1^1	37.0	32.0	27.0	**37.0**	47.0	32.0	42.0	37.0	42.0
Energy	-.3358	-.3376	-.3383	-.3340	-.3311	-.3337	-.3310	-.3298	-.3332
↔ 01	1.424	1.425	1.425	1.425	1.431	1.425	1.431	1.434	1.425
↔ 02	1.465	1.465	1.465	1.465	1.462	1.465	1.465	1.469	1.465
↔ 11	1.087	1.087	1.087	1.087	1.085	1.087	1.085	1.085	1.087
↔ 11′	1.095	1.095	1.095	1.095	1.089	1.095	1.091	1.093	1.095
↔ 22	1.086	1.086	1.086	1.086	1.087	1.086	1.088	1.088	1.086
↔ 22′	1.086	1.086	1.086	1.086	1.084	1.086	1.085	1.086	1.086
∢ 011	127.0	127.2	127.4	127.4	127.2	127.6	127.5	127.8	127.2
∢ 011′	119.2	119.0	118.8	118.8	118.4	118.6	118.5	118.5	119.0
∢ 022	126.5	126.3	126.1	126.5	126.0	126.3	126.0	126.2	126.7
∢ 022′	119.3	119.5	119.7	119.3	119.5	119.5	119.8	119.9	119.0
PB 1	2.63	2.49	2.33	2.33	1.91	2.15	2.05	2.36	2.49
PB 2	2.54	2.23	1.91	2.54	4.91	2.23	4.46	3.94	2.82

Table 7.9. Variation of the twelve remaining internal coordinates around the intersection of the reaction path for the panel $\Phi=90^{0}$

δ	120.2	125.0	125.0	129.9	129.9	130.0	134.8	135.0	139.7
δ_1^1	24.0	19.1	29.1	14.2	24.2	34.0	19.3	29.0	24.3
Energy	-.3521	-.3541	-.3467	-.3551	-.3485	-.3402	-.3496	-.3417	-.3431
↔ 01	1.438	1.438	1.434	1.439	1.436	1.431	1.438	1.431	1.438
↔ 02	1.443	1.445	1.455	1.448	1.456	1.457	1.458	1.457	1.469
↔ 11	1.091	1.088	1.087	1.085	1.084	1.085	1.082	1.085	1.080
↔ 11′	1.080	1.083	1.084	1.086	1.085	1.100	1.087	1.100	1.087
↔ 22	1.082	1.083	1.083	1.083	1.084	1.078	1.085	1.078	1.086
↔ 22′	1.095	1.093	1.097	1.095	1.097	1.088	1.096	1.088	1.098
∢ 011	127.1	127.4	127.1	127.7	127.4	127.2	127.8	127.8	127.7
∢ 011′	119.4	119.5	119.1	119.5	119.2	118.7	119.2	118.2	119.1
∢ 022	125.2	124.9	124.9	124.8	124.6	127.1	124.5	126.8	124.0
∢ 022′	120.4	120.9	120.4	121.2	120.9	118.7	121.4	119.1	121.6
PB 1	9.00	8.27	7.97	7.50	7.31	6.61	6.58	6.10	5.64
PB 2	4.39	3.42	5.42	2.44	4.40	4.34	3.37	3.76	4.42

Table 7.10. Variation of the twelve remaining internal coordinates around the intersection of the reaction path for the panel $\Phi=92^{0}$

δ	120.4	125.4	125.2	130.1	130.0	130.2	135.0	135.0	139.9
δ_1^1	11.7	16.8	6.9	12.0	2.0	22.0	17.1	7.0	12.1
Energy	-.3695	-.3648	-.3704	-.3661	-.3707	-.3590	-.3605	-.3664	-.3611
↔ 01	1.444	1.441	1.444	1.442	1.444	1.437	1.439	1.438	1.440
↔ 02	1.425	1.434	1.427	1.435	1.430	1.444	1.444	1.430	1.440
↔ 11	1.081	1.083	1.080	1.082	1.080	1.085	1.084	1.076	1.080
↔ 11′	1.088	1.089	1.089	1.092	1.091	1.093	1.094	1.098	1.097
↔ 22	1.083	1.085	1.083	1.084	1.084	1.086	1.086	1.082	1.084
↔ 22′	1.088	1.088	1.087	1.088	1.088	1.084	1.086	1.089	1.086
∢ 011	125.3	126.0	125.8	126.2	126.1	126.2	126.6	126.6	127.1
∢ 011′	120.3	119.8	120.2	119.9	120.3	119.6	119.5	119.5	119.1
∢ 022	125.5	124.8	125.2	124.9	125.0	124.6	124.4	125.9	125.2
∢ 022′	121.3	121.1	121.9	121.8	122.4	121.0	121.7	122.3	122.1
PB 1	10.91	10.48	10.15	9.38	9.33	9.48	8.69	8.19	7.67
PB 2	3.30	5.05	1.97	3.25	0.62	6.17	4.66	1.62	2.92

Table 7.11. Variation of the twelve remaining internal coordinates around the intersection of the reaction path for the panel $\Phi=94^{\circ}$

δ_1	120.0	125.0	125.0	130.0	130.0	130.0	135.0	135.0	140.0
δ_1^1	-1.0	-6.0	4.0	-1.0	-11.0	9.0	-6.0	4.0	-1.0
Energy	-.3834	-.3840	-.3805	-.3811	-.3843	-.3765	-.3813	-.3769	-.3771
↔ 01	1.447	1.447	1.447	1.447	1.447	1.447	1.447	1.447	1.447
↔ 02	1.416	1.416	1.416	1.416	1.416	1.416	1.416	1.416	1.416
↔ 11	1.083	1.083	1.083	1.083	1.083	1.083	1.083	1.083	1.083
↔ 11′	1.090	1.090	1.090	1.090	1.090	1.090	1.090	1.090	1.090
↔ 22	1.083	1.083	1.083	1.083	1.083	1.083	1.083	1.083	1.083
↔ 22′	1.092	1.092	1.092	1.092	1.092	1.092	1.092	1.092	1.092
∠ 011	122.4	123.5	123.5	124.5	124.5	124.5	125.5	125.5	126.4
∠ 011′	123.3	122.4	122.4	121.6	121.6	121.6	120.8	120.8	120.1
∠ 022	125.5	125.2	125.4	125.5	124.7	124.9	125.2	125.4	125.5
∠ 022′	121.5	121.6	121.5	121.5	121.8	121.7	121.6	121.5	121.5
PB 1	11.89	11.23	11.23	10.50	10.50	10.50	9.68	9.68	8.79
PB 2	0.60	3.59	-2.39	0.60	6.56	-5.38	3.59	-2.39	0.60

Table 7.12. Variation of the twelve remaining internal coordinates around the intersection of the reaction path for the panel $\Phi=96^{0}$

δ_1	120.2	125.0	125.0	130.0	129.8	130.0	134.8	134.8	139.7
δ_1^1	-14.2	-19.0	-9.0	-14.0	-23.6	-4.0	-18.7	-8.9	-13.6
Energy	-.3950	-.3955	-.3937	-.3942	-.3959	-.3911	-.3946	-.3917	-.3921
↔ 01	1.436	1.436	1.437	1.437	1.435	1.437	1.436	1.438	1.437
↔ 02	1.406	1.410	1.412	1.412	1.414	1.412	1.415	1.414	1.418
↔ 11	1.090	1.091	1.092	1.092	1.090	1.092	1.091	1.091	1.091
↔ 11′	1.091	1.092	1.092	1.092	1.093	1.092	1.093	1.092	1.093
↔ 22	1.084	1.081	1.079	1.079	1.080	1.079	1.078	1.078	1.077
↔ 22′	1.086	1.088	1.088	1.088	1.090	1.088	1.090	1.087	1.089
∢ 011	120.3	121.3	121.3	122.6	122.0	122.6	123.2	123.3	124.0
∢ 011′	123.9	123.1	123.4	122.3	122.7	122.3	121.9	121.8	121.3
∢ 022	125.3	124.6	125.3	124.7	123.8	125.6	124.2	124.6	124.4
∢ 022′	121.5	121.9	121.7	122.0	122.2	121.6	122.5	122.4	122.5
PB 1	16.60	16.09	15.05	14.06	15.88	14.06	14.03	12.99	12.70
PB 2	6.95	9.29	4.12	6.38	11.70	1.84	8.32	3.31	5.30

Table 7.13. Variation of the twelve remaining internal coordinates around the intersection of the reaction path for the panel Φ=98°

δ_1	129.9	124.9	129.6	134.6	139.7	134.9	129.9	125.0	120.2
δ_1^1	-26.7	-31.9	-36.5	-31.5	-26.7	-21.9	-17.0	-22.1	-27.2
Energy	-.4042	-.4037	-.4040	-.4045	-.4036	-.4033	-.4029	-.4038	-.4034
↔ 01	1.430	1.432	1.431	1.429	1.429	1.431	1.431	1.431	1.436
↔ 02	1.411	1.411	1.419	1.419	1.417	1.410	1.410	1.408	1.407
↔ 11	1.083	1.083	1.084	1.083	1.081	1.080	1.089	1.088	1.087
↔ 11′	1.090	1.091	1.093	1.093	1.092	1.090	1.091	1.091	1.091
↔ 22	1.082	1.084	1.082	1.080	1.080	1.082	1.080	1.082	1.083
↔ 22′	1.089	1.089	1.091	1.091	1.090	1.089	1.088	1.089	1.088
∢ 011	120.5	119.3	120.1	121.3	122.6	121.9	120.5	119.4	118.3
∢ 011′	123.1	123.8	123.0	122.4	121.8	122.6	123.2	123.9	124.3
∢ 022	122.4	121.8	120.7	121.7	122.2	123.1	124.0	123.8	122.8
∢ 022′	122.4	121.9	121.9	122.2	122.7	122.1	122.1	121.8	121.5
PB 1	17.87	19.59	19.41	17.36	14.99	15.44	16.67	18.44	20.55
PB 2	13.89	17.83	20.52	16.87	12.76	10.87	7.93	11.47	15.82

Table 7.14. Variation of the twelve remaining internal coordinates around the intersection of the reaction path for the panel $\Phi=100^{o}$

δ_1	**130.0**	125.0	129.3	134.4	139.5	135.0	130.2	125.3	120.6
δ_1^1	-40.0	-45.0	-49.4	-44.5	-39.7	-35.0	-30.3	-35.5	-40.7
Energy	-.4111	-.4085	-.4087	-.4112	-.4121	-.4119	-.4118	-.4109	-.4085
↔ 01	1.428	1.428	1.426	1.423	1.422	1.428	1.428	1.430	1.434
↔ 02	1.416	1.416	1.423	1.420	1.418	1.416	1.410	1.412	1.414
↔ 11	1.086	1.086	1.086	1.085	1.085	1.086	1.086	1.086	1.088
↔ 11′	1.090	1.090	1.092	1.091	1.090	1.090	1.091	1.092	1.093
↔ 22	1.084	1.084	1.086	1.085	1.084	1.084	1.082	1.083	1.083
↔ 22′	1.089	1.089	1.091	1.091	1.090	1.089	1.088	1.090	1.091
∢ 011	118.3	115.9	116.9	118.4	119.8	120.5	119.1	117.7	116.2
∢ 011′	122.5	123.8	122.6	122.5	122.5	121.2	122.7	122.8	122.9
∢ 022	119.1	116.9	116.9	118.6	120.2	121.1	121.3	119.9	118.2
∢ 022′	122.6	123.6	122.5	122.5	122.6	121.7	122.5	122.4	122.2
PB 1	24.04	25.82	26.69	23.53	20.31	22.09	21.71	24.56	27.28
PB 2	22.12	24.47	26.70	22.97	19.10	19.64	16.49	20.73	24.89

Table 7.15. Variation of the twelve remaining internal coordinates around the intersection of the reaction path for the panel $\Phi=120^{0}$

δ_1	130.0	125.0	130.0	135.0	140.0	135.0	140.0	125.0	120.0
δ_1'	-42.0	-47.0	-52.0	-47.0	-42.0	-37.0	-32.0	-37.0	-42.0
Energy	-.4608	-.4580	-.4577	-.4607	-.4614	-.4614	-.4612	-.4606	-.4576
↔ 01	1.380	1.380	1.380	1.373	1.375	1.380	1.388	1.387	1.380
↔ 02	1.373	1.373	1.373	1.377	1.378	1.373	1.371	1.370	1.373
↔ 11	1.085	1.085	1.085	1.084	1.083	1.085	1.086	1.085	1.085
↔ 11′	1.086	1.086	1.086	1.089	1.088	1.086	1.089	1.089	1.086
↔ 22	1.084	1.084	1.084	1.085	1.085	1.084	1.084	1.083	1.084
↔ 22′	1.085	1.085	1.084	1.086	1.087	1.085	1.086	1.085	1.085
∢ 011	118.3	116.4	118.3	118.0	119.6	120.1	120.5	119.0	114.4
∢ 011′	122.8	124.1	122.8	122.4	121.8	121.7	122.1	122.7	125.5
∢ 022	118.6	116.9	115.0	118.5	119.5	120.3	119.9	119.0	118.6
∢ 022′	123.0	124.1	125.3	122.8	122.5	122.1	122.6	123.0	123.0
PB 1	19.64	21.07	19.64	20.98	17.66	18.08	15.93	18.54	22.34
PB 2	17.84	19.56	21.44	19.10	16.89	15.99	14.42	16.74	17.84

Table 7.16. Variation of the twelve remaining internal coordinates around the intersection of the reaction path for the panel $\Phi=140^{0}$

δ_1	120.0	125.1	125.0	130.4	130.0	130.0	135.0	135.0	140.0
δ_1^1	-45.0	-40.1	-50.0	-35.8	-45.0	-55.0	-40.0	-50.0	-45.0
Energy	-.4815	-.4848	-.4818	-.4856	-.4850	-.4817	-.4855	-.4849	-.4854
↔ 01	1.348	1.350	1.348	1.349	1.348	1.348	1.348	1.348	1.348
↔ 02	1.346	1.343	1.346	1.342	1.346	1.346	1.346	1.346	1.346
↔ 11	1.084	1.086	1.084	1.087	1.084	1.084	1.084	1.084	1.084
↔ 11′	1.084	1.088	1.084	1.087	1.084	1.084	1.084	1.084	1.084
↔ 22	1.084	1.081	1.084	1.081	1.084	1.084	1.084	1.084	1.084
↔ 22′	1.083	1.086	1.083	1.083	1.083	1.083	1.083	1.083	1.083
∢ 011	116.1	119.0	117.6	120.4	119.1	119.1	120.4	120.4	121.7
∢ 011′	125.0	123.0	123.9	122.6	122.8	122.8	121.8	121.8	120.9
∢ 022	119.7	120.5	118.4	121.1	119.7	116.9	121.0	118.4	119.7
∢ 022′	122.5	122.0	123.5	121.8	122.5	124.6	121.6	123.5	122.5
PB 1	17.06	13.65	16.11	9.31	15.04	15.04	13.86	13.86	12.58
PB 2	13.65	11.72	14.82	9.85	13.65	15.87	12.39	14.82	13.65

Table 7.17. Variation of the twelve remaining internal coordinates around the intersection of the reaction path for the panel $\Phi=160^{0}$

δ_1	125.0	130.0	130.0	135.0	135.0	135.0	140.0	140.0	145.0
δ_1^1	-45.0	-40.0	-50.0	-35.0	-45.0	-55.0	-40.0	-50.0	-45.0
Energy	-.4948	-.4966	-.4949	-.4953	-.4966	-.4948	-.4953	-.4966	-.4953
↔ 01	1.326	1.326	1.326	1.326	1.326	1.326	1.326	1.326	1.326
↔ 02	1.326	1.326	1.326	1.326	1.326	1.326	1.326	1.326	1.326
↔ 11	1.083	1.083	1.083	1.083	1.083	1.083	1.083	1.083	1.083
↔ 11′	1.083	1.083	1.083	1.083	1.083	1.083	1.083	1.083	1.083
↔ 22	1.083	1.083	1.083	1.083	1.083	1.083	1.083	1.083	1.083
↔ 22′	1.082	1.082	1.082	1.082	1.082	1.082	1.082	1.082	1.082
∢ 011	120.1	120.6	120.6	121.1	121.1	121.1	121.6	121.6	122.0
∢ 011′	123.1	122.6	122.6	122.1	122.1	122.1	121.7	121.7	121.3
∢ 022	121.1	121.6	120.5	122.1	121.1	119.9	121.6	120.5	121.1
∢ 022′	122.1	121.6	122.6	121.2	122.1	123.1	121.6	122.6	122.1
PB 1	6.27	5.87	5.87	5.42	5.42	5.42	4.92	4.92	4.39
PB 2	5.96	5.41	6.46	4.83	5.96	6.91	5.41	6.46	5.96

VIII. REFERENCES

A. Almenningen, O. Bastiansen and M. Traetteberg, Acta Chem. Scand. 13, 1699 (1959).

R. O. Angus, Jr., M. W. Schmidt and R. P. Johnson, J. Am. Chem. Soc. 107, 532 (1985).

F. W. Bobrowicz and W. A. Goddard, in Methods of Electronic Structure Theory, edited by H. F. Schaefer, III (Plenum Press, New York, 1977), p. 79 and references therein.

N. Bodor, M. J. S. Dewar and Z. B. Maksic, J. Am. Chem. Soc. 95, 5245 (1973).

W. T. Borden, Tetrahedron Lett. 5, 447 (1967).

W. T. Brady, in The Chemistry of Ketenes, Allenes and Related Compounds, edited by S. Patai (John Wiley, Interscience, New York, 1980), p. 298 and references therein.

U. Burkert and N. L. Allinger, Molecular Mechanics (American Chemical Society, Washington, D.C., 1982), and references therein.

P. Carsky and M. Urban, Ab Initio Calculations, Methods and Applications in Chemistry, edited by G. Berthier, M. J. S. Dewar, H. Fischer, K. Fukui, H. Hartmann, H. H. Jaffe, J. Jorther, W. Kutzelnigg, K. Ruedenberg, E. Scrocco and W. Zeil (Springer-Verlag, Berlin, 1980), and references therein.

O. L. Chapman, Pure Appl. Chem. 40, 511 (1974).

L. M. Cheung, K. R. Sundberg and K. Ruedenberg, Int. J. Quantum Chem. 16, 1103 (1979).

Y.- N. Chiu, J. Am. Chem. Soc. 104, 6937 (1982).

P. W. Dillon and G. R. Underwood, J. Am. Chem. Soc. 99, 2435 (1977).

M. G. Dombek, Ph.D. Dissertation, Iowa State University, (1977).

T. H. Dunning, D. C. Cartwright, W. J. Hunt, P. J. Hay and F. W. Bobrowicz, J. Chem. Phys. 64, 4755 (1976).

T. H. Dunning and P. J. Hay, in Methods of Electronic Structure Theory, edited by H. F. Schaefer, III (Plenum Press, New York, 1977), p. 1.

M. Dupuis and H. F. King, J. Chem. Phys. 68 3998 (1978).

M. Dupuis, D. Spangler and J. J. Wendoloski, Nat. Resour. Comput. Chem. Software Cat. 1, Prog. No. QG01 (GAMESS), (1980).

C. E. Dykstra, J. Am. Chem. Soc. 99, 2060 (1977).

C. E. Dykstra and H. F. Schaefer, III, in The Chemistry of Ketenes, Allenes and Related Compounds, edited by S. Patai (John Wiley, Interscience, New York, 1980), p. 1 and references therein.

C. Edmiston and K. Ruedenberg, Rev. Mod. Phys. 35, 457 (1963).

S. T. Elbert, L. M. Cheung and K. Ruedenberg, Nat. Resour. Comput. Chem. Software Cat. 1, Prog. No. QM01 (ALIS), (1980).

D. F. Feller, Ph.D. Dissertation, Iowa State University, (1979).

D. F. Feller and K. Ruedenberg, Theoret. Chim. Acta 52, 231 (1979).

D. F. Feller, M. W. Schmidt and K. Ruedenberg, J. Am. Chem. Soc. 104, 960 (1982).

A. T. Hagler, E. Huler and S. Lifson, J. Am. Chem. Soc. 96, 5319 (1974).

F. Hegelund, J. L. Duncan and D. C. McKean, J. Mol. Spectrosc. 65, 366 (1977).

W. J. Hehre, R. Ditchfield, R. F. Stewart and J. A. Pople, J. Chem. Phys. 52, 2769 (1970).

W. J. Hehre, R. F. Stewart and J. A. Pople, Symp. Faraday Soc. 2, 15 (1968).

W. J. Hehre, R. F. Stewart and J. A. Pople, J. Chem. Phys. 51, 2657 (1969).

G. Herzberg, Electronic Spectra of Polyatomic Molecules (Van Nostrand Reinhold, New York, 1966).

N. Honjou, J. Pacansky and M. Yoshimine, J. Am. Chem. Soc. 106, 5361 (1984).

N. Honjou, J. Pacansky and M. Yoshimine, Ab Initio Studies of the C_3H_4 Surface: I. SCF and CI Study of Structures and Stabilities of Isomers, J. Am. Chem. Soc., submitted (1985).

H. Hopf, in The Chemistry of Ketenes, Allenes and Related Compounds, edited by S. Patai (John Wiley, Interscience, New York, 1980), p. 779 and references therein.

W. J. Hunt, P. J. Hay and W. A. Goddard, J. Chem. Phys. 57, 738 (1972).

R. P. Johnson, Chemistry Department, Iowa State University, private communication (1985).

R. P. Johnson and M. W. Schmidt, J. Am. Chem. Soc. 103, 3244 (1981).

W. M. Jones and D. L. Krause, J. Am. Chem. Soc. 93, 551 (1971).

W. M. Jones and J. M. Walbrick, J. Org. Chem. 34, 2217 (1969).

W. M. Jones and J. W. Wilson, Jr., Tetrahedron Lett. 21, 1587 (1965).

W. M. Jones, J. W. Wilson, Jr., and F. B. Tutwiler, J. Am. Chem. Soc. 85, 3309 (1963).

K. Kirby-Docken and B. Liu, J. Chem. Phys., 66, 4309 (1977).

K. Krogh-Jespersen, J. Comp. Chem. 3, 571 (1982).

B. Lam, Ph.D. Dissertation, Iowa State University, (1984).

B. Lam and R. P. Johnson, J. Am. Chem. Soc. 105, 7479 (1983).

J. M. Lehn and G. Ourisson, Bull. Soc. Chim. Fr., 1113 (1963).

J. E. Lennard-Jones, Proc. R. Soc. London, Ser. A 106, 463 (1924).

G. C. Lie and E. Clementi, J. Chem. Phys. 60, 1275 (1974); 60, 1288 (1974).

R. C. Lord and P. Venkatesvarlu, J. Chem. Phys. 20, 1237 (1952).

J. W. McIver, Jr., and A. Komornicki, Chem. Phys. Lett. 10, 303 (1971).

J. W. McIver, Jr., and A. Komornicki, J. Am. Chem. Soc. 94, 2625 (1972).

A. G. Maki and R. A. Toth, J. Mol. Spectrosc. 17, 136 (1965).

A. Y. Meyer and N. L. Allinger, Tetrahedron 31, 1971 (1975).

J. N. Murrell and K. J. Laidler, Trans. Far. Soc. 64, 371 (1968).

J. N. Murrell and G. L. Pratt, Trans. Far. Soc. 66, 1680 (1970).

D. J. Pasto, M. Haley and D. M. Chipman, J. Am. Chem. Soc. 100, 5272 (1978).

L. C. Pauling, The Nature of the Chemical Bond, 3rd edition (Cornell University Press, Ithaca, N.Y., 1960).

P. Pechukas, J. Chem. Phys 64, 1516 (1976).

J. A. Pople and R. K. Nesbet, J. Chem. Phys. 22, 571 (1954).

R. C. Raffenetti, J. Chem. Phys. 58, 4452 (1973).

B. O. Roos, Int. J. Quantum Chem. 14, 175 (1980).

B. O. Roos, P. R. Taylor and P. E. M. Siegbahn, Chem. Phys. 48, 157 (1980).

C. C. J. Roothaan, Rev. Mod. Phys. 23, 69 (1951).

W. R. Roth, F. Ruf and P. W. Ford, Chem. Ber. 107, 48 (1974).

K. Ruedenberg, Phys. Rev. Lett. 27, 1105 (1971).

K. Ruedenberg, L. M. Cheung and S. T. Elbert, Int. J. Quantum Chem. 16, 1069 (1979).

K. Ruedenberg, M. W. Schmidt, M. M. Gilbert and S. T. Elbert, Chem. Phys. 71, 41 (1982); 71, 51 (1982); 71, 65 (1982).

K. Ruedenberg and R. Poshusta, Adv. Quantum. Chem. 6, 267 (1972).

K. Ruedenberg and K. R. Sundberg, in Quantum Science, edited by J. L. Calais, O. Goscinski, J. Linderberg and Y. Ohrn (Plenum Press, New York, 1976), p. 505.

W. Runge, in The Chemistry of Ketenes, Allenes and Related Compounds, edited by S. Patai (John Wiley, Interscience, New York, 1980), p. 45 and references therein.

W. I. Salmon, L. M. Cheung and K. Ruedenberg, J. Chem. Phys. 57, 2776 and 2787 (1972).

W. I. Salmon and K. Ruedenberg, J. Chem. Phys. 57, 2791 (1972).

H. F. Schaefer, III, editor, Methods of Electronic Structure Theory (Plenum Press, New York, 1977), and references therein.

H. B. Schlegel, J. Comp. Chem. 3, 214 (1982).

M. W. Schmidt, Ph.D. Dissertation, Iowa State University, (1982).

M. W. Schmidt and K. Ruedenberg, J. Chem. Phys. 71, 3951 (1979).

R. Seeger, R. Krishnan, J. A. Pople and P. von R. Schleyer, J. Am. Chem. Soc. 99, 7103 (1977).

P. E. M. Siegbahn, J. Almlof, A. Heiberg and B. O. Roos, J. Chem. Phys. 74, (1981).

P. E. M. Siegbahn, A. Heiberg, B. O. Roos and B. Levy, Physica Scripta 21, 323 (1980).

D. M. Silver, E. L. Mehler and K. Ruedenberg, J. Chem. Phys. 52, 1174 (1970); 52, 1181 (1970); 52, 1206 (1970).

V. Staemmler, Theoret. Chim. Acta 45, 89 (1977).

R. E. Stanton and J. W. McIver, Jr., J. Am. Chem. Soc. 97, 3632 (1975).

R. F. Stewart, J. Chem. Phys. 52, 431 (1970).

T. J. Stierman and R. P. Johnson, J. Am. Chem. Soc. 107, 0000 (1985).

P. Valtazanos and K. Ruedenberg, The Inversion of Methane, unpublished (1985).

A. C. Wahl and G. Das, in Methods of Electronic Structure Theory, edited by H. F. Schaefer, III (Plenum Press, New York, 1977), p. 51 and references therein.

J. M. Walbrick, J. W. Wilson, Jr., and W. M. Jones, J. Am. Chem. Soc. 90, 2895 (1968).

A. Warshel and S. Lifson, J. Chem. Phys. 53, 582 (1970).

D. H. Wertz and N. L. Allinger, Tetrahedron 30, 1579 (1974).

K. B. Wiberg and J. J. Wendoloski, J. Am. Chem. Soc. 98, 5465 (1976).

E. B. Wilson, J. C. Decius and P. C. Cross, Molecular Vibrations (McGraw-Hill, New York, 1955).

F. J. Wodarczyk and E. B. Wilson, J. Chem. Phys. 56, 166 (1972).

L. G. Yaffe and W. A. Goddard, Phys. Rev. A 13, 1682 (1976).

IX. ACKNOWLEDGEMENTS

I owe a deep personal as well as scientific debt to Professor Klaus Ruedenberg. It has been my privilege to work under his supervision and to have had the opportunity to learn from him, and I also deeply appreciate his help in every other way.

My sincere gratitude to Dr. Stephen T. Elbert for his help throughout the years and for his unfailing willingness to share his extensive knowledge of computers and computer programming with me. A very special thanks to Dr. Michael W. Schmidt for his untiring and cheerful guidance during my first years in this group. No question was ever too dumb for him to answer! My appreciation also to Professor Philip M. Warner for first introducing us to the problem, to Shoichi Okuyama and David L. Phillips for their contribution to some parts of this project and to Professor Richard P. Johnson for many interesting and helpful discussions.

My family and I had many friends in Ames and I would like to thank them all for everything they did to make our long stay here enjoyable. I would, however, like to express my special gratitude to Dilys and Achilles Avraamides and to Charlotte and David Bruner. My thanks also to all our friends in Greece and most of all to Pericles Nicolaides for providing support and encouragement when it was most needed.

Christos and Kathy Saccopoulos provided us with a sense of family and security away from home and no thanks is sufficient to repay this. I also owe thanks to all members of my family for their patience, love and understanding, and especially to my mother, Maria, my mother-in-law, Frosso Saccopoulos, and to my sister and brothers and sister-in-law, Tassos and Myrto Arvanitis and Pericles and Elina Saccopoulos. Above all, to my children, Frosso and Maria-Lisa who, even when I least deserved it, somehow always managed to find a way to show their love for me and make me feel that my efforts were worth it.

But the deepest debt of gratitude I owe to my wife, Penny. Her courage, strength, understanding and, above all, love I will never be able to repay. It is not enough to say that, but for her, this dissertation would never have been written. If it were not for her, her confidence and vision, I would not even have been here to start this work. It is therefore to her that I dedicate this dissertation with all my love.